International Scientific-Technical and Production Journal

The Paton WELDING JOURNAL

March 2012 # 3

English translation of the monthly «Avtomaticheskaya Svarka» (Automatic Welding) journal published in Russian since 1948

Founders: *E.O. Paton Electric Welding Institute of the NAS of Ukraine*
International Association «Welding»

Publisher: *International Association «Welding»*

Address:
E.O. Paton Electric Welding Institute,
International Association «Welding»,
11, Bozhenko str., 03680, Kyiv, Ukraine
Tel.: (38044) 200 82 77
Fax: (38044) 200 81 45
E-mail: journal@paton.kiev.ua
http://www.nas.gov.ua/pwj
URL: www.rucont.ru

State Registration Certificate
KV 4790 of 09.01.2001

Subscriptions:
$324, 12 issues per year,
postage and packaging included.
Back issues available.

CONTENTS

MODELLING OF PROCESSES OF HEAT-, MASS- AND ELECTRIC TRANSFER IN COLUMN AND ANODE REGION OF ARC WITH REFRACTORY CATHODE

I.V. KRIKENT[1], **I.V. KRIVTSUN**[2] and **V.F. DEMCHENKO**[2]
[1]Dneprodzerzhinsk State Technical University, Dneprodzerzhinsk, Ukraine
[2]E.O. Paton Electric Welding Institute, NASU, Kiev, Ukraine

Numerical analysis of thermal, electromagnetic and gas-dynamic characteristics of plasma of free-burning arc in argon at atmospheric pressure with tungsten cathode and copper water-cooled anode was performed in the anode region and column of welding arc based on self-consistent mathematic model of processes of heat-, mass- and electric transfer. Results of calculation of current density on the anode and heat flow in the anode are compared with the available experimental data. It is shown that considering of the anode potential drop in the model provides more accurate predictions of the characteristics of heat and electric interaction of arc plasma with anode surface.

Keywords: *fusion welding, electric arc, refractory cathode, arc characteristics, modelling of heat-, mass- and electric transfer*

Information about thermal, electric and dynamic effects of arc on welded metal is necessary for efficient application of the electric arc as a heat source in fusion welding. Investigation of welding arcs using the mathematic modelling methods [1–8] seems to be relevant since experimental determination of characteristics of the welding arc important from technological point of view such as density of electric current and heat flow over the surface of welded part is complicated due to high values of temperature of arc plasma and metal surface temperature, small geometry of region of arc fixation and series of other factors.

Let us consider the electric arc with refractory cathode burning in inert gas at atmospheric pressure. The main attention will be given to the processes taking place in a column and anode region of the arc since theory and mathematic models of cathode phenomena, including processes in a near-cathode plasma, were developed in sufficient details for such an arc [9–12]. Study [13] proposed a self-consistent mathematic model of indicated processes for conditions of nonconsumable electrode welding and plasma welding. The aim of the present work is a verification of given model by means of numerical investigation of distributed characteristics of plasma of column and anode region of a free-burning arc with tungsten cathode and copper water-cooled anode and comparison of obtained results with available experimental data.

Two interconnected models are included in the self-consistent mathematic model of the processes of energy-, mass- and electric transfer in the column and anode region of the welding arc with refractory cathode in accordance with approach applied in [13]:

- model of arc column describing interaction of thermal, electromagnetic, gas-dynamic and diffusion processes in multicomponent plasma of the arc column;
- model of anode region which allows determining characteristics of thermal and electric interaction of arc with anode surface (part), necessary for analysis of thermal, electromagnetic and hydro-dynamic processes in welded metal.

Model of the anode region of arc with evaporating anode proposed in study [13] allows calculating distribution of anode potential drop $U_a = -\Delta\varphi$ along the anode surface and density of heat flow q_a, being entered in the anode by arc, depending on current density on the anode j_a, temperature of electrons of plasma near the anode T_{ea} as well as temperature of its surface T_s. Distribution of j_a and T_{ea} along the anode surface can be determined with sufficient accuracy in modelling of the arc with refractory cathode based on the model of arc column with self-consistent boundary conditions on the anode.

Comparison of calculation value $\Delta\varphi$ with one experimentally measured for the case of application of the arc with tungsten cathode and copper water-cooled anode burning in argon at atmospheric pressure (arc current 200 A, 10 mm length) was carried out for verification of conformity of selected model of anode processes. The following experimental data [14, 15] were used in calculations: $j_a = 3.5 \cdot 10^6$ A/m^2, $T_{ea} =$ = 9840 K, T_s = 720 K, that provides $\Delta\varphi$ = 4.04 V. Obtained calculation value complies with experimentally measured $\Delta\varphi$ = 4.01 V [15] with high accuracy. Figures 1 and 2 show applied in further calculation dependencies of $\Delta\varphi$ and q_a on temperature of electrons in the near-anode plasma and density of electric current on the anode for the free-burning argon arc with refractory cathode and copper water-cooled anode.

Model of isothermal plasma (temperature of electrons equals temperature of heavy particles) was used in describing the processes of heat-, mass- and electric transfer in column plasma of the considered arc, and distribution of all its characteristics as axial-symmetric would be considered. The corresponding system of differential equations represented in a cylindrical coordinate system $\{r, \vartheta, z\}$ has the following appearance [13]:

• continuity equation

$$\frac{\partial \rho}{\partial t} + \frac{1}{r}\frac{\partial}{\partial r}(r\rho v) + \frac{\partial}{\partial z}(\rho u) = 0, \qquad (1)$$

where ρ is the mass density of plasma; v, u are the radial and axial components of its speed;

• motion equations

$$\rho\left(\frac{\partial v}{\partial t} + v\frac{\partial v}{\partial r} + u\frac{\partial v}{\partial z}\right) = -\frac{\partial p}{\partial r} - j_z B_\varphi + \frac{2}{r}\frac{\partial}{\partial r}\times$$
$$\times\left(r\eta\frac{\partial v}{\partial r}\right) + \frac{\partial}{\partial z}\left[\eta\left(\frac{\partial u}{\partial r} + \frac{\partial v}{\partial z}\right)\right] -$$
$$- 2\eta\frac{v}{r^2} - \frac{2}{3}\frac{\partial}{\partial r}\left\{\eta\left[\frac{1}{r}\frac{\partial (rv)}{\partial r} + \frac{\partial u}{\partial z}\right]\right\}, \qquad (2)$$

$$\rho\left(\frac{\partial u}{\partial t} + v\frac{\partial u}{\partial r} + u\frac{\partial u}{\partial z}\right) = -\frac{\partial p}{\partial z} + j_r B_\varphi + 2\frac{\partial}{\partial z}\times$$
$$\times\left(\eta\frac{\partial u}{\partial z}\right) + \frac{1}{r}\frac{\partial}{\partial r}\left[r\eta\left(\frac{\partial u}{\partial r} + \frac{\partial v}{\partial z}\right)\right] -$$
$$- \frac{2}{3}\frac{\partial}{\partial z}\left\{\eta\left[\frac{1}{r}\frac{\partial (rv)}{\partial r} + \frac{\partial u}{\partial z}\right]\right\}, \qquad (3)$$

where p is the pressure; j_z, j_r are the axial and radial components of current density in the arc; B_φ is the azimuth component of vector of magnetic induction; η is the coefficient of dynamic viscosity;

• energy equation

$$\rho C_p\left(\frac{\partial T_p}{\partial t} + v\frac{\partial T_p}{\partial r} + u\frac{\partial T_p}{\partial z}\right) = \frac{1}{r}\frac{\partial}{\partial r}\times$$
$$\times\left(r\chi\frac{\partial T_p}{\partial r}\right) + \frac{\partial}{\partial z}\left(\chi\frac{\partial T_p}{\partial z}\right) + \frac{k}{e}\times$$
$$\times\left\{j_r\frac{\delta[(5/2-\delta)T_p]}{\partial r} + j_z\frac{\partial[(5/2-\delta)T_p]}{\partial z}\right\} +$$
$$+ \frac{j_r^2 + j_z^2}{\sigma} - \psi, \qquad (4)$$

where C_p is the specific heat capacity of plasma considering ionization energy; T_p is the plasma temperature; χ is the coefficient of heat conductance; k is the Boltzmann constant; e is the charge of electron; δ is the thermodiffusion constant; ψ is the energy loss for radiation in approximation of optically thin plasma;

• equations of electromagnetic field

$$\frac{1}{r}\frac{\partial}{\partial r}\left(r\sigma\frac{\partial \varphi}{\partial r}\right) + \frac{\partial}{\partial z}\left(\sigma\frac{\partial \varphi}{\partial z}\right) = 0, \qquad (5)$$

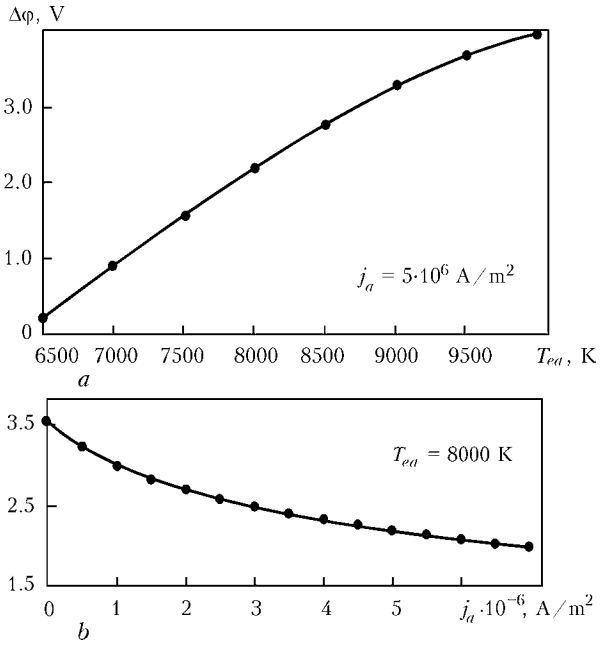

Figure 1. Dependence of potential differences between the boundary of arc column and anode surface on temperature of electrons in the anode region (*a*) and density of electric current on the anode (*b*) for argon arc with copper water-cooled anode

$$B_\varphi(r, z) = \frac{\mu^0}{r}\int_0^r j_z(\xi, z)\xi d\xi, \qquad (6)$$

where φ is the electric potential; σ is the plasma specific electric conductivity; μ^0 is the universal magnetic constant;

$$j_r = -\sigma\frac{\partial \varphi}{\partial r}, \quad j_z = -\sigma\frac{\partial \varphi}{\partial z}. \qquad (7)$$

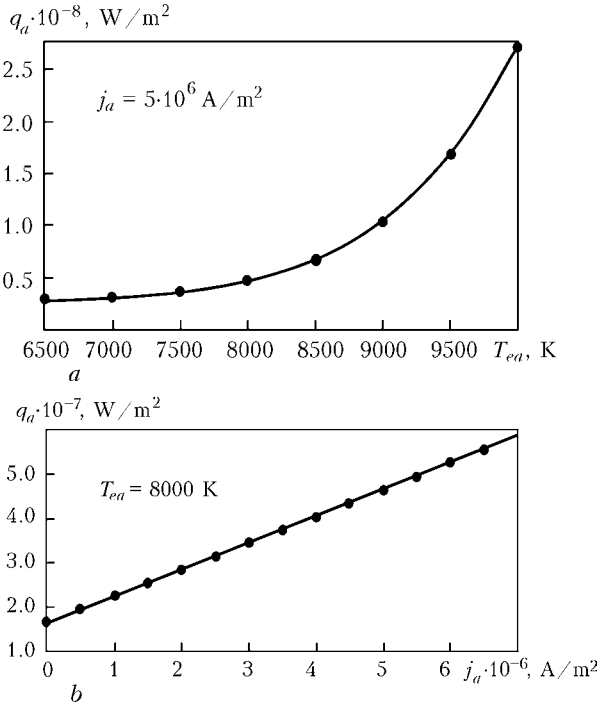

Figure 2. Dependence of heat flow in the anode on temperature of electrons in the anode region (*a*) and density of electric current on the anode (*b*) for argon arc with copper water-cooled anode

Thermodynamic characteristics ρ, C_p, coefficients of transfer η, χ, δ, σ and loss of energy for irradiation ψ of arc plasma depending on its temperature, pressure and composition are to be put for closing the system of equations (1)–(7). Study [16], for example, provides indicated dependencies for isothermal argon plasma of atmospheric pressure.

Corresponding initial and boundary conditions are to be set for solving the system of differential equations (1)–(5) describing the processes of heat-, mass- and electric transfer in the arc column. Initial distributions of speed and temperature of plasma have no fundamental importance since physical fields are established sufficiently quickly in the arc discharge. For example, zero values can be set for speed, and temperature in the region of current channel can be chosen such as to provide plasma conductivity character for the argon arc.

Boundary conditions for desired functions ($\vec{V} = \{v, 0, u\}$, T_p, φ) were formulated in the following way for case of considered here arc with tungsten cathode and copper water-cooled anode.

«Adhesion» conditions are fulfilled for plasma speed $\vec{V}$ on the surface of anode (plane $z = L$):

$$\vec{V}|_{z=L} = 0. \qquad (8)$$

The following condition of energy balance [13] takes place on the boundary of plasma of the arc column with the anode region:

$$-\chi \frac{\partial T_p}{\partial z}\Big|_{z=L} + j_a \frac{k}{e}\left(\frac{5}{2} - \delta\right) T_p|_{z=L} = \Delta\varphi j_a + q_a, \qquad (9)$$

where $j_a = -j_z|_{z=L}$ is the current density on the anode.

Electric potential of the anode surface can be considered constant and equal zero at good approximation. Then the boundary condition for potential on the boundary of arc column with the anode region can be written as

$$\varphi|_{z=L} = \Delta\varphi. \qquad (10)$$

Potential drop Δφ in expressions (9), (10) is calculated according to the model of the anode region [13] at $T_{ea} = T_p|_{z=L}$ (see Figure 1).

The conditions for vector of speed near the cathode (plane $z = 0$) are set in the following way:

$$v|_{z=0} = 0, \quad u|_{z=0} = u_0, \qquad (11)$$

where u_0 is determined by consumption of shielding gas and diameter of nozzle for its feeding.

We will take the following conditions for temperature and electric potential in the near cathode zone of arc:

$$T_p|_{z=0} = T_k(r), \quad \sigma \frac{\partial \varphi}{\partial z}\Big|_{z=0} = j_k(r), \qquad (12)$$

where distribution of plasma temperature $T_k(r)$ and current density under the cathode $j_k(r)$ are chosen according to the recommendations of study [12].

It can be indicated in the zone of shielding gas supply that

$$T_p|_{z=0} = T_{env}, \quad \frac{\partial \varphi}{\partial z}\Big|_{z=0} = 0, \qquad (13)$$

where T_{env} is the temperature of environment.

The boundary conditions for speed, temperature of plasma and electric potential on the axis of symmetry of the system are set in the standard way (see, for example, [1, 3]).

We can write [3] on the outer boundary of calculation area ($r = R$) for speed of plasma and electric potential

$$\frac{\partial(\rho v r)}{\partial r}\Big|_{r=R} = 0, \quad u|_{r=R} = 0, \quad \frac{\partial \varphi}{\partial r}\Big|_{r=R} = 0. \qquad (14)$$

The boundary condition for temperature of plasma at $r = R$ will be determined depending on moving direction of the plasma flow:

$$\begin{aligned} &T_p|_{r=R} = T_{env} \text{ at } v|_{r=R} \le 0, \\ &\frac{\partial T_p}{\partial r}\Big|_{r=R} = 0 \text{ at } v|_{r=R} > 0. \end{aligned} \qquad (15)$$

A finite-difference method was used for numerical solving of the system of differential equations (1)–(5) with the boundary conditions (8)–(15). Calculation data for argon plasma [16] were used for determination of the thermodynamic and transport characteristics of plasma included in equations (1)–(5). Common Lagrangian–Eulerian method [17, 18] adapted to the conditions of compressible media was used at numerical solution of the gas-dynamic and thermal tasks.

A zone φ of positive values, caused by the presence of reverse potential drop on the anode layer, appears over the surface of anode, as can be seen from results of calculation of the electric potential (Figure 3, *a*). The maximum values of gradient of potential and current density in the arc column can be observed near the cathode (Figure 3, *b*). The maximum temperature of arc plasma (Figure 4, *a*) is also achieved in this place that is caused by high intensity of Joule heat sources. Density of electric current rapidly reduces (see Figure 3, *b*) as the distance from the cathode increases. Pattern of plasma movement in the arc column (see Figure 4, *b*) character for the arc with refractory cathode is caused by a force field formed at such current distribution. The maximum values of plasma speed on the axis of symmetry (up to 350 m/s) provide efficient transfer of heat energy from the hottest zone near the cathode to the anode surface. As can be seen from Figure 4, *a*, convective heat transfer determines the temperature field in the arc plasma to a substantive level. This fact explains significant elongation of isotherms along the anode surface.

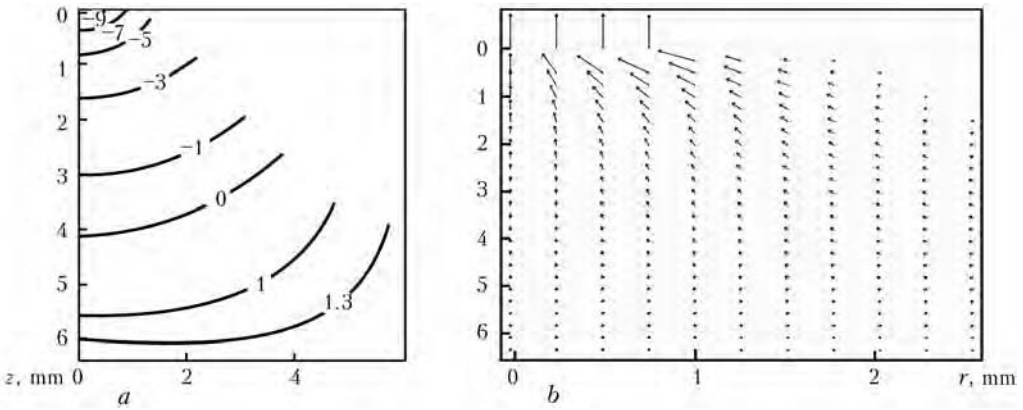

Figure 3. Fields of electric potential (*a*) and current density (*b*) in the column of free-burning arc in argon with tungsten cathode and copper water-cooled anode (max $|\vec{j}| = 8 \cdot 10^7$ A/m^2)

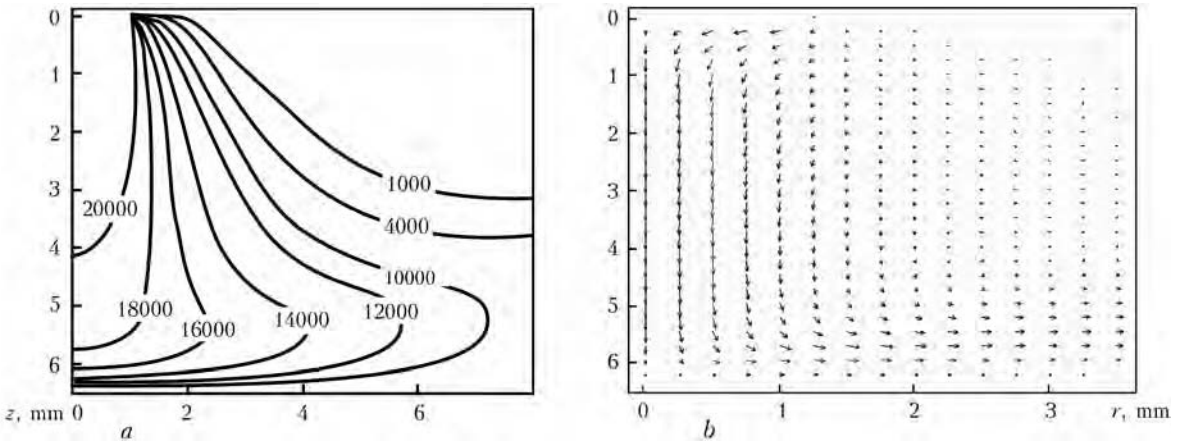

Figure 4. Fields of temperature (*a*) and speed (*b*) of plasma in the column of free-burning arc in argon with tungsten cathode and copper water-cooled anode (max $|\vec{V}| = 8 \cdot 10^7 = 350$ m/s)

Figure 5 shows that the maximum value of $\Delta\varphi$ in the near-anode region is caused by higher values of T_{ea} near the axis of symmetry. Certain increase of the potential drop on a periphery of region of anode arc fixation is caused by extremely small value of current density in this region of the anode surface.

Figure 6 shows a comparison of calculation data of radial distribution of electric current density on the anode and heat flow in the anode with experimental ones [14]. Sufficiently good matching of calculation distributions $j_a(r)$ and $q_a(r)$ with experimental ones is observed for arc of 200 A current. Some differences in calculation and experimental data near the axis of symmetry can be related with the errors of mathematic modelling as well as with the problems of reconstruction of distributed characteristics on integral parameters, measured in [14]. Compliance of the results of mathematic modelling and experimental data for arc of 100 A can be described as sufficiently satisfactory.

The numerical analysis of distributed characteristics in the column and anode region of the electric arc with tungsten cathode and copper water-cooled

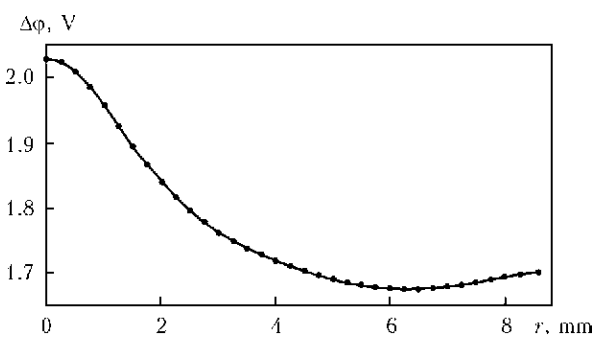

Figure 5. Radial distribution of potential drop in the anode region for free-burning arc in argon with tungsten cathode and copper water-cooled anode (I = 200 A, L = 6.3 mm, T_s = 720 K)

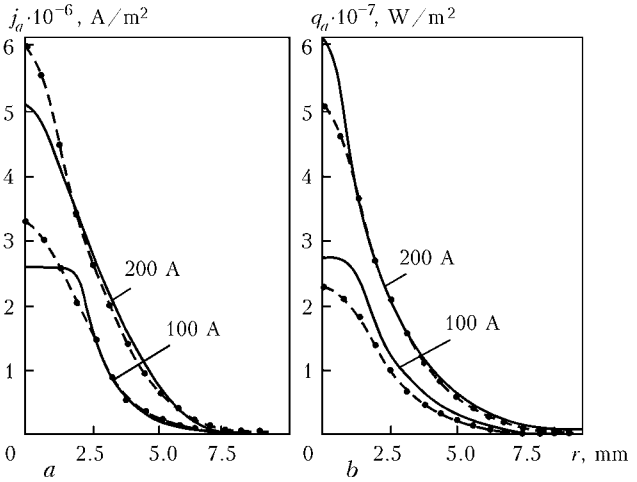

Figure 6. Radial distributions of current density on the anode (*a*) and heat flow in the anode (*b*) for free-burning arc in argon with tungsten cathode and copper water-cooled anode (L = 6.3 mm) [14]: dashed curves — calculation; solid — experimental data

anode and comparison of obtained results with available experimental data performed in this study on the whole are an evidence of adequacy of the self-consistent model proposed in study [13] for processes of heat-, mass- and electric transfer in the anode region and column of welding arc in nonconsumable electrode welding and plasma welding in inert gas.

1. Hsu, K.C., Etemadi, K., Pfender, E. (1983) Study of the free-burning high-intensity argon arc. *J. Appl. Phys.*, 54(**3**), 1293–1301.
2. Hsu, K.C., Pfender, E. (1983) Two-temperature modeling of the free-burning high-intensity arc. *Ibid.*, 54(**8**), 4359–4366.
3. Zhu, P., Lowke, J.J., Morrow, R. et al. (1995) Prediction of anode temperatures of free burning arcs. *J. Phys. D: Appl. Phys.*, **28**, 1369–1376.
4. Lowke, J.J., Morrow, R., Haidar, J. (1997) A simplified unified theory of arcs and their electrodes. *Ibid.*, **30**, 2033–2042.
5. Haidar, J. (1999) Non-equilibrium modeling of transferred arcs. *Ibid.*, **32**, 263–272.
6. Fan, H.G., Kovacevic, R. (2004) A unified model of transport phenomena in gas metal arc welding including electrode, arc plasma and molten pool. *Ibid.*, **37**, 2531–2544.
7. Hu, J., Tsai, H.L. (2007) Heat and mass transfer in gas metal arc welding. Pt 1: The arc. *Int. J. Heat and Mass Transfer*, **50**, 833–846.
8. Tanaka, M., Yamamoto, K., Tashiro, S. et al. (2008) Metal vapour behaviour in gas tungsten arc thermal plasma during welding. *Welding in the World*, 52(**11/12**), 82–88.
9. Mojzhes, B.Ya., Nemchinsky, V.A. (1972) To theory of high pressure arc on refractory cathode. *Zhurnal Tekhnich. Fiziki*, 42(**5**), 1001–1009.
10. Mojzhes, B.Ya., Nemchinsky, V.A. (1973) To theory of high pressure arc on refractory cathode. Pt 2. *Ibid.*, 43(**11**), 2309–2317.
11. Zhukov, M.F., Kozlov, N.P., Pustogarov, A.V. et al. (1982) *Near-electrode processes in arc discharges*. Novosibirsk: Nauka.
12. Wendelstorf, J., Simon, G., Decker, I. et al. (1997) Investigation of cathode spot behaviour of atmospheric argon arcs by mathematical modeling. In: *Proc. of 12th Int. Conf. on Gas Discharges and Their Applications* (Germany, Greifswald, 1997), Vol. 1, 62–65.
13. Krivtsun, I.V., Demchenko, V.F., Krikent, I.V. (2010) Model of the processes of heat, mass and charge transfer in the anode region and column of the welding arc with refractory cathode. *The Paton Welding J.*, **6**, 2–9.
14. Nestor, O.H. (1962) Heat intensity and current density distributions at the anode of high current, inert gas arcs. *J. Appl. Phys.*, 33(**5**), 1638–1648.
15. Sanders, N.A., Pfender, E. (1984) Measurement of anode falls and anode heat transfer in atmospheric pressure high intensity arcs. *Ibid.*, 55(**3**), 714–722.
16. Boulos, M.I., Fauchais, P., Pfender, E. (1997) *Thermal plasmas: Fundamentals and applications*. Vol. 1. New-York; London: Plenum Press.
17. Lyashko, I.I., Demchenko, V.F., Vakulenko, S.A. (1981) Version of dynamics equation splitting method of viscous incompressible fluid on Lagrangian-Eulerian networks. *Doklady AN UkrSSR*, Series A, 43–47.
18. Demchenko, V.F., Lesnoj, A.B. (2000) Lagrangian-Eulerian method for numerical solution of multidimensional problems of convective diffusion. *Dopovidi NAN Ukrainy*, **11**, 71–75.

EFFICIENCY OF ELECTRODYNAMIC TREATMENT OF WELDED JOINTS OF AMg6 ALLOY OF DIFFERENT THICKNESS

L.M. LOBANOV, N.A. PASHCHIN and **O.L. MIKHODUJ**
E.O. Paton Electric Welding Institute, NASU, Kiev, Ukraine

Influence of design features of fastening the samples of AMg6 alloy and its welded joints in the grips of testing machine on decrease in deformation resistance at electrodynamic treatment is shown. It is established that the effectiveness of electrodynamic effect is decreased with increase in thickness of metal being treated.

Keywords: *welded joints, aluminium alloy, electrodynamic treatment, initial stresses, current discharge, charge voltage, system of specimen fastening, efficiency of treatment, decrease of deformation resistance*

The methods of treatment of metallic materials by pulse electromagnetic fields are ever more widely used in control of stressed state of elements of welded structures [1, 2]. One of the methods of pulse effect by electric current on metals and alloys is electrodynamic treatment (EDT). The investigations of mechanisms of influence of EDT on stressed state of aluminium alloys [3], structural steels [4, 5] and also welded joints of these materials were conducted. The results presented in the works [1, 3–5] were obtained using developed experimental methods based on tension of flat specimens, their treatment by current discharges with in-process control of change in tension force which was taken as evaluation characteristics of EDT.

At the same time it is known [6] that conditions of fastening of specimens being investigated in the grips of testing machine have considerably greater influence on resistance of metallic materials to deformation at dynamic loads than at static ones. The same concerns the deformation processes initiated in the metals and alloys by passing of charges of electric current [7].

Thus, it is obvious that during evaluation of EDT process efficiency it is necessary to consider the design system of fastening the specimens being treated. Moreover, basing on the analysis of fractograms of fractures of AMg6 alloy it is assumed that the efficiency of electrodynamic effect is deceased with increase in thickness of metal being treated [8]. The quantitative evaluation of EDT efficiency depending on thickness of treated material allows distinguishing the range of values of power parameters of electrodynamic effect defining the applicability of this method of treatment in the engineering practice.

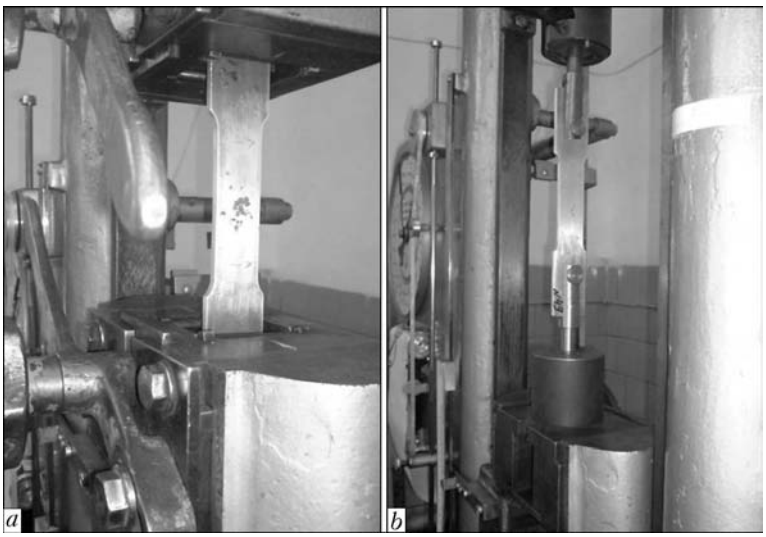

Figure 1. Appearance of assemblies of fastening of specimens in TsDM-10 machine using wedge-type grips (*a*) and pins connected with П-shaped cramps (*b*)

The aim of this work was the investigation of influence of thickness of specimens of welded joints of aluminium AMg6 alloy and also design features of their fastening in testing machine on the efficiency of electrodynamic effects.

To evaluate the EDT effect on decrease of level of initial stresses in the material, the tests were carried out after preliminary tension of flat specimens of AMg6 alloy of rectangular section with sizes of a test part and head of, respectively, 150 × 30 and 120 × × 40 mm and thickness from 2.5 to 10 mm. To generate the pulse current the installation was used described in the work [5], and EDT was performed by the contact of a copper electrode with the surface of metal on the test part of the specimen, as is shown in the work [3].

The tension of specimens was performed in the rupture machine TsDM-10 of class 2 with a maximal load at tension of 98,000 N, speed of deformation was 0.1 mm/s and temperature 293 K. The machine was completed with a mechanical drive of tension, a manual system of precise adjustment of load, a pendulum force meter and relates to the devices with a closed loading system. The choice of given type of machine excludes possibility of uncontrolled deformation and fracture of specimen at dynamic loading which in number of cases occurs while using loading devices with an automatic maintaining of deformation speed [7].

The EDT was conducted by series in 5–6 pulses at charge voltage U = 500 V and capacity of capacitor battery C = 6600 μF which corresponded to the energy of accumulated charge of 800 J. The treatment of specimens of base metal and butt welded joints of AMg6 alloy, preliminary loaded up to the values of initial stresses σ_0 from 50 to 140 MPa, was performed.

The investigations of influence of design peculiarities of fastening of specimens in the grips of machine for decrease of σ_0 values in EDT were carried out on the basis of comparison of two variants of design of assembly for fastening the heads of specimens (Figure 1). In the first variant the fastening was performed by wedge-type grips, the jaws of which were matched with the area of contact surface of heads of specimen (Figure 1, *a*). In the second variant the specimen was fastened by cylindrical pins joined by П-shape cramps of the machine traverse (Figure 1, *b*). The cross sections of working platform and heads of test specimens were in compliance with the requirements of GOST 1497–84.

The comparative evaluation was carried out in EDT of specimens of 5 mm thickness after tension to

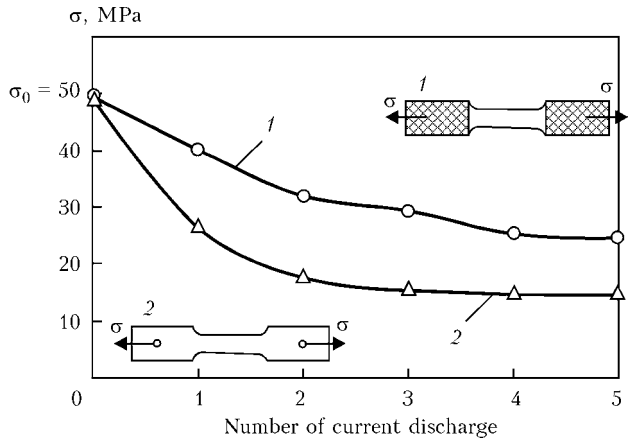

Figure 2. Influence of design features of fastening of specimens of AMg6 alloy on decrease of stresses σ in EDT: *1* — fastening using wedge-type grips; *2* — the same, but with П-shaped cramps

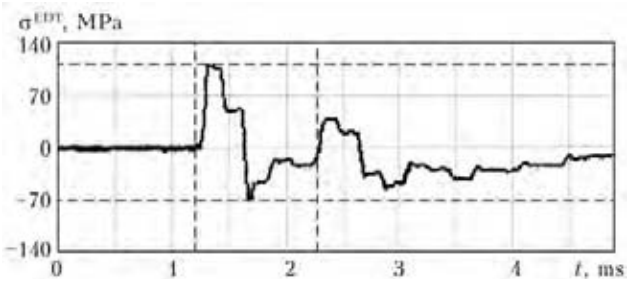

Figure 3. Wave of dynamic stresses σ^{EDT} in the specimen of AMg6 alloy at single electrodynamic effect with charge energy of 800 J

the values of σ_0 = 50 MPa. The treatment of specimens was performed by the series of five current pulses. The changes in values of stresses in EDT for both variants of fastening of specimens are presented in Figure 2, where it is seen that fixation of specimen using pin (curve *2*) is characterized by more intensive decrease of values of stresses as compared to the fastening using the wedge-type grips (curve *1*). Here, the difference of values of stresses in curves *1* and *2* after five current pulses amounted to 40–50 % , which is connected with difference in design features of specimen fastening. In case of the specimen fastening using pin, at the moment of electrodynamic effect the conditions of interaction occur, defined as a contact of pin–hole pair [9] on the surface of their matching. The area of the contact corresponded to the print of a pin on the surface of a head hole, matched with it after single electrodynamic effect, and was equal to 5 mm^2. In case of fastening using wedge-type grips the interaction of specimen head with two jaws of a traverse grip occurs along the lines of matching of total length of 80 mm (width of specimen head is 40 mm), that determines the area of contact interaction of 200 mm^2.

To evaluate the dynamic load influencing the specimen in the fastening zone, the distribution of longitudinal waves of stresses initiated by electrodynamic effect caused by treatment was investigated. The flat specimen of rectangular section of AMg6 alloy was used after tension to the values of initial stresses corresponding to 50 MPa. On the front and reverse surface of test part of the specimen along the central longitudinal axis two tensors (r = 200 Ohm) with 10 mm base were positioned. The sensors were positioned at the distance of 70 mm from the centre of specimen, the surface of which was treated by a single current discharge under the conditions corresponding to the charge voltage of 500 V. The record of values of sensors was carried out by two-channel digital oscillograph PCS Welleman at the scanning of 0.5 ms.

During calculation of dynamic stresses the dynamic modulus of elasticity E_d for aluminium alloys was taken equal to static one of E = 70,000 MPa [10]. The amplitude values of stress wave, averaged across the thickness of metal, are presented in Figure 3. It is seen from the Figure that the range of amplitude is 178 MPa, from which 108 MPa are valid for tensile stresses. Moreover, the residual plastic deformation in the zone of measuring by tensors was not recorded. This fact is proved by the works [3, 11] where it is pointed out that area of plastic deformation in EDT is localized in the area of energy release of electrodynamic effect.

Coming from the experimentally obtained maximal values of stress of load wave, presented in Figure 3, the approximate evaluation of stressed state of metal of specimens in the places of their fastening on traverses of testing machine was carried out. In accordance with the work [6] it is necessary to account for the correlation of conditional yield strength at dynamic loads $\sigma^d_{0.2}$, the value of which is determined by the relation [10]

$$\sigma^d_{0.2} = \chi\sigma^{st}_{0.2},$$

where $\sigma^{st}_{0.2}$ is the conditional yield strength in static tension, MPa; χ is the coefficient of dynamics.

According to the work [10] the χ value for aluminium alloys was taken equal to 2, and $\sigma^{st}_{0.2}$ of AMg6 alloy, obtained from the results of tests of metal in initial state, was 140 MPa. Considering χ, the value of dynamic yield strength $\sigma^d_{0.2}$ was 280 MPa.

In case of fastening using wedge-type grips the values of dynamic tensile stresses are 81 MPa. In addition of dynamic stresses with initial stresses of specimen σ_0 = 50 MPa, their summed value does not exceed 131 MPa, which is considerably lower than $\sigma^d_{0.2}$.

In pin-type fastening the values of dynamic stresses are 324 MPa, that during addition with initial stresses is 374 MPa, which exceeds $\sigma^d_{0.2}$. According to the carried out evaluation using the pin-type system of fastening, in the area of a hole the local yielding is developing, leading to its deformation. It imposes certain restrictions to applicability of pin fastenings during development of experimental methods of investigation of influence of dynamic and pulse loads on stressed state of structural materials.

The investigations of influence of thickness of metal on efficiency of EDT during treatment of specimens of AMg6 alloy and its welded joints with thickness of test part of 30 mm were carried out. Here, the thickness of specimens of base metal was preset 2.5 and 10 mm and welded joints — 2.5, 4, 5 and 10 mm. The latter were produced by cutting from plates of 400 × 400 mm sizes TIG-welded with a filler in the installation ASTV-2M. The welding conditions of specimens of AMg6 alloy are given in the Table.

It should be noted that section area in the region of weld reinforcement during increase of thickness of metal being welded can change, that is due to the technology of welding. This can have a negative influence on validity of results in comparison of values of efficiency of EDT of specimens of different thickness treated at equal power parameters of electrodynamic effects. To increase the accuracy of measuring

Conditions of automatic welding of plates of AMg6 alloy of different thickness used for EDT (U_a = 18 V)

Plate number	δ, mm	I, A	v_w, mm/s
1	2.5	170	5.55
2	4	200	3.33
3	5	250	3.33
4	10	480	2.50

results the reinforcement on the specimens was removed by machining to the value of thickness of base metal.

Before the treatment the specimens were subjected to static tension up to the value of initial stress σ_0 = = 140 MPa which corresponds to maximal value of a longitudinal component of residual welding stresses in AMg6 alloy.

The treatment of surface of central part of specimens was performed by a series of six pulses (n = 6) at the parameters of electrodynamic effect corresponding to energy of accumulated charge of 800 J. After each pulse the decrease of level of initial stresses $\Delta\sigma$ was recorded. The evaluation characteristic of influence of thickness of treated metal on EDT efficiency was relative efficiency $\frac{\Delta\sigma}{\sigma_0}\cdot 100$ %.

Dependence of influence of thickness of metal being treated on EDT efficiency is presented in Figure 4, *a*, from which it is seen that maximal values of $\frac{\Delta\sigma}{\sigma_0}\cdot 100$ % are achieved after the first pulse current in the whole range of thicknesses being examined (n = = 1). During comparison of values of efficiency of EDT of base metal and welded joints for minimal thicknesses of 2.5 mm (Figure 4, *a*, curves *1′* and *1*) and maximal 10 mm (Figure 4, *a*, curves *4′* and *4*) it can be seen that $\frac{\Delta\sigma}{\sigma_0}\cdot 100$ % values for base metal are 10–12 % lower than those for the welded joints. It is connected with the presence of residual stresses in the specimens of welded joints. In a number of works, for example [3, 7], it is shown that direct dependence of efficiency of electrodynamic effects on the values of elastic tensile stresses applied to the specimen in the process of EDT is observed.

During comparison of parameters of efficiency of electrodynamic effect in EDT of welded joints of 2.5 and 4 mm thickness (Figure 4, *a*, curves *1* and *2*) the values of $\frac{\Delta\sigma}{\sigma_0}\cdot 100$ % are differed by 2–5 % during the whole cycle of treatment. The maximal values of EDT efficiency during increase in thickness of specimens from 4 to 10 mm (curves *2–4*) are decreased, respectively, from 25 to 15 %, i.e. the $\frac{\Delta\sigma}{\sigma_0}\cdot 100$ % values are decreased as a whole with increase in thickness of metal. As is seen from Figure 4, *a*, the values of EDT efficiency with charge energy of 800 J are close to maximal ones in the range of thicknesses of 2.5–4 mm.

The evaluation of decrease of resistance of metal to deformation in EDT of specimens of welded joints of AMg6 alloy of thickness from 2.5 to 10 mm after the first (n = 1) and finishing (n = 6) pulse currents (Figure 4, *b*, curves *5* and *6*) was made. If maximal value $\frac{\Delta\sigma}{\sigma_0}\cdot 100$ % at n = 6 to take for each of sections

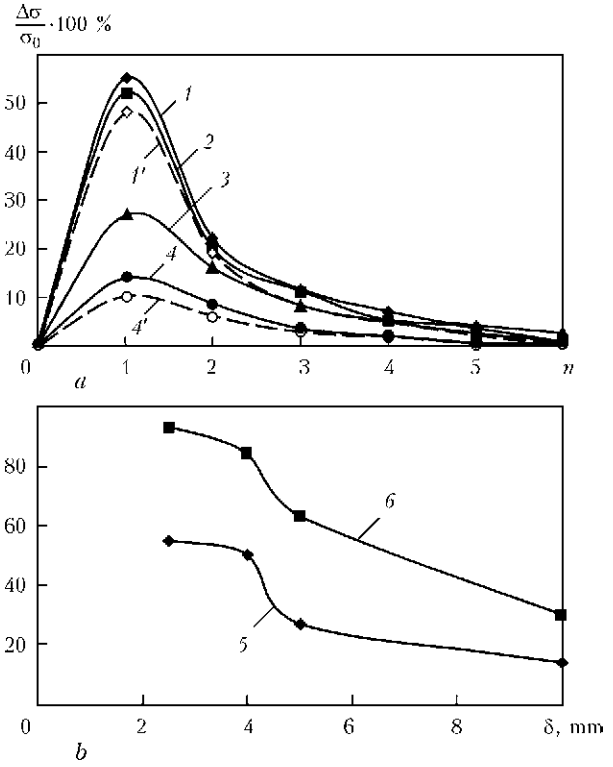

Figure 4. Dependence of EDT efficiency on number of current discharges n for specimens of base metal (BM) and welded joints (WJ) of AMg6 alloy (*a*) and on the thickness of specimens (*b*): *1*, *1′* — δ = 2.5 mm for BM and WJ; *2* — 4 mm for WJ and BM; *3* — 5 mm for WJ; *4*, *4′* — 10 mm for WJ and BM; *5* — n = 1; *6* — 6

being investigated as 100 %, then it is seen during comparison of curves *5* and *6* at the regions corresponding to the thicknesses 2.5 and 4 mm that influence of the first current pulse (curve *5*) on EDT efficiency is 60 %.

The similar values of influence of the first current pulse for the thicknesses of 5 and 10 mm were, respectively, 0.50 and 0.35. Having analyzed the data of Figure 4, it can be concluded that in the range of thicknesses of 2.5–4 mm the increase in values of EDT efficiency during comparison with specimens 5–10 mm thick takes place. The values of efficiency for the thicknesses of 2.5 and 4 mm are very close. It evidences that processes of deformation of metal as a result of electrodynamic effect for the thicknesses of 2.5–4 mm and 5–10 mm are different. It can be assumed that linear character of decrease in values of $\frac{\Delta\sigma}{\sigma_0}\cdot 100$ % with increase in thickness from 5 to 10 mm is connected with elastic-plastic deformation of metal during treatment. With increase of thickness of specimens the fraction of plastic component of deformation is decreased with accompanied growth of elastic one. Deformation of specimens of 2.5–4 mm thickness takes place under the conditions when metal has almost exhausted the elastic properties and close to plastic yielding, that is proved by steep areas of curves *5* and *6*.

To confirm the abovementioned assumption about difference of processes of deformation of welded joints

of AMg6 alloy in the ranges of thicknesses of 2.5–4 and 5–10 mm, the approximate evaluation of specific dynamic load, corresponding to stored charge energy of 800 J, was performed. According to the results of tests on longitudinal tension, it was established that value of static yield strength $\sigma^{st}_{0.2}$ for welded joints of AMg6 alloy of 2.5–10 mm thickness in initial state is 130 MPa. Considering the accepted dynamics coefficient value $\chi = 2$ based on the work [10], the value of dynamic yield strength $\sigma^{d}_{0.2}$ was 260 MPa. In the work [12] the experimental evaluation of dynamic load was carried out, corresponding to the accumulated energy of 800 J, the value of which was 20,461 N, and the period of increment up to maximal value was 0.0013 s. The value of dynamic stresses σ^{EDT} at the thickness of specimens of 2.5 mm is equal to 273 MPa which exceeds $\sigma^{d}_{0.2}$. At the thickness of 4 mm the relation $\sigma^{EDT} = 0.75\sigma^{d}_{0.2}$ is valid which proves that maximal values of dynamic stresses are close to dynamic yield strength. The obtained relations σ^{EDT} and $\sigma^{d}_{0.2}$ determine the steep nature of curves *5* and *6* in Figure 4, *b* within the range of thicknesses 2.5–4 mm. During treatment of specimens of 5 and 10 mm thickness the electrodynamic effect is in the area of elastic dynamic loads which correspond to monotonous area of curves *5* and *6* in Figure 4, *b*, and efficiency of EDT is determined by the area of plastic deformation in the area of current pulse energy release [3, 11].

CONCLUSIONS

1. It was established that in case of pin-type fastening of heads of specimens of AMg6 alloy in testing machine the values of tensile stresses, decreased by 50 % during electrodynamic effects, were recorded as compared with those obtained in fastening by wedge-type grips.

2. It is shown that values of EDT efficiency of welded joints of AMg6 alloy are decreased with increase in thickness of metal being treated.

1. Lobanov, L.M., Pashchin, N.A., Loginov, V.P. et al. (2005) Application of electric pulse treatment of structural elements to extend their service life (Review). *The Paton Welding J.*, **11**, 19–23.
2. Stepanov, G.V., Babutsky, A.I., Mameev, I.A. et al. (2011) Redistribution of residual welding stresses after treatment by pulse electromagnetic field. *Problemy Prochnosti*, **3**, 123–131.
3. Lobanov, L.M., Pashchin, N.A., Loginov, V.P. (2007) Change of the stress-strain state of welded joints of aluminium alloy AMg6 after electrodynamic treatment. *The Paton Welding J.*, **6**, 7–14.
4. Lobanov, L.M., Pashchin, N.A., Loginov, V.P. et al. (2007) Effect of electrodynamic treatment on stressed state of welded joints on steel St3. *Ibid.*, **7**, 6–8.
5. Lobanov, L.M., Pashchin, N.A., Skulsky, V.Yu. et al. (2006) Influence of electrodynamic treatment on the stress-strain state of heat-resistant steels. *Ibid.*, **5**, 8–11.
6. Bell, J.F. (1984) *Experimental principles of mechanics of deformed solids*. Pt 2: Finite deformations. Moscow: Nauka.
7. Strizhalo, V.A., Novogrudsky, L.S., Vorobiov, E.V. (2008) *Strength of materials at cryogenic temperatures taking into account the effect of electromagnetic fields*. Kiev: G.S. Pisarenko IPP.
8. Lobanov, L.M., Pashchin, N.A., Loginov, V.P. (2010) Specifics of structure formation of aluminium alloys AMg5, AMg6 under action of electric current pulses. *Visnyk Ukr. Materialozn. Tov.*, **3**, 33–42.
9. Gudchenko, V.M., Lyutsau, V.G. (1971) Structural changes of surface layers of ShKh-15 steel in conditions of pulsed contact loading. In: *High-speed deformation*. Moscow: Nauka.
10. Ionov, V.N., Ogibalov, P.M. (1975) *Stresses in bodies under pulse loading*. Moscow: Vysshaya Shkola.
11. Lobanov, L.M., Makhnenko, V.I., Pashchin, N.A. et al. (2007) Features of formation of plastic deformations at electrodynamic treatment of welded joints of St3 steel. *The Paton Welding J.*, **10**, 7–11.
12. Lobanov, L.M., Pashchin, N.A., Cherkashin, A.V. et al. (2012) Efficiency of electrodynamic treatment of aluminium alloy AMg6 and its welded joints. *Ibid.*, **1**, 2–6.

INFLUENCE OF AUSTENITIZING MODE ON LOCAL FRACTURE SUSCEPTIBILITY OF WELDED JOINTS OF 03Kh16N9M2 STEEL

Yu.V. POLETAEV
Volgodonsk Affiliate of South-Russian State Technical University, Volgodonsk, RF

Influence of parameters of thermal cycle of austenitizing on formation of structural and chemical homogeneity and local fracture resistance of HAZ metal in production welded joints of austenitic steel 03Kh16N9M2 was investigated. It is established that development of processes of formation and growth of carbides and carbonitrides, stimulating welded joint susceptibility to local fracture, is difficult in low-carbon HAZ metal. Inexpediency of conducting high-temperature heat treatment, i.e. austenitizing of welded joints of 03Kh16N9M2 steel, is proved experimentally, as repeated heating up to T = 1323–1373 K for 1–4 h did not promote an improvement of HAZ metal resistance to local fracture.

Keywords: *arc welding, welded joints, low-carbon austenitic steel, heat-affected zone, structural and chemical microinhomogeneity, austenitizing, high-temperature low-frequency loading, local fracture*

With increase of unit power and working parameters of nuclear power plants with liquid-metal coolant the total extent of welded joints of austenitic steel increases markedly and is equal to tens of kilometers, while site welded joints are not subjected to austenitizing. Under these conditions the problem of ensuring the quality, strength and brittle fracture resistance of welded joints, including local fracture of HAZ metal at working temperature above 773 K, becomes particularly urgent.

At present there is no common opinion on effectiveness of austenitizing as a reliable technological method of prevention of local fracture of welded joints in high-temperature service [1–4]. It is established that austenitizing promotes lowering of long-term strength of welded joints [2, 5, 6] and increases the probability of appearance of intercrystalline fracture in the fusion zone [7–9], which is an even more embrittled zone of welded joint HAZ.

Thus, apriori application of autenitizing without an appropriate assessment of its influence on the structure and service properties of HAZ metal of specific welded joints of each studied steel grade can promote lowering of operational reliability.

The objective of this work is experimental substantiation of the possibility of eliminating austenitizing of welded joints on low-carbon austenitic steel 03Kh16N9M2 without the hazard of lowering of the resistance to local fracture of HAZ metal under the conditions of high-temperature (823 K) low-frequency low-cycle loading.

03Kh16N9M2 steel was studied using production melts of 6.5 and 40 t weight, melted from pure charge in the main electric arc furnace of the A.A. Zhdanov Izhora Plant. Chemical composition of this steel was, wt.%: 0.03 C; 1.22 Mn; 0.21 Si; 16.07 Cr; 10.37 Ni; 2.05 Mo; 0.20 Cu; 0.01 S and 0.007 P, and its mechanical properties corresponded to the requirements of normative documents.

Welded joints of 03Kh16N9M2 steel were made by standard technology of manufacturing welded assemblies of BN-800 reactor plant under the conditions of OJSC EMK-ATOMMASH. Manual arc welding was conducted with specially developed electrodes of TsT-46 grade. Welded joints were tested in as-welded condition and after austenitizing at T = 1323 K (soaking duration is 1–4 h) in keeping with the recommendations on heat treatment of welded structures of nuclear power plants with fast-breeder reactors from steel of Kh18N9 type. Heat treatment mode simulated the conditions of heating and cooling of large-sized welded structures. Also tested were welded samples subjected to austenitizing at T = 1373 K with 1 h soaking that corresponded to possible deviation from maximum temperature at furnace heating. Heterogeneity of mechanical properties between the weld metal and metal of HAZ is as-welded condition is quite high. The highest hardness of welded joints is observed in weld metal, and the lowest — in the base metal. Increased strength and hardness of weld metal is explained by its developed substructure and work hardening in welding. Microhardness measurement in PMT-3 instrument (100 g load) also revealed a section of «work-hardened» base metal, adjacent to the fusion line of about 0.1–0.3 mm length that is commensurate with the dimensions of overheated zone. Microhardness of this section is on the level of microhardness values of weld metal. Austenitizing eliminates the work hardening and leads to smoothing of mechanical heterogeneity, without, however, eliminating it completely.

Unlike steel stabilized by titanium [10], in the HAZ metal of non-stabilized 03Kh16N9M2 steel a considerable dissolution of carbides occurs after welding. This is attributable to the fact that chromium carbides are less stable than titanium carbides, and dissolve in

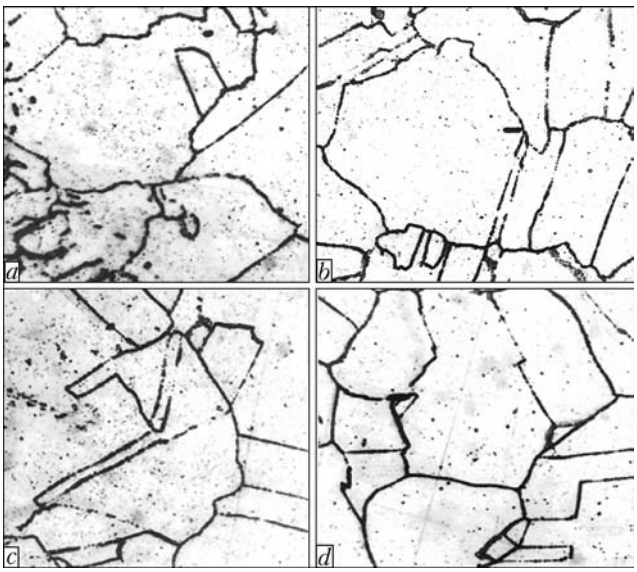

Figure 1. Microstructures (×700) of HAZ metal of 03Kh16N9M2 steel at different distance from the weld: *a* — fusion line; *b* — 0.1 mm; *c* — 0.5 mm; *d* — base metal

the HAZ metal during welding. Base metal of 03Kh16N9M2 steel has an equilibrium structure with a large number of twins, while finely dispersed carbides are absent in the grain body. Second phase precipitates are found on some part of grain boundaries. Electron microscopy studies and electron diffraction are indicative of the fact that these are plate-like carbides of $Me_{23}C_6$ type [10]. Now a large part of intergranular boundaries is free from precipitates. In HAZ metal sections directly adjacent to the fusion line (Figure 1), grain size became larger as a result of welding heat impact. Second phase precipitates are noticeable on some part of new boundaries. As shown by electron diffraction, these are also carbides of $Me_{23}C_6$ type. It is obvious that this section was heated above 1373–1473 K during welding that resulted in grain growth

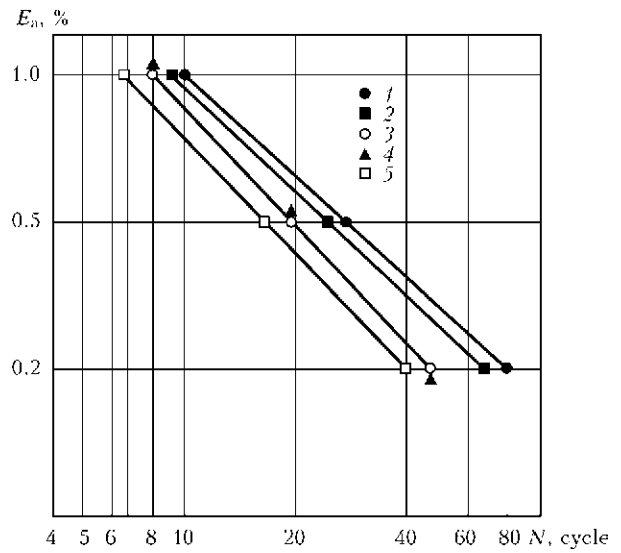

Figure 2. Influence of austenitizing on fatigue life of welded joints of 03Kh16N9M2 steel with Mesnager notch at T = 823 K: *1* — base metal; *2* — welded joint in as-welded condition; *3* — same at T = 1323 K, τ = 1 h; *4* — same at T = 1323 K, τ = 4 h; *5* — same at T = 1373 K, τ = 1 h

in it. During cooling in the temperature range of carbide initiation (723–1123 K), precipitation of fine dendritic carbides took place on some part of the boundaries with maximum free energy and largest segregations of carbon atoms. The farther from the fusion line, the smaller is the quantity and dimensions of precipitates along the grain boundaries.

After heat treatment HAZ metal microstructure practically did not change and consisted of austenite holyhedrons with individual inclusions of large chromium carbides. Weld metal structure, which had a dendritic structure in as-welded condition, changed to the greatest degree. After austenitizing weld metal acquired the structure of polyhedral austenite with a large amount of uniformly distributed globular ferritic phase.

Thus, while changing the metal structure, heat treatment leads to reduction of structural and mechanical heterogeneity of the welded joint, without, however, eliminating it completely. It is believed that austenitizing leads to increase of welded joint resistance to local fracture, which was not, however, confirmed by test results.

Assessment of welded joint susceptibility to formation and development of local fractures at high-temperature low-cycle loading was performed in keeping with the operational procedure of work [11]. Tested were prismatic samples with a transverse weld with one edge notch made along the fusion line. Samples were deformed by the schematic of alternating cyclic bending with soaking duration of 24 h in the tension half-cycle at T = 823 K.

As is seen from Figure 2, none of the heat treatment modes restores welded joint properties to base metal level. This is indicative of incomplete healing of microdamage on grain boundaries, arising during welding [5]. Welded samples in as-welded condition and after austenitizing at T = 1323 K with soaking for 1 h have practically the same fatigue life. Increase of soaking up to 4 h led to extension of fatigue life by only 1.2 times. At the same time, heating up to T = 1373 K increases brittle fracture susceptibility of welded joints.

Fracture diagrams and curves of fatigue crack growth rate are shown in Figures 3 and 4, respectively. In as-welded condition during the first four loading cycles welded joint strengthening is observed, namely increase of σ_{ef} in the cycles. Then the deformation process is stabilized and a crack forms at N_{fr} = 18 cycles. After austenitizing, the duration of the process of welded joint strengthening rises noticeably. After heating at T = 1323 K with 4 h soaking strengthening goes on for eight cycles. Then the deformation process is stabilized and a crack forms at N_{fr} = 21 cycles. After heat treatment at the temperature of 1323 and 1373 K with 1 h soaking the shape of $\sigma_{ef} = f(N)$ curve is unstable. After four cycles strengthening is over, and the deformation process is stabilized. Then strengthening is observed again, which goes on right up to crack formation (at N_{fr} = 17 and 14 cycles, respectively).

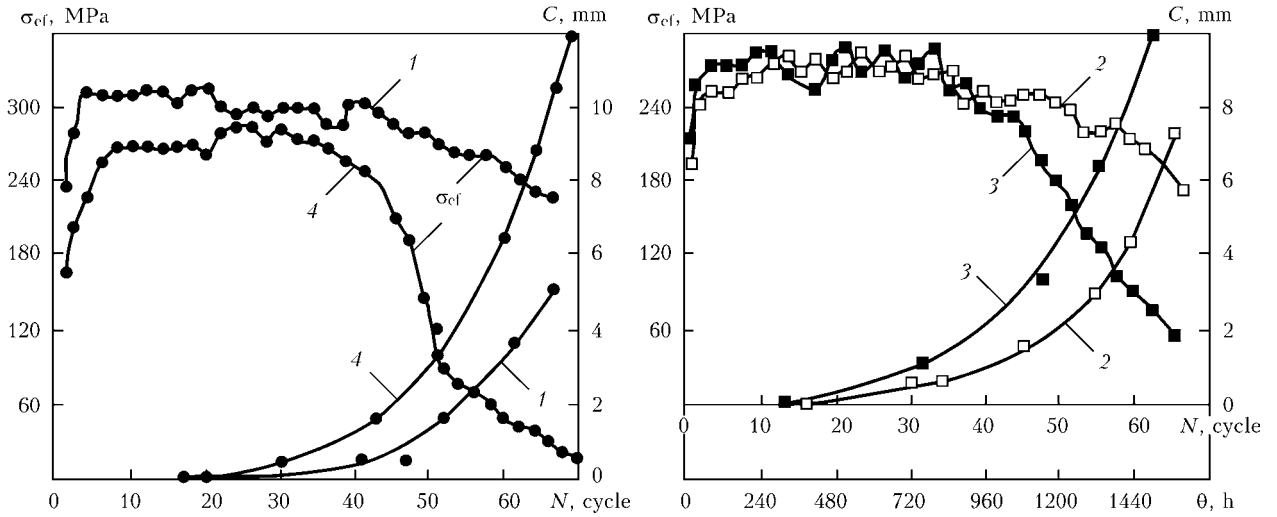

Figure 3. Fracture diagrams of welded joints of 03Kh16N9M2 steel at E_a = 0.5 %, τ = 24 h, T = 823 K: *1* — as-welded condition; *2* — austenitizing at T = 1323 K, τ = 1 h; *3* — same at 1373 K, τ = 1 h; *4* — same at 1323 K, τ = 4 h

Kinetics of fracture development was studied on the base of 50 cycles from the moment of crack formation. At testing in as-welded condition in the range of the first 14 loading cycles stable crack development with a constant rate equal to $7 \cdot 10^{-3}$ mm/cycle (see Figure 4) is observed, while strengthening and softening sections can be seen on $\sigma_{ef} = f(N)$ curve (see Figure 3). At N = 14 cycles the first salient point forms on $V = f(N)$ curve. In the range of 14–26 cycles accelerated crack propagation occurs. After 26 cycles the sample looses its load-carrying capacity that points to a constant relatively small lowering of σ_{ef} in each cycle and second salient point on $V = f(N)$ curve. At further deformation crack propagation process is characterized by a practically constant acceleration. After 50 loading cycles crack depth was about 5 mm, and its growth rate was about $100 \cdot 10^{-3}$ mm/cycle.

Shape of $\sigma_{ef} = f(N)$ curves in welded joints after heat treatment at T = 1323 and 1373 K with soaking for 4 h, during the first four cycles is characterized by stable development of the crack at a constant rate of $38 \cdot 10^{-3}$ mm/cycle. At subsequent loading σ_{ef} rises as a result of considerable resistance to crack propagation. After N = 14 cycles loss of sample load-carrying capacity takes place that is particularly noticeable after the 22nd cycle. Intensity of fracture propagation rises. After 50 loading cycles the crack has reached the depth of 11.8 mm and growth rate of $236 \cdot 10^{-3}$ mm/cycle.

Shape of $\sigma_{ef} = f(N)$ curves for welded joints after autenitizing at T = 1323 and 1373 K with 1 h soaking is the same. The fracture process, however, is characterized by different intensity. In a sample treated at T = 1323 K loss of load-carrying capacity occurs after 24 cycles. In the range of 24–50 cycles periodically recurring sections of softening and stabilization can be singled out on $\sigma_{ef} = f(N)$ curve, that is indicative of a jump-like nature of crack growth and its subsequent deceleration, so that several salient points and sections with different acceleration of crack propagation are observed on $V = f(N)$ curve. In a sample treated at T = 1373 K loss of load-carrying capacity occurs after 14 loading cycles. At subsequent cycles an abrupt lowering of σ_{ef} value is observed, which is due to intensive crack propagation. In the range of 14–50 cycles two sections with different inclination to abscissa axis can be singled out on $V = f(N)$ curve. After 50 loading cycles, in welded joints, treated at T = 1323 and 1373 K, crack depth was equal to 6.9 and 9.9 mm, respectively, and crack growth was $138 \cdot 10^{-3}$ and $198 \cdot 10^{-3}$ mm/cycle.

Lowering of welded joint crack resistance after austenitizing is related to a change of fracture location. Welded joints in as-welded condition are characterized by formation and development of local fracture in the HAZ metal at the distance of 1–3 grains from the fusion line (Figure 5, *a*). Here, development of several cracks occurs with approximately the same intensity. After austenitizing local fracture develops predominantly along the fusion line (Figure 5, *b*). Even at formation of several cracks the crack along

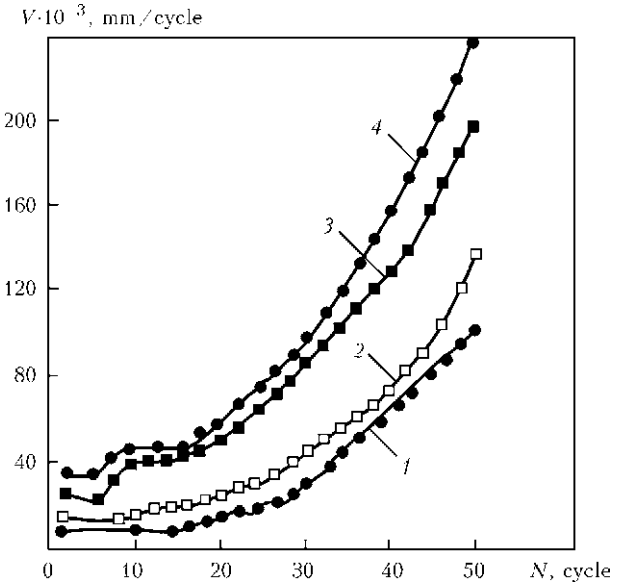

Figure 4. Dependence of intensity of local fracture of 03Kh16N9M2 welded joints on autenitizing mode: *1–4* — same as in Figure 3

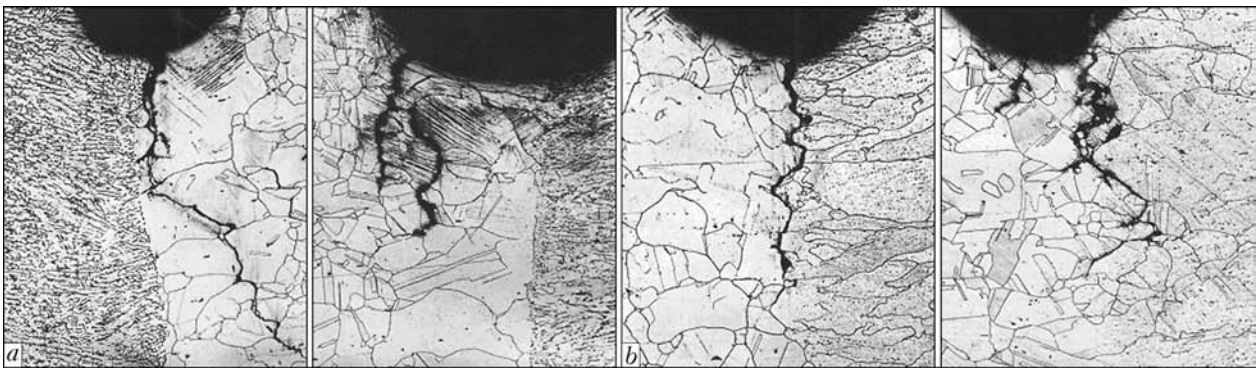

Figure 5. Nature of fracture of 03Kh16N9M2 welded joints with Mesnager notch in as-welded condition (*a*) and after austenitizing (*b*) (×100)

the fusion line develops more intensively. In both the cases brittle (tear) intergranular fracture is observed.

Change of fracture site can be explained as follows. In as-welded condition the HAZ metal forms a work-hardened zone of 0.1–0.3 mm length adjacent to the weld and having a higher hardness on the level of that of weld metal. At deformation of such a heterogeneous joint, strain localizing, damage accumulation and intergranular fracture at low-frequency low-cycle loading will occur on the boundary of the hard (strengthened) and soft regions. Austenitizing eliminates post-weld work-hardening of the metal of HAZ and weld and facilitates producing a more homogeneous joint. In this case, however, weld metal also has higher strength than the base metal, thus leading to strain localizing already on the fusion line. High chemical and structural heterogeneity of this HAZ region promotes a more intensive development of intergranular fracture.

Thus, it is experimentally proved that austenitizing in the temperature range of 1323–1373 K of 1–4 h duration does not promote any increase of local fracture resistance of 03Kh16N9M2 steel welded joints under the conditions of low-frequency low-cycle loading. More over, at deviation from the recommended heat treatment mode, lowering of crack resistance is observed, which is related to localizing of intergranualr fracture on the fusion line. Obtained results allowed substantiating elimination of performance of high-temperature heat treatment, i.e. austenitizing of 03Kh16N9M2 welded joints.

Based on the results of evaluation testing of production welded joints, a permission of RF GOSTEKhNADZOR was obtained, and certified procedures and recommended parameters of welding mode, and welding consumables for welded structure fabrication from 03Kh16N9M2 steel were incorporated into PN AEG-7-008–89, PN-AEG-7-009–89 and PN AEG-7-010–89 normative-technical documents that will allow a long-term and reliable operation of welded joints in as-welded condition at up to 923 K temperature.

CONCLUSIONS

1. Integrated study of the influence of austenitizing mode parameters on formation of a stable and local fracture resistant structure of HAZ metal in production welded joints of 03Kh16N9M2 austenitic steel was performed.

2. It is established that low content of carbon in 03Kh16N9M2 steel makes it difficult for the process of formation and growth of the most probable $Me_{23}C_6$ carbide to run, that ensures a low sensitivity to welding heating and preservation of the structurally stable condition of HAZ metal at subsequent high-temperature low-frequency low-cycle loading.

3. It is proved experimentally that performance of high-temperature heat treatment, i.e. austenitizing at T = 1323 K of 1–4 h duration, does not promote an increase of local fracture resistance of 03Kh16N9M2 steel welded joints. Deviation (heating up to T = 1373 K) from the recommended austenitizing mode promotes the manifestation of local fracture susceptibility of HAZ metal under the conditions of low-frequency low-cycle loading, simulating the non-stationary mode of high-temperature operation of welded structures of nuclear power plants with liquid metal coolant.

1. Zemzin, V.N., Shron, R.Z. (1978) *Heat treatment and properties of welded joints*. Leningrad: Mashinostroenie.
2. Nikitin, V.M. (1974) About mechanism of formation of chemical heterogeneity in near-weld zone. *Svarochn. Proizvodstvo*, **9**, 55–57.
3. Zemzin, V.N., Zhitnikov, N.P. (1972) Conditions of crack formation in near-weld zone in welded joints during heat treatment. *Avtomatich. Svarka*, **2**, 1–5.
4. Krutasova, E.I. (1981) *Reliability of power equipment metal*. Moscow: Energoizdat.
5. Zemzin, V.N. (1972) *Heat resistance of welded joints*. Leningrad: Mashinostroenie.
6. Yarkovoj, V.S., Muromtsev, B.I., Komissarov, V.G. (1969) Long-term strength of base metal and welded joints of steels 08Kh18N9 and 07Kh16N9M2. *Avtomatich. Svarka*, **6**, 38–40.
7. Rajkhman, A.Z., Svyatsky, B.S., Bely, V.E. (1968) About service reliability of welded joints of high pressure steam pipelines. *Teploenergetika*, **7**, 17–21.
8. Ratner, A.V. (1962) On causes of deformation-free fracture of steam pipeline joints of austenitic steels. *Ibid*., **8**, 12–18.
9. Fedosov, A.I., Gorelkin, B.G. (1965) Tests of full-scale welded joints of steam pipelines from austenitic steel 12Kh18N12T. In: *Experimental tests of strength of turbine discs, blades and steam pipelines*: TsNIITMash Sci. and Techn. Information, Issue 56. Moscow: ONTI TsNIITMash, 100–106.
10. Poletaev, Yu.V., Malinovsky, V.K., Batieva, N.M. (1986) Change of austenitic steel structure in welding and thermal ageing. In: *Properties and technology of welding of high-alloy steels and alloys*: Transact. of TsNIITMash, No. 197. Moscow: ONTI TsNIITMash, 5–11.
11. Tarnovsky, A.I., Poletaev, Yu.V., Zubchenko, A.S. (1982) Procedure for examination of welded joint damage accumulation at low-cycle creep. *Avtomatich. Svarka*, **11**, 15–17.

DISLOCATION MODEL OF HYDROGEN-ENHANCED LOCALIZING OF PLASTICITY IN METALS WITH BCC LATTICE*

A.V. IGNATENKO, I.K. POKHODNYA, A.P. PALTSEVICH and **V.S. SINYUK**
E.O. Paton Electric Welding Institute, NASU, Kiev, Ukraine

A mechanism of the influence of hydrogen-enhanced localizing of plasticity on the stage of initiation of a submicrodefect and growth of a macrocrack in metal with bcc lattice is proposed. A mathematical model of hydrogen embrittlement in metals with bcc lattice was constructed, which allows for the effect of hydrogen-enhanced localizing of plasticity and hydrogen influence on surface energy of a submicrocrack. It is established that metal susceptibility to hydrogen embrittlement is increased with grain size refinement.

Keywords: *arc welding, welded joints, high-strength low-alloyed steels, hydrogen brittleness model, metals with bcc lattice, grain size, hydrogen-enhanced localizing of plasticity, brittle fracture*

In welding of HSLA steels there exists the probability of initiation of hydrogen-induced cold cracks in the welded joint, which are a manifestation of hydrogen brittleness (HB) of metal under specific conditions of thermodeformational cycle of welding [1]. This phenomenon is based on the mechanism of hydrogen interaction with dislocations [2–5], leading to a change of properties of dislocation clusters [6, 7].

Properties of both individual dislocations and dislocation clusters largely determine the mechanical properties of metals. The difference between theoretical yield point and the really observed value, metal capability for plastic deformation, strengthening, temperature dependence of yield point and many other properties are attributed to presence of dislocations in the real metals [8–12]. Main regularities of HB are also well described in terms of dislocation theory that is confirmed by experiments correlating plastic deformation rate in the metal and its HB sensitivity [1, 2, 13], as well as electron microscopy studies of hydrogen influence on behaviour of dislocation clusters and microcrack growth [14]. Under the impact of hydrogen, metal mechanical characteristics can deteriorate several times, and it is important to take it into account in prediction of the reliability and fatigue life of structures. This work describes HB mechanism allowing for the effect of hydrogen-enhanced localizing of plastictiy (HLP) on micro- and macrolevels and physicomathematical model of dislocation interaction in hydrogen-containing metal with bcc lattice.

Physical model of HB. Dislocations are capable of interacting with each other owing to presence of stress fields around them. Two edge dislocations of one sign located in one slip plane are repulsed with force F_D inversely proportional to distance r between them [15]:

$$F_D \sim 1/r. \quad (1)$$

In hydrogen-containing metal the nature of interaction of edge dislocations changes somewhat. In addition to the force of interaction with the stress field of adjacent dislocation F_D, an additional force is applied to the edge dislocation that is caused by interaction of this dislocation stress field with hydrogen atoms concentrated around the adjacent dislocation [6, 7]. Thus, an additional force of attraction F_H arises between two edge dislocations of one sign located in one slip plane, which is caused by presence of hydrogen atoms around the dislocations. The magnitude of this force depends on metal temperature and hydrogen concentration. The force of interaction of hydrogen atom with edge dislocation rises in inverse proportion to the square of distance between them [16]. Therefore, allowing for certain approximations, dependence of force F_H on distance between the dislocations has the following form:

$$F_H = \frac{\alpha}{r^2}, \quad (2)$$

where α is the coefficient of proportionality.

Therefore, in hydrogen-containing metal the resultant force of interaction is smaller than that in metal without hydrogen. Effect of reduction of the resultant force of interaction between edge dislocations $F_{RES} = F_D - F_H$ in the metal, containing hydrogen, was experimentally confirmed in [14], and was called hydrogen-enhanced localized plasticity.

*Work was performed with the support of State Fund of Fundamental Research of Ukraine (Grant of President of Ukraine for supporting young scientists F32/237–2011).

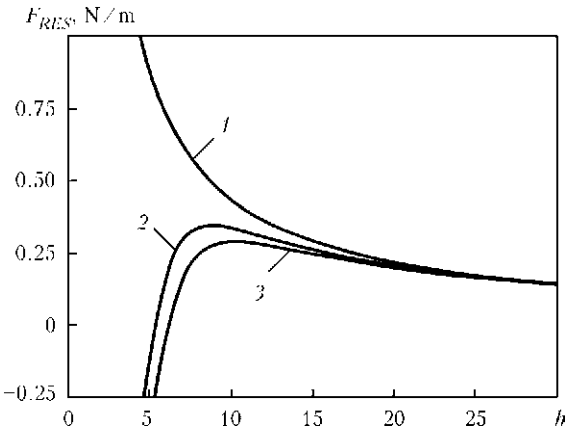

Figure 1. Dependence of resulting force of interaction of two edge dislocations F_{RES} on distance between them h (in modules of Burgers vector) at different concentration of diffusible hydrogen (metal temperature T = 300 K) [17]: *1* — 0; *2* — 5; *3* — 10 cm^3/100 g

In work [17] it is shown that a low hydrogen concentration characteristic for metal of welded joints from HSLA steels [18] is sufficient for appearance of the effect of HLP in iron. The limiting stage of initiation of a submicrodefect is the coalescence of two first dislocations in the cluster tip, as a much smaller force is required for dislocation joining the already formed submicrodefect [19]. Therefore, reduction of F_{RES} magnitude essentially facilitates coalescence of edge dislocations into microdefect nucleus. In hydrogen-containing iron the value of force, required for coalescence of the first two edge dislocations into submicrodefect nucleus, can drop 2 times and more (Figure 1). Therefore, under certain conditions presence of Cottrell atmospheres essentially changes the properties of dislocation clusters, leading to a change of metal mechanical properties.

As is seen from Figure 1, in hydrogen-containing metal there is a certain threshold distance between the dislocations, after achievement of which hydrogen influence on the force of interaction of dislocations rises noticeably. Therefore, hydrogen presence starts affecting the macroscopic strength of the metal after the dislocation density has reached a certain threshold value.

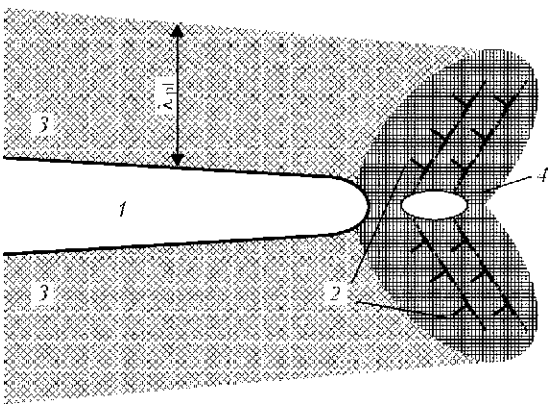

Figure 2. Schematic of macrocrack growth in the metal: *1* — macrocrack; *2* — field of plastic deformations ahead of its tip; *3* — layer of plastically deformed metal; *4* — microdefect

Initiation and propagation of a submicrocrack in the metal grain allowing for the effect of HLP be divided into three stages:

- hydrogen atoms concentrate around edge dislocations present in the cluster, thus reducing the force of repulsion between the dislocations and faciliting their coalescence;
- under the impact of external stresses the dislocations in the cluster tip coalesce and form a submicrocrack nucleus. Hydrogen present on these dislocations is partially entrapped by submicrocrack stress field, and partially penetrates into its volume;
- submicrocrack growth leads to fracture of metal grain and formation of a stable microdefect, which is capable of growing up to macrodimensions under the impact of external stresses and hydrogen.

One of the most probable mechanisms of macrocrack development in the metal is formation of a microdefect ahead of its tip and its subsequent coalescence with the crack (Figure 2) [10]. Under the impact of stresses, a plastic strain region forms in the metal ahead of the growing crack tip. During crack growth it leads to formation under its surface of a layer of plastically deformed metal, λ_{pl}, the thickness of which depends on applied load: the higher the load, which should be applied for formation of a microdefect ahead of the crack tip, the greater the λ_{pl}. Energy required for macrocrack growth consists of two parts — energy of free surface formation, and energy of subsurface layer of plastically deformed metal. In the metal not containing hydrogen, specific energy required to form such a layer, is by several orders of magnitude higher than the specific energy of crack-free surfaces [20]. Owing to the effect of HLP, the stress required to form a microdefect ahead of macrocrack tip, decreases considerably. Therefore, in a sample containing hydrogen value of λ_{pl} and percent of plastically deformed metal are much lower than in metal without hydrogen. Effect of HLP reduces the most energy-consuming component of crack growth, namely, formation of a subsurface layer λ_{pl}. Therefore, in hydrogen-containing metal with bcc lattice, macrocrack propagation should proceed in a more brittle mode, and should require much less energy, which is exactly what was observed in the experiments [1, 2].

Based on the proposed HB mechanism, an assumption can be made about the difference in fracture processes on macrolevel in samples of one and the same metal with and without hydrogen. While at the initial stage of plastic deformation dislocation density is low, change of dislocation structure in the samples proceeds in a similar mode, irrespective of hydrogen content. It means that at mechanical testing on macrolevel metal properties practically coincide. With increase of metal plastic deformation dislocation density rises. When as a result of increase of dislocation density the average distance between them reaches a certain

threshold value, the effect of HLP will be manifested in hydrogen-containing metal. As a result, more intensive formation of submicrodefects starts in the metal that will lead to an irreversible change of the mechanical properties of such a metal on macrolevel.

Thus, there should be a threshold plastic deformation, the value of which depends on metal sensitivity to HB, testing temperature and hydrogen concentration. If metal containing hydrogen is deformed to a smaller degree of plastic deformation, then after hydrogen degassing its mechanical properties will recover. After achievement of threshold plastic deformation, however, owing to presence of a large number of microdefects in the sample, metal properties after degassing will not recover, and it will still fail in a more brittle manner than the metal that did not contain any hydrogen initially.

HB mathematical model. Dislocation rearrangements leading to initiation and propagation of a submicrocrack in hydrogen-containing metal can be described with application of either force [3, 19] or energy criterion [21, 22]. Application of force criterion of submicrocrack initiation, when behaviour of each individual dislocation is calculated proceeding from forces acting on it, gives a more detailed picture and is easily realized, when studying the behaviour of a small number of dislocations, as it was shown in the case of two dislocations interaction. Nonetheless, an energy criterion of submicrocrack initiation and propagation is used in this work for calculations. This is related to the fact that if a cluster has five and more dislocations, then in case of application of force approach for calculation the derived system of equations has no analytical solution, even when there are no Cottrell atmospheres around the dislocation. Now, allowing for hydrogen influence makes such calculations more complicated by an order of magnitude. For metal containing no hydrogen the problem of dislocation behaviour in a large cluster can be solved, if continuum model of the cluster is considered instead of discrete dislocations [11, 15, 19]. With such a problem definition the cluster is characterized not by the position of each individual dislocation, but by dislocation density $\rho(x)$ in a point. However, as shown by calculations, continuum model gives an inadequate assessment of the stressed state inside the cluster proper [11]. Therefore, when allowing for the influence of the effect of HLP, when it is the question of interaction inside the dislocation cluster proper, this continuum model cannot be applied. Energy criterion of submicrocrack formation and growth allows circumventing this problem.

At simulation of metal HB the classical schematic of submicrocrack formation from a plane cluster of edge dislocations was taken as a basis. In the case of metal containing no hydrogen, the total energy of plane cluster of edge dislocations–submicrocrack system is equal to [10, 21–24]

$$W = \frac{nb^2G}{4\pi(1-\nu)} \ln \frac{4d}{L} + \frac{(N-n)^2b^2G}{4\pi(1-\nu)} \times \\ \times \ln \frac{4\pi\sqrt{e}(1-\nu)d}{(N-n)Gb} \tau_{eff} - \frac{\pi(1-\nu)L^2}{8G} \sigma^2 + 2\gamma L, \quad (3)$$

where b is the Burgers vector; G is the shear modulus; ν is the Poisson's ratio; L is the submicrocrack length; n is the number of dislocations which formed the submicrocrack; N is the maximum number of dislocations in the cluster; σ is the principal normal stress; γ is the specific surface energy of the metal which changes as a result of hydrogen impact; d is the size of metal grain; e is the Napierian base; τ_{eff} is the effective tangential stress in the slip plane.

Penetrating into the submicrocrack volume, hydrogen decreases its specific surface energy. During submicrocrack growth its volume increases, and dislocations joining it contribute new portions of hydrogen. This leads to a constant change of hydrogen pressure inside the submcirocrack and to a change of metal specific surface energy. Therefore, in case of hydrogen-containing metal, the last addendum in equation (3) should be replaced by integral

$$2 \int_0^{L_f} \gamma(L, N, n, T) dL, \quad (4)$$

where L_f is the final length of the submicrocrack.

In hydrogen-containing metal the work which should be done to bring together dislocations removed from each other to distance r, is found from the following equation:

$$\int_{+\infty}^{r} F_{RES} dr = \int_{+\infty}^{r} F_X dr - \int_{+\infty}^{r} F_H dr, \quad (5)$$

where $\int_{+\infty}^{r} F_X dr$ is the work which should be done in the metal containing no hydrogen, and, therefore, it is already allowed for in equation (3).

With shortening of the distance between the dislocations, their stress fields are superposed. As a result, the energy of the bond of hydrogen with dislocations becomes higher. Let us assume that at the beginning, when dislocations are located at a considerable distance from each other, the total energy of their bond with hydrogen is equal to W_d, and when they are at distance r – W_d^r from each other, then according to the law of energy conservation

$$\int_{+\infty}^{r} F_H dr = W_d^r - W_d. \quad (6)$$

Therefore, hydrogen, located on dislocations during shortening of interdislocation spacing, gives part of its potential energy to the submicrocrack

nucleus, thus reducing the work required for dislocation coalescence:

$$\int_{+\infty}^{0} F_H dr = W_L^0 - W_d, \qquad (7)$$

where W_L^0 is the energy of hydrogen bond with submicrocrack nucleus.

Integrating over the entire region taken up by Cottrell atmosphere, we will find the energy of the bond of hydrogen with edge dislocation per a unit of length:

$$W_d = \int\int_{\Omega_d} u_d(x, y) C_d(x, y) dx dy \qquad (8)$$

where Ω_d is the area taken up by Cottrell atmosphere around the dislocation; $C_d(x, y)$ is the hydrogen concentration calculated on the basis of Fermi–Dirac statistics.

Energy of interaction of a hydrogen atom, located in point (x, y) relative to dislocation nucleus, is calculated from equation [16]

$$u_d(x, y) = -\frac{Ay}{x^2 + y^2}, \qquad (9)$$

where A is the material constant determined experimentally.

In the first approximation at evaluation of the energy of hydrogen bond with submicrocrack W_L the latter can be regarded as a superdislocation. Therefore, W_L value is found in a similar way:

$$W_L = \int\int_{\Omega_L} U_L(x, y) C_L(x, y) dx dy \qquad (10)$$

where Ω_L is the region taken up by Cottrell atmosphere around the submicrocrack; $U_L(x, y)$ is the energy of the bond between hydrogen atom and submicrocrack.

Allowing for equations (7), (8) and (10), total change of submicrocrack energy caused by hydrogen and $(N - n)$-dislocations that did not join the defect can be written as

$$W_H = -(W_L + (N - n)W_d) = -\int\int_{\Omega_L} U_L C_L dx dy - (N - n) \int\int_{\Omega_d} u_d C_d dx dy \qquad (11)$$

Allowing for equations (3), (4) and (11), energy of plane cluster of edge dislocations–submicrocrack system for hydrogen-containing metal is equal to

$$W = \frac{(nb)^2 G}{4\pi(1 - \nu)} \ln \frac{4d}{L_f} + \frac{(N - n)^2 b^2 G}{4\pi(1 - \nu)} \ln \frac{4\pi\sqrt{e}(1 - \nu)d}{(N - n)Gb} \tau_{eff} - \frac{\pi(1 - \nu)L_f^2}{8G} \sigma^2 + 2\int_0^{L_f} \gamma dL - \int\int_{\Omega_L} U_L C_L dx dy - (N - n) \int\int_{\Omega_d} u_d C_d dx dy \qquad (12)$$

To calculate the behaviour of dislocations and submicrocrack, it is necessary to differentiate equation (12) by L_f and n. Derived equations are used to determine the conditions, at which the submicrocrack becomes unstable, i.e. breaks up.

At calculation it was assumed that the maximum slip length of edge dislocation is equal to grain size, while hydrogen concentration in the metal is equal to 10 $cm^3/100$ g.

Quantity of hydrogen, which is transferred by edge dislocation to the site of submicrocrack initiation, was determined on the basis of relationships proposed in [25]. Number of dislocations in the cluster N and τ_{eff} was evaluated on the basis of Hall–Petch relationship [11].

Derived relationships were the basis to perform computer simulation of fracture of iron grain with bcc lattice by dislocation mechanism (Figure 3). In calculation it was assumed that in the temperature range T = 350–250 K shear modulus and Poisson's ratio remain constant. Therefore, breaking stress of a grain of metal not containing hydrogen, will also remain constant in this range. If HLP is taken into account in the mathematical model, the stress, which is to be applied to break the grain, decreases, and microdefect length and number of dislocations joining it increase. In some cases, lowering of the strength of hydrogen-

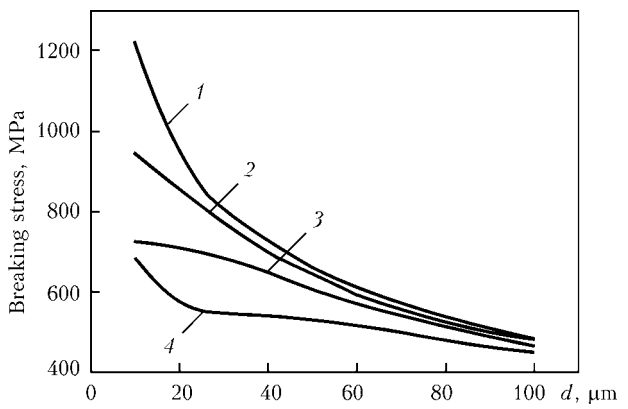

Figure 3. Dependence of breaking stress of grain of iron with bcc lattice on its size d at different temperatures: *1* — grain of metal without hydrogen at T = 350–250; *2* — 350; *3* — 300; *4* — 250 K

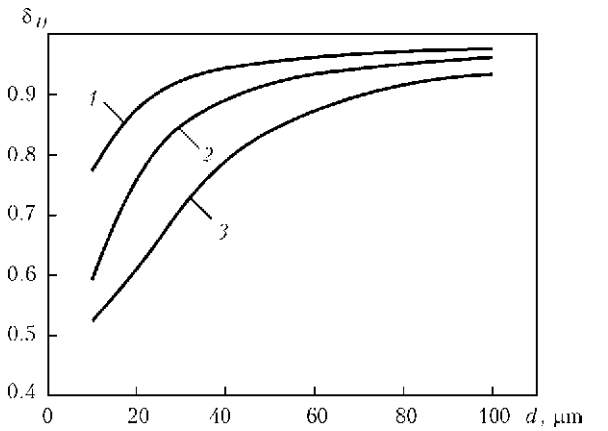

Figure 4. Dependence of relationship $\delta_H = S_C^H / S_C^0$ on size of grain d at different temperatures: *1* — T = 350; *2* — 300; *3* — 250 K

containing iron is equal to 40–50 % of the nominal value. A certain increase of breaking stress on curve *4* in Figure 3 at d = 25–10 μm is attributable to the nature of HB temperature-rate dependence [1, 2]. It is seen that in the metal containing hydrogen the effect of saturation can be manifested, when grain refinement practically does not increase its strength (see Figure 3). Therefore, increase of steel strength due to grain refinement is rational only up to a certain limit value of d. Note that d value depends on metal sensitivity to HB, hydrogen concentration and operating temperature range.

Metal susceptibility to HB can be expressed through decrease of breaking stress [1]:

$$\delta_H = S_C^H / S_C^0,$$

where S_C^H, S_C^0 is the true breaking stress of metal grain with and without hydrogen, respectively. According to performed calculations at comparatively large values of grain size d (in the range from 100 up to 50 μm), dependence of the degree of lowering of metal brittle strength δ_H can be approximated by a straight line (Figure 4). This is in agreement with experimental data given in [2, 26], which were obtained for armco-iron and low-carbon steel. At further grain refinement, however, metal sensitivity to BH rises abruptly. At other conditions being equal, grain refinement raises the degree of lowering of metal brittle strength. It should be noted that the absolute value of breaking stress S_C^H of hydrogen-containing metal still grows somewhat with grain refinement (see Figure 3).

As was noted above, in calculation it was assumed that the length of dislocation slipping is equal to grain size d. Therefore, according to the results given in Figure 4, HB degree rises with shortening of free sliding length of dislocations. Thus, derived conclusion on higher HB susceptibility of metal with finer grain can be interpreted as a theoretical explanation for the experimental fact that metal HB susceptibility rises with increase of its strength.

CONCLUSIONS

1. A mechanism of HB of metals with bcc lattice was proposed, which allows for the effect of hydrogen-enhanced localizing of ductility on the micro- and macrolevel.

2. A model of fracture of metal grain by the dislocation mechanism for hydrogen-containing metal was improved.

3. It is shown that at all other conditions being equal metal grain refinement will lead to an increase of HB degree, although the absolute value of breaking stress of hydrogen-containing metal increases with grain refinement.

4. It is shown that for hydrogen-containing metal increase of its strength due to grain refinement it rational only up to a certain limit, which depends on hydrogen concentration, operating temperature and HB sensitivity.

1. Pokhodnya, I.K., Yavdoshchin, I.R., Paltsevich, A.P. et al. (2004) *Metallurgy of arc welding. Interaction of metal with gases*. Ed. by I.K. Pokhodnya. Kiev: Naukova Dumka.
2. Kolachev, B.A. (1985) *Hydrogen brittleness of metals*. Moscow: Metallurgiya.
3. Morozov, L.S., Chechulin, B.B. (1967) *Hydrogen brittleness of metals*. Moscow: Metallurgiya.
4. Pokhodnya, I.K., Stepanyuk, S.N., Shvachko, V.I. (2000) Role of temperature in hydrogen-induced cracking of structural steels and welded joints. *The Paton Welding J.*, **2**, 2–7.
5. Pokhodnya, I.K., Shvachko, V.I., Utkin, S.V. (2002) Effect of hydrogen on equilibrium of a dislocation submicrocrack in α-iron. *Fiz.-Chim. Mekhanika Materialiv*, **1**, 7–14.
6. Birnbaum, H.K., Sofronis, P. (1994) Hydrogen-enhanced localized plasticity — a mechanism for hydrogen-related fracture. *Mat. Sci. and Eng. A*, **176**, 191–202.
7. Birnbaum, H.K., Sofronis, P. (1995) Mechanics of the hydrogen-dislocation-impurity interactions — increasing shear modulus. *J. Mech. Phys. Solids*, 43(**1**), 49–90.
8. Gulyaev, A.P. (1986) *Physical metallurgy*. Moscow: Metallurgiya.
9. Milman, Yu.V., Trefilov, V.I. (2010) On physical nature of temperature dependence of yield strength. *Poroshk. Metallurgiya*, **7/8**, 3–18.
10. Vladimirov, V.I. (1986) *Physical nature of metal fracture*. Moscow: Metallurgiya.
11. Hirth, J., Lothe, J. (1972) *Theory of dislocation*. Moscow: Atomizdat.
12. Frenkel, Ya.I. (1972) *Introduction to theory of metals*. Leningrad: Nauka.
13. Shvachko, V.I. (2000) Hydrogen brittleness of iron alloys with bcc lattice. *Voprosy Atomnoj Nauki i Tekhniki*, **5**, 79–86.
14. Robertson, I.M. (2001) The effect of hydrogen on dislocation dynamics. *Eng. Fracture Mech.*, **68**, 671–692.
15. Landau, L.D., Lifshits, E.M. (1987) *Theoretical physics*. Vol. 7: Elasticity theory. Moscow: Nauka.
16. Cottrell, A. (1964) *Theory of dislocation*. Moscow: Mir.
17. Ignatenko, O.V., Pokhodnya, I.K. (2010) Hydrogen induced localized plasticity in iron with BCC lattice. In: *Proc. of 18th Europ. Conf. on Fracture of Materials and Structure from Micro to Macroscale* (Dresden, 2010). Dresden: ESIS, DVM.
18. Paltsevich, A.P. (1999) Chromatographic method for determination of hydrogen content in components of electrode coatings. *Avtomatich. Svarka*, **6**, 45–48.
19. Vladimirov, V.I., Khannanov, Sh.Kh. (1969) Interaction of dislocation cluster with dislocation crack. *Fizika Tv. Tela*, 11(**6**), 1667–1676.
20. Panasyuk, V.V. (1968) *Limit equilibrium of brittle solids with cracks*. Kiev: Naukova Dumka.
21. Stroh, A.N. (1954) The formation of cracks as a result of plastic flow. Pt 1. *Proc. of Roy. Soc. of London A*, **223**, 404–414.
22. Kotrechko, S.A., Meshkov, Yu.Ya., Mettus, G.S. (1988) Brittle fracture of polycrystalline metals in complex stressed state. *Metallofizika*, 10(**6**), 46–55.
23. Garofalo, F., Chou, Y.T., Ambegaokar, V. (1960) Effect of hydrogen on stability of microcracks in iron and steel. *Acta Metall.*, 8(**8**), 504–512.
24. Pokhodnya, I.K., Shvachko, V.I., Utkin, S.V. (2002) Effect of hydrogen on equilibrium of dislocation submicrocrack in α-iron. *Fiz.-Khim. Mekhanika Materialov*, **1**, 1–8.
25. Ignatenko, A.V. (2007) Mathematical model of transportation of hydrogen by edge dislocation. *The Paton Welding J.*, **9**, 23–27.
26. Ostash, O.P., Vitvittsky, V.I. (2011) Duality of hydrogen effect on mechanical behavior of steels and structural optimization. *Fiz.-Khim. Mekhanika Materialov*, **4**, 4–19.

NON DESTRUCTIVE TESTING OF WELDED JOINTS

IMPROVEMENT OF RELIABILITY OF MAIN GAS PIPELINES BY USING REPEATED IN-PIPE FLAW DETECTION

D.P. VARLAMOV[1], **V.N. DEDESHKO**[1], **V.A. KANAJKIN**[2] and **O.I. STEKLOV**[2]
[1]Closed Joint Stock Company «Research and Production Association «Spetsmash», Moscow, RF
[2]Gubkin Russian State University of Oil and Gas, Moscow, RF

It is shown that the presence of a large number of abnormalities in welded joints is hazardous for safe operation of the system of main gas pipelines not only because of the probability of failure of the welded joints, but also because of formation of an additional factor, i.e. initiation and propagation of stress corrosion cracking defects in a zone of intersection of longitudinal and circumferential welds.

Keywords: *welded pipelines, integrity, in-pipe flaw detection, general and local corrosion, stress corrosion cracking, abnormal circumferential welded joints*

Stability of delivery of gas to consumers in the Russian Federation, countries of the Western and Eastern Europe, as well as of the Balkan Region is inseparably connected to the reliability and safety of operation of the unified system of gas pipelines of Company «Gazprom». The Russian gas industry exhibits a gradual growth of volumes of gas production, the forecast for 2020 being 670 bln m^3. However, the unified gas transportation system built as far back as under the Soviet Union underwent substantial changes because of disintegration of the Soviet Union. Today the multiline corridors of main gas pipelines pass through foreign countries, and inspection of their condition depends in many respects on foreign partners. On the average, service life of the entire system of main gas pipelines of the former Soviet Union has amounted to 30 years or more.

At present, both the Russian Federation and foreign countries have worked out the technology for maintaining integrity of main gas pipelines and putting them into repair on a timely basis to ensure their safe operation and increase productivity under the rated gas pressure. The key stages of the technology for maintaining integrity of main gas pipelines are as follows:

- subjecting pipelines to regular in-pipe flaw detection (IPFD) procedures with an interval of 3–5 years;
- estimation of hazard of detected defects and monitoring of their development;
- timely performance of repair-and-renewal operations on the defects that are hazardous for integrity of main gas pipelines.

Modern development of the market economy under conditions of severe competition imposes increasingly serious requirements to elaboration of the most advanced technologies, their consistency in the process of manufacture of materials and parts, and in provision of services. In this case, quality and reliability, as well as durability of the products play a decisive role in successful activities of not only individual enterprises, but also entire branches of economy of the country. Therefore, inspection of the condition of materials and quality of products becomes highly topical. The latest science and technology achievements and developments, i.e. thermal, optical, X-ray, different types of hard and soft radiation, ultrasound, eddy currents, magnetic fields and other methods of physical metals science, are used to provide continuous improvement of the procedures used to test pipes in main pipelines [1].

The pipes laid down with violation of design solutions, especially in mountain, irregular and swamp lands, as well as the pipes having relative residual welding stresses in heat-affected zones of the welds or in zones of complete bending of plate edges, are particularly hazardous for main pipelines, as zones of local stresses in metal are nearly the most important cause of initiation and propagation of defects of the type of stress corrosion cracking (SCC). In view that the exact location of SCC defects in underground gas pipelines can hardly be predicted even by using many known methods of physical metals science, while ultrasonic IPFD of gas pipelines is too costly, the efforts in the industry are aimed at development of magnetic IPFD.

Magnetic flaw detection equipment. Magnetic flaw detection equipment developed during the last 15 years by CJSC «RPA «Spetsneftegaz» for inspection of main oil and gas pipelines can be rated as

Figure 1. Cleaning piston

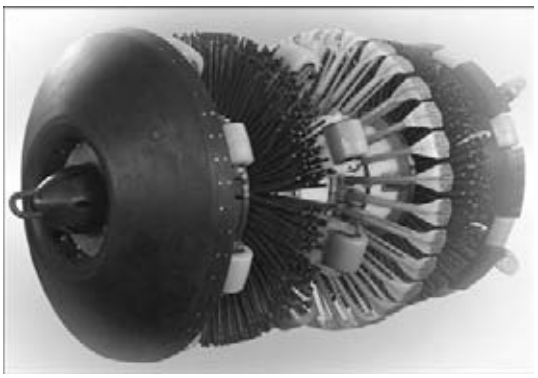

Figure 3. Electron multi-channel profile measurement gear

important achievements [2]. Development of domestic flaw detection gears allows comprehensive diagnostic examination of the conditions of pipelines and estimation of hazard of the detected damages in pipes. The IPFD system consists of several gears, each performing its function, where the starting sequence makes it possible to remove garbage and deposits from a pipe, determine the profile of pipes and possibility of passage of the flaw detection gears through the route, magnetise a pipeline and reveal the character and location of a damage at a high degree of precision. The system of gears for IPFD is shown in Figures 1–5.

The cleaning piston (Figure 1) designed for cleaning the internal cavity of a pipeline from garbage and deposits is equipped with calibration plates for initial determination of passability of a pipeline length.

The cleaning magnetic in-pipe one-section piston with a by-pass device (Figure 2) is intended for cleaning the internal cavity of a pipeline from ferromagnetic deposits and initial magnetisation. This is the first domestic in-pipe gear with a speed (by-pass) control device.

The electron multi-channel profile measurement gear (Figure 3) serves to reveal dents, crimps and out-of-roundness of a pipe, fix their sizes and locations on route of a gas pipeline, sense transverse welds, and initially detect corrosion defects.

The magnetic in-pipe two-section flaw detector for longitudinal magnetisation with a by-pass device (Figure 4), having the run speed regulation coefficient equal to 6, is meant to reveal defects of the type of metal losses on the internal and external surfaces of the pipe wall:

- general and pitting corrosion, transverse grooves, transverse cracks and abnormalities in transverse welds;
- defects of a mechanical origin, such as scores and scratches;
- defects of a metallurgical character — in-wall laminations and non-metallic inclusions.

The magnetic in-pipe two-section flaw detector for transverse magnetisation with a by-pass device (Figure 5) is designed for detection of SCC defects, transverse cracks, defects of the type of metal losses (general and pitting corrosion, longitudinal grooves), abnormalities in longitudinal welds, longitudinally oriented defects of a mechanical origin (scores, scratches), and defects of a metallurgical origin (in-wall laminations, non-metallic inclusions).

The flaw detector is equipped with an active by-pass having the run speed regulation coefficient equal to 6, which provides decrease in speed from 12 (speed of transportation of product via a pipe) to 2–3 m/s (optimal speed for magnetic flaw detection).

Analysis of unsoundness of welded joints, defects of general and local corrosion, and SCC defects in an extended multi-line system of main pipelines. This study presents analysis of unsoundness of an extended system of main gas pipelines with a diameter of 1420 mm conducted on a base of several sequential IPFDs by «Spetsneftegaz» by using a complete set of the equipment.

Analysis of unsoundness covered the scheme of propagation of such damages as general and local corrosion defects, SCC defects, abnormal circumferential welds, arrangement of the pipes laid down in sections,

Figure 2. Cleaning magnetic in-pipe one-section piston with by-pass device

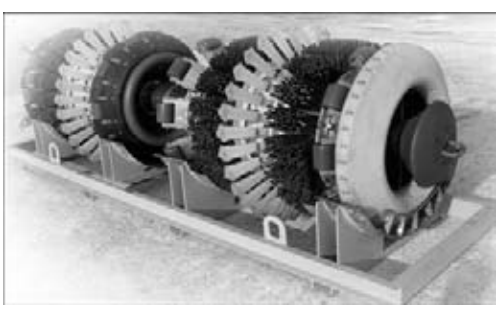

Figure 4. Magnetic in-pipe two-section flaw detector for longitudinal magnetisation with by-pass device

Figure 5. Magnetic in-pipe two-section flaw detector for transverse magnetisation with by-pass device

depending on the wall thickness and type of manufacture of the pipes over the major length of a region.

The data of estimation of unsoundness of 28 sections in the Western Siberia (two IPFDs were conducted with an interval of 4–5 years) on six parallel lines of the main gas pipeline were considered. It should be noted that a section extends to a distance from one compressor station (CS) to the other, the average length of one section being approximately 100 km [3].

General and local corrosion defects. Figure 6 shows zonality of propagation of general corrosion defects related to the explicit impact by relief and water cut. This can be seen at CS 9 and 10 — on all the lines, between CS 12 and 13 — on four lower lines at the end of the section, at CS 13 and 14 in the middle of the section — on four lower lines, and at the end of the section — on lines 1 and 2.

The total quantity of the general corrosion defects is high for the enterprise, and in many sections after the third IPFD the quantity of the defects substantially increased. No common regularity was fixed for propagation of the general corrosion defects over the section length, and the maxima were observed at the beginning, in the centre or at the end of a section on all parallel lines.

As established from the investigation results on the effect of the level of stresses and identification of a component of stresses that determines cracking and crack propagation path, corrosion cracks are caused by tensile components of stresses independently of the loading method. For all metals the time to cracking continuously decreases with growth of stresses. Increase of stresses caused by external loading, as well as of residual stresses leads to weakening and violation of continuity of protective films, growth of the concentration of elasto-plastic strains in microcracks and at the apex of a propagating crack, and to intensification of mechanical, corrosion and sorption processes related to the concentration of strains. Intensification of all related processes with increase in stresses results in acceleration of corrosion cracking.

Almost every section of all lines of gas pipelines in Western Siberia is subjected to SCC defects (Figure 7). The quantity of the SCC defects grows from inspection to inspection despite the efforts made to remove the earlier revealed defects. The new SCC defects are detected in sections where before they were absent, and they continue to be fixed in the sections where the SCC defects were already revealed and removed. Alarming is the fact of detection of the SCC defects in the third IPFD in second halves of the sections. The clear zonality of propagation of the SCC defects can be seen along the length of the sections

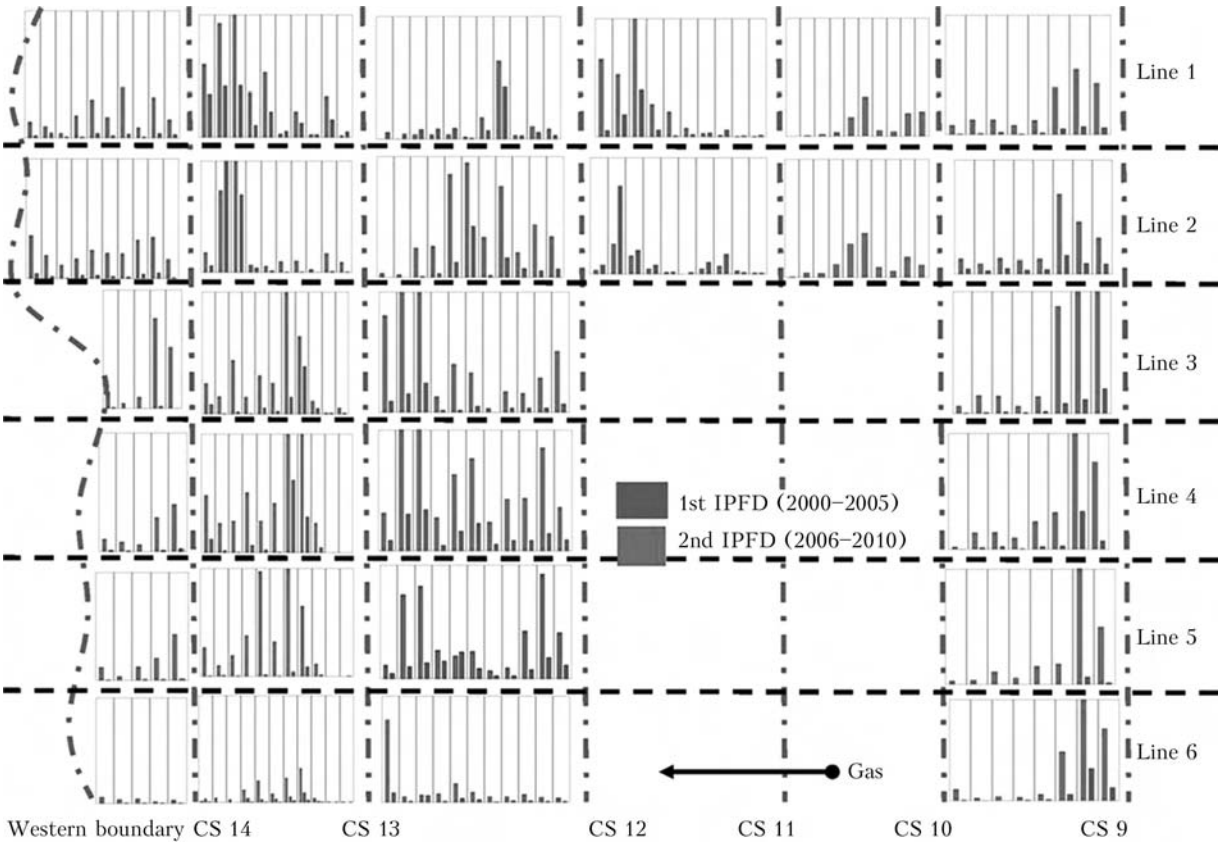

Figure 6. General and local corrosion defects of pipelines in Western Siberia: scale *0Y* in all diagrams consists of 0–800 defects; scale *0X* — length of the sections divided by 10 km

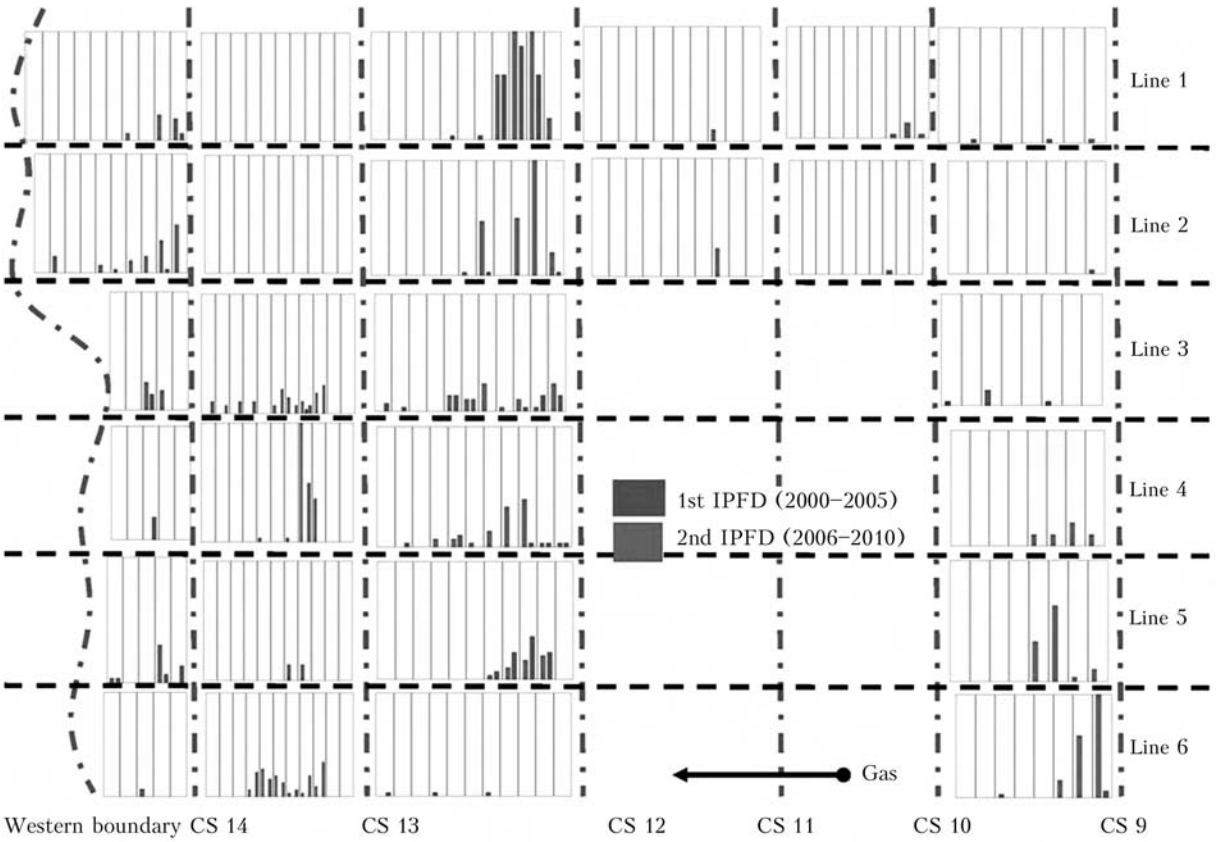

Figure 7. SCC defects of pipelines in Western Siberia: scale *0Y* in all diagrams consists of 0–30 defects; scale *0X* — length of the sections divided by 10 km

(there are much more SCC defects in the first half of the sections). The quantity of the SCC defects is substantially different in the same zones on parallel lines of gas pipelines, this being another evidence of a considerable effect of the wall thickness and type of the pipes laid down in the sections.

Abnormal circumferential welded joints. Specific features determining causes, character, kinetics and mechanism of corrosion fractures of the welded joints are attributable mainly to the thermal-deformation effect of the welding process, which causes unfavourable changes in properties of metal and its stressed state, this aggravating the negative impact of the environment.

Analysis of causes and mechanisms of failures of the welded joints on pipelines shows that fracture begins, as a rule, from the plane surface defects located mostly in the root layers of the welds. In all the cases, to ensure reliable and safe operation of a pipeline it is necessary to prevent development of a defect before it transforms into a through crack. Plane defects, i.e. cracks, lacks of penetration and undercuts, are most dangerous. One of the most common defects in butt welding of pipes is lack of penetration in the weld root. Often this defect combines with edge displacement. In the field welds it is difficult to technologically avoid formation of lacks of penetration and edge displacements [4].

Figure 8 shows abnormalities in the welded joints detected from the results of IPFD in the Central Region and in the Western Siberia. The Central Region was taken for comparison as a region with the best natural-climatic conditions for operation of main gas pipelines. It should be emphasised that the type of abnormality of a circumferential weld is established from the results of IPFD and requires a more precise definition using the external diagnostic equipment. A limited capability of the magnetic method used for IPFD, having a sufficient degree of reliability in identification of the type of abnormality, is shown in the first column of the diagram in Figure 8.

Unexpected corrosion-mechanical fractures of the welded joints and structures to form cracks of the avalanche type, caused by the combined impact of the environment and stresses under static (corrosion cracking), repeated static and cyclic loadings, are very hazardous.

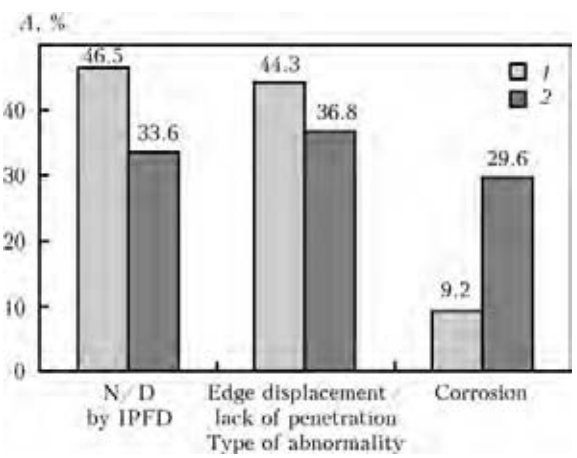

Figure 8. Types of abnormalities *A* in joints revealed in third IPED in the Central Region (*1*) and Western Siberia (*2*)

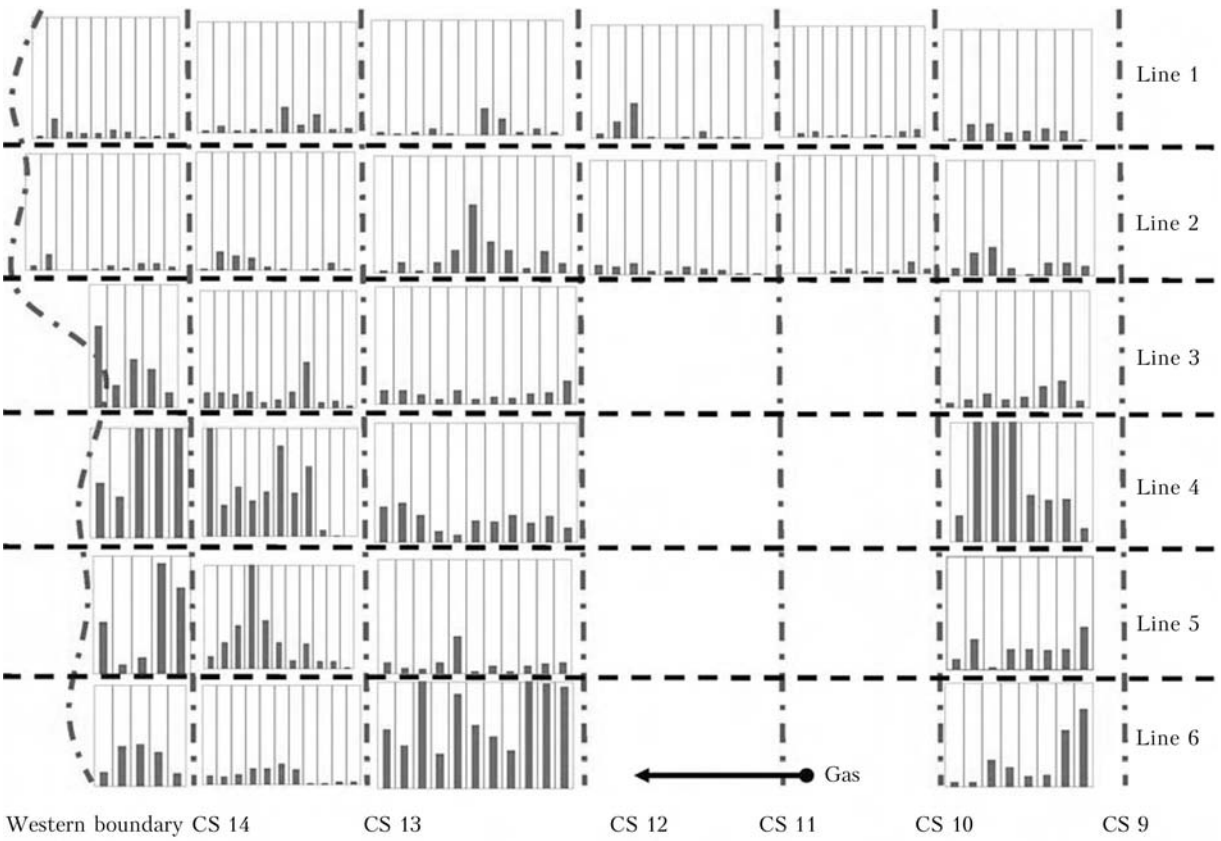

Figure 9. Abnormal circumferential welds on pipelines in Western Siberia: scale *0Y* in all diagrams consists of 0–100 defects; scale *0X* — length of the sections divided by 10 km

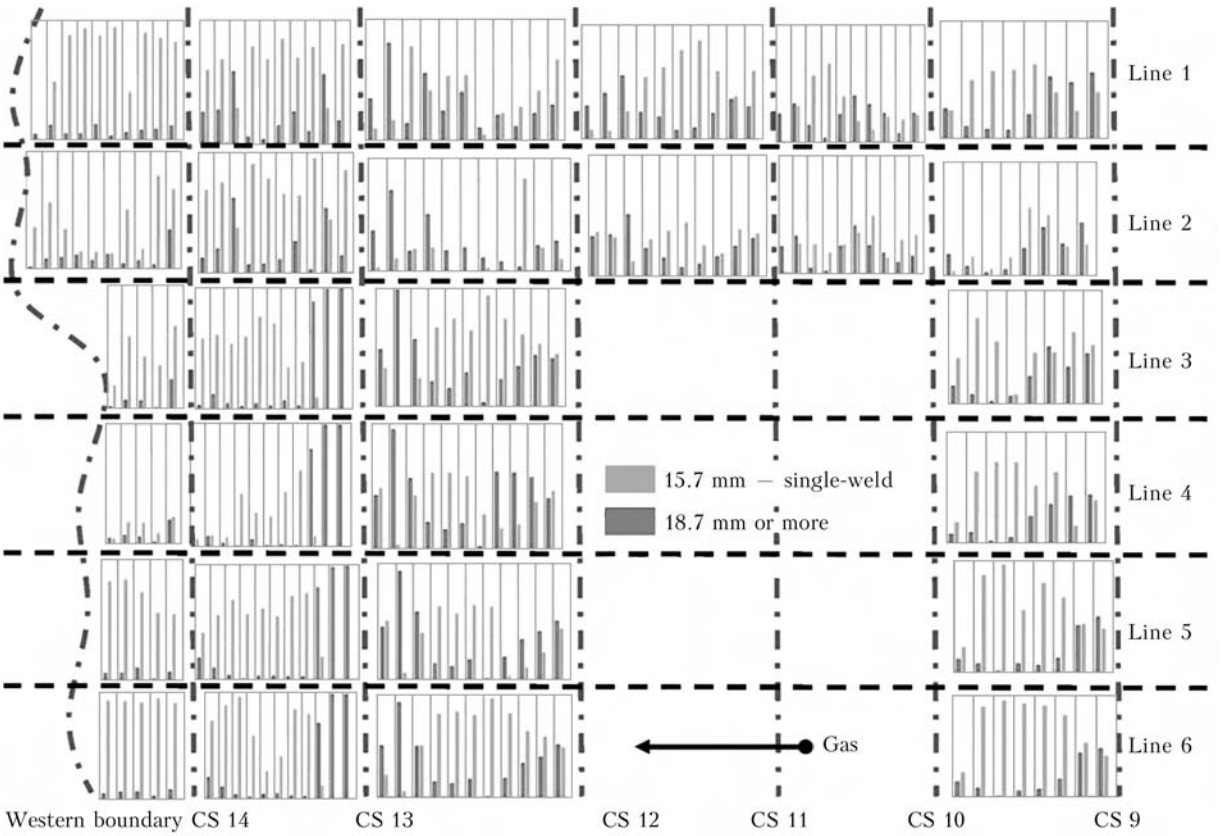

Figure 10. Distribution of pipes in sections depending on wall thickness and type of manufacture of pipes in Western Siberia: scale *0Y* in all diagrams consists of 0–900 pipes; scale *0X* — length of the sections divided by 10 km

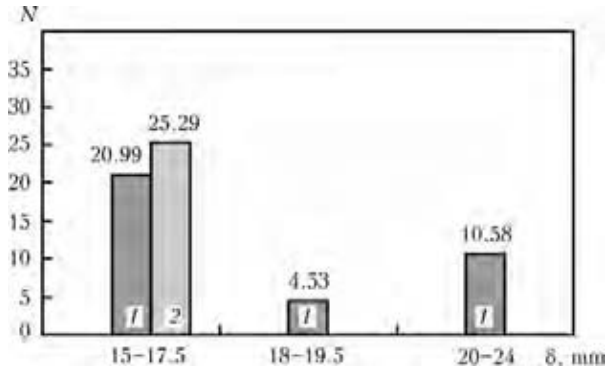

Figure 11. Specific quantity of SCC defects depending on wall thickness δ and type of manufacture of single-weld (*1*) and spiral-welded (*2*) pipes 1420 mm in diameter: *N* — quantity of pipes with SCC defects per 100,000 pipes

In the Central Region and Western Siberia apoproximately half of all abnormal joints are of a serious danger for operation of gas pipelines (lacks of penetration or edge displacements). The presence of such a large number of edge displacements and lacks of penetration in the Central Region is related, first of all, to the quality of construction, rather than to the natural-climatic conditions, this being indicative of a low level of corrosion in the joints (9.3 % in the Central region, and 29.6 % in the Western Siberia).

Many abnormal circumferential welds were fixed in the Western Siberia (Figure 9). This is associated with severe natural-climatic conditions exerting a considerable effect on the quality of construction and service conditions of gas pipelines.

Characteristics of pipes laid down in the main gas pipeline system. The sensitivity to technological and service effects, the types of failures of main gas pipelines and the importance of ageing are different for different generations of steels welded, which are meant for the oil and gas industry, such as low-carbon, low-alloy, and low-alloy steels with microadditions of active carbide-forming elements. The effect of corrosive environments, fluctuations of temperatures, working loads and stresses change with time the structure and properties of the metal used, compared to its initial characteristics.

The factor of dependence of the amount of SCC defects in a section and pipes laid down in it (wall thickness and type of manufacture of a pipe) is most pronounced in the Western Siberia (Figure 10). For example, almost no SCC defects were fixed in a section of CS 12 and 13 on the sixth line by any IPFD, whereas they were present in large quantities in the rest of the sections. The indirect dependence of the stressed state on a complex relief of land (presence of thin-walled pipes surrounded by a large quantity of thick-walled ones) and amount of SCC defects was also seen.

According to the data of statistical analysis conducted on 5 mln pipes with over 6000 SCC defects revealed in them (Figure 11), the thin-walled pipes (15.0–17.5 mm) were proved to be 2–3 times more sensitive to the SCC defects than the pipes with a wall thickness of more than 18 mm.

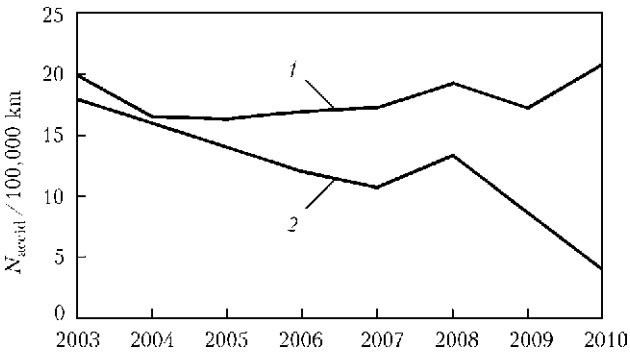

Figure 12. Effect of growth of the scopes of IPFD on decrease in failure rate: *1* — scope of flaw detection, thou km; *2* — failure rate, quantity of accidents a year per 100,000 km

Among the thin-walled pipes, the single-weld pipes had more SCC defects than the double-weld pipes [5]. As approximately 1/3 of all the pipes laid down in the extended multi-line system of main gas pipelines with a diameter of 1420 mm are the thin-walled double-weld pipes, IPFD is the only efficient method for prevention of emergency fractures.

IPFD performed annually on 18,000–20,000 km of large-diameter gas pipelines belonging to «Gazprom» made it possible to substantially improve their reliability and safety, and ensure the failure-free transportation of gas to consumers in Russia and abroad. According to the IPFD data, this was provided due to a 5 times decrease in the failure rate achieved in the last 10 years by applying selective repair and re-insulation of hazardous sections of gas pipelines (Figure 12).

CONCLUSIONS

1. To ensure safe operation of the system of main gas pipelines, it is necessary to continuously implement a set of the measures meant to timely reveal and remove defects from a linear part of the pipelines by using multiple IPFDs, and conduct comprehensive analysis of the state of the pipes and prediction of the amount of defects for the next 3–5 years.

2. A large number of abnormalities of the welded joints is hazardous for safe operation of the main gas pipeline system not only because of the probability of fracture of a welded joint, but also because of formation of an additional factor consisting in initiation and propagation of SCC defects in the zone of intersection of longitudinal and circumferential welds.

3. IPFD is the most efficient method for prevention of emergency fractures of pipes in the extended multi-line system of main gas pipelines.

1. Mazur, I.I., Ivantsov, O.M. (2004) *Safety of pipeline systems*. Moscow: Elina.
2. Steklov, O.I. (1990) *Resistance of materials and structures to stress corrosion*. Moscow: Mashinostroenie.
3. Kanajkin, V.A. (2009) *In-pipe magnetic flow detection of main pipelines*. Ekaterinburg: UrO RAN.
4. Varlamov, D.P., Kanajkin, V.A., Matvienko, A.F. (2008) *Monitoring of defects in main gas pipelines*. Ekaterinburg: UrO RAN.
5. Varlamov, D.P., Kanajkin, V.A., Matvienko, A.F. et al. (2010) *Analysis of stress corrosion defects in main gas pipelines*. Ekaterinburg.

APPLICATION OF WELDING TECHNOLOGIES AT REALIZATION OF EUROPEAN PROGRAM ON NEW RENEWABLE ENERGY SOURCES*

A. KLIMPEL
Silesian Polytechnical Institute, Gliwice, Poland

Analysis of the strategy of EuroUnion outlined in the European Strategic Energy Technology Plan (SET-Plan) was performed. Design of high-power wind generators for application on land and at sea is described, as well as modern structural materials and design solutions of towers, blades and load-carrying structures of nacelles. Directions of investigation of modern welding technologies to be applied in manufacture of up to 20 MW wind generators are proposed.

Keywords: *welded structures, renewable energy, wind generators, European plan, new structural materials, new welding technologies, installation work*

At the end of 2010 the European Commission approved a new program «The European Strategic Energy Technology Plan» (SET-Plan) [1], the main objective of which is lowering the emissions of hothouse gases (CO_2) and development of effective energy technologies. This initiative is based primarily on cooperation with the European Industrial Initiatives and covers the following fields: bioenergy; CO_2 collection and accumulation; power networks, fuel elements and hydrogen; nuclear energy; solar and wind energy.

In each of the above-mentioned fields technologies of welding, surfacing, thermal spraying and cutting have an important role. These technologies, unfortunately, are usually not taken into account or treated as those of secondary importance. A group of experts was formed, including the author of this paper, the purpose of which is development of concepts of fundamental and applied investigations in the field of technology of materials for construction of high-power sea wind generators. Analysis of the documents of «SET-Plan Wind Energy» shows that modern welding technologies should have one of the leading roles in construction of sea wind generators of up to 20 MW power. In is anticipated that in 2030 in the EuroUnion wind power will generate electric energy of up to 280–400 GW. Under «SET-Plan Wind Energy» program for which approximately 6 bln Euros will be allocated, it is intended to built up to ten new generation test wind turbines of 10–20 MW power; not less that four test structures of high power sea wind turbines located in zones with different wind conditions, in the sea coastal strip and in open sea in deep waters that will require application of welding technologies.

There exists a multitude of national and international organizations and societies, which, in particular, coordinate cooperation between industry and research centers [2–25]. Denmark now is keeping the leading role in the world market among countries producing energy by wind power, where in 2010 already 20 % of the total energy was produced from wind power (in Poland it was just 2.6 %). By the data of Polish Society of Wind Power in 2010 about 1096 MW of electric energy was produced by ground wind power stations (0 — sea wind power stations), and based on 2020 prediction about 1.6 GW will be produced by 10,893 sea wind turbines and 14.4 GW will be produced by 2100 ground wind turbines, including 600 private turbines [26]. As predicted in the report by J. Beurskens, Director of WE@SEA Scientific Program of Dutch government [4], Poland so far is only a potential territory for construction of sea wind power stations and does not look good against the background of 2030 prediction for the countries of Baltic and Northern Sea regions. According to this prediction, it is anticipated that sea wind power stations in 2030 will produce electric energy of the following power: more than 4 GW (Denmark), 6 (The Netherlands), 4 (Belgium), 33 (Great Britain) and 25 (Germany).

Ground and sea wind generators, made in a wide power range from various structural materials, are given in Figures 1–5 and Table 1. Quite a lot of wind generator manufacturers are present in the world wind energy market, among which the following European companies have the leading role [13–19], %: VESTAS (Denmark) — 12.5–15.0; ENERCON (Germany) — 8.5–10.5; GAMESA (Spain) — 6.5–8.0; SIEMENS WIND POWER (Germany and Denmark) — 5.0–6.0; REPOWER (Germany) — 3.5–4.5; GE WIND ENERGY (USA) — 12.0–14.0; SINOVEL (China) — 9.0–11.0; GLODWIND (China) — 7.0–8.0; DONGFANG ELECTRIC (China) — 6.0–6.5; SUZLON (India) — 6.0–6.5.

*Paper was earlier published in «Biuletyn Instytutu Spawalnictwa w Gliwicach» Journal, № 2, 2011. Translating into Russian was performed by Prof. E. Turyk.

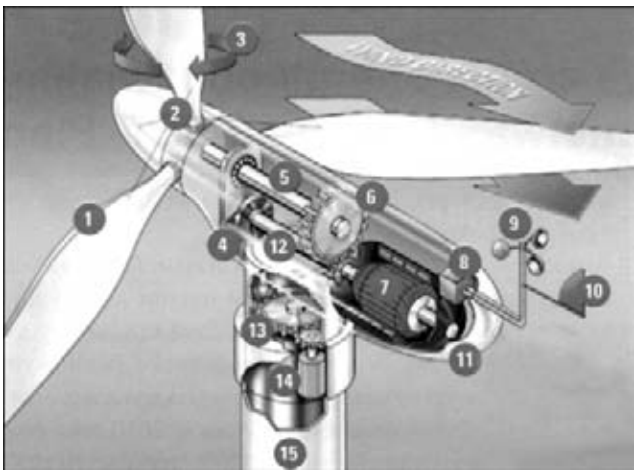

Figure 1. Schematic of a wind generator: *1* — blades; *2* — rotor; *3* — system of blade rotation in rotor bushing; *4* — system of deceleration of rotor rotation; *5* — drive shaft with low speed of rotation; *6* — transmission; *7* — generator; *8* — control system; *9* — wind speed measuring instrument; *10* — system of wind direction monitoring; *11* — nacelle; *12* — shaft with high rotation speed; *13*, *14* — drive and motor of nacelle rotation system; *15* — tower

Weight fraction and fraction of costs for manufacturing of the main load-carrying assemblies of wind generator structure (rotor bushing, nacelle load-carrying structure and tower) not only depend on wind generator power and its dimensions, but also show how important is the component role in wind generator structure [1–25] (see Figures 1–3, Table 2). Towers of high power wind generators (more than 2 MW) are made by welding from steel with medium yield point, usually S355 NL. Load-carrying structures of

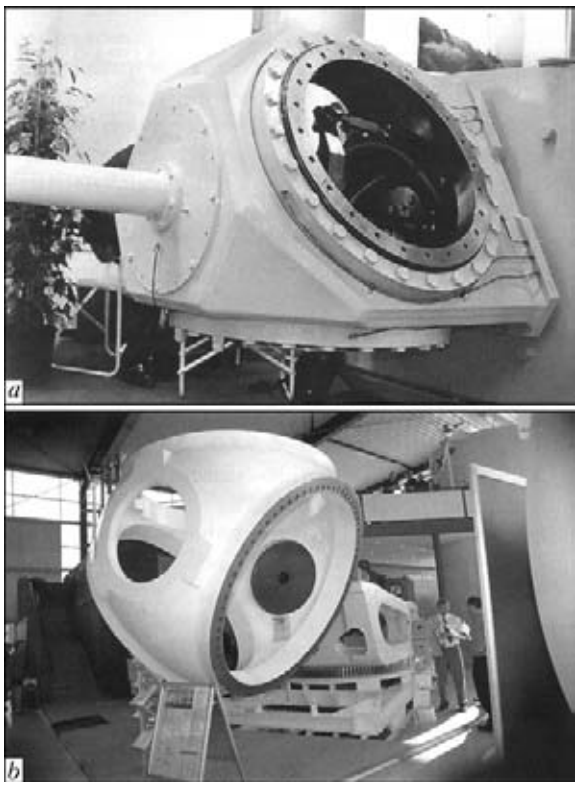

Figure 2. Appearance of a bushing of wind generator rotor: *a* — welded structure from sheet steel; *b* — casting from spheroidized cast iron of 15 t mass

Figure 3. Mounting a powerful wind generator nacelle on wind generator tower

the nacelle and rotor bushing are made in the form of heavy castings from spheroidized cast iron, one-piece or sectioned, welded by MAG-process, as well as from forged steel elements, joined by MAG, and sheet steel, most often S355 NL [11–20]. Generator rotor (bushing and blades) is a more expensive component of wind generator and at the same time a component, of which super high reliability requirements are made. Technologies of making rotor bushings from composite materials are developed [25]. Currently applied main production processes in manufacturing of wind generator structure elements are given in Table 3.

Note that one of the main technological features of EurouUnion Program «SET-Plan Wind Energy» is construction of sea wind generators of up to 20 MW power at simultaneous lowering of energy production costs. Analysis of documents [1–9] shows that the fundamental and applied research in the field of materials technology should be focused on improvement of modern structural materials, and, therefore, also welding technologies and materials. Main structural elements of high-power wind generators (more than 2 MW), such as rotor, nacelle and tower, should be

Figure 4. Constructions of wind generators with their base in the sea coastal strip (*a*) and floating ones (*b*)

Table 1. Wind generators of maximum power from different manufacturers and their parameters [13–18]

Wind generator	Electric power, MW	Rotor diameter, m	Tower type	Tower height, m
VESTAS-V112-3.0	3.0	112	Steel pipe	Depending on location
ENERCON-E126	7.5	127	Tubular, steel	135
GAMESA-G128-4.5 MW	4.5	128	Tubular — steel or stressed reinforced concrete	120
SIEMENS SWT-3.6-107	3.6	107	Tubular, steel	80 or depending on location
REPOWER-6M	6.15	126	Same	100–117 on land 85–95 at sea
GE WIND ENERGY GE 4.0	4.0	110	»	No data
SET-Plan	20.0	160–250	No data	120–160
Note. Sea wind generator VESTAS-V112-3.0 has the following nacelle size, m: 6.8 height, 12.8 length, 4.0 width.				

Table 2. Weight fraction and fraction of costs for the main structural elements of wind generators [1–24]

Structural element	Tentative mass of turbines of 2–3 MW power, t	Weight fraction, %	Cost fraction, %	Material
Tower	200	50–68	10–25	Steel, stressed reinforced concrete
Entire nacelle (load-carrying structure + transmission + generator)	70	25–40	40–65	Steel, copper, aluminium, special metal alloys, etc.
Load-carrying nacelle structure	11.5 (cast-welded structure)	6–8	No data	Steel, spheroidized cast iron
Rotor	40	10–20	20–30	Steel, spheroidized cast iron, fiberglass plastic or plastic reinforced by carbon fibre, wood and epoxy resins
Rotor bushing		6.5–7.0	No data	Spheroidized cast iron
Three blades		No data	Same	Fiberglass plastic or plastic reinforced by carbon fibre, wood and epoxy resins

made from materials with a high specific fatigue strength at simultaneous lowering of manufacturing costs. To fulfill these requirements, the purpose of fundamental and applied research should be lowering of the mass of rotor (bushing + blades), nacelle (drive shaft, transmission, generator, control system, rotor unit drive) and tower.

Figure 5. Appearance of the first free-floating wind energy turbine of Siemens and StatoilHydro installed on September 8, 2009 in the North Sea

Towers of powerful generators, both sea and ground, are an element subjected to the highest fatigue load. At present towers are built from thick-walled pipes of a conical shape with a about 3 % convergence, more seldom with a truss structure (made by RUUKI in Europe» [19]), as well as hybrid structure (reinforced concrete or completely concrete) [18–22]. When mounting sea wind generators, one of the most complicated technological problems is development of the technology of mounting tower elements and their base structure on the sea bottom, as well as technology of fastening to the bottom at great depth, or realization of floating tower structure (see Figures 4 and 5). All the world and European programs are focused on applied studies to find tower design solutions, mounting its elements, as well as development and application of composite materials with very high yield point, providing an essential increase of strength properties, lowering of wind tower mass and product cost [1–26]. More than 90 % of the constructed towers of powerful wind generators are made from low-alloyed steels, mainly, of type S355 NL ($\sigma_{0.2}$ = 345–355 MPa) [11–23]. The basic technology of producing welded joints

Table 3. Main production processes of fabrication of wind generator structural elements and technological tasks

Structural element	Base material	Manufacturing processes	Ttechnological tasks
Tower	Steel	Continuous casting with controlled rolling, welding	Production of higher quality steel with better weldability, high-quality welding consumables, lowering of production costs, development of high-quality welding technologies
Load-carrying nacelle structure	Same Cast iron	Continuous casting with controlled rolling, welding, casting	Production of steel of a higher quality and better weldability, high-quality welding consumables, lowering of manufacturing costs. Mastering the technology of casting cast iron large-sized billets, improvement of their quality
Rotor bushing	Steel Cast iron Composite materials	Forging, casting, welding	Production of steel of a higher quality with better weldability, high-quality welding consumables, lowering of production costs. Mastering the technology of casting cast iron large-sized billets, as well as technology of fabrication of high-quality structures from composite materials

in the processes of manufacturing powerful wind generators is automatic submerged-arc welding [29–35]. At the same time, also investigations on welding technology are performed for mounting tower steel elements instead of expensive bolted joints [27, 28], although steels with good weldability with 1100–1300 MPa yield point (WELDOX 110 and WELDOX 1300) and up to 25.4 mm plate thickness are available in the European market.

It is expedient to complement the EuroUnion «SET-Plan Wind Energy» Program, which is now at the stage of development of basic and applied research, with the following: investigation of the technology of laser hybrid welding of butt and tee joints of plate metal from steel with a high yield point both in the shop and in the conditions of tower section mounting (instead of bolted joints) [36–56]; investigations on development of high-quality filler materials for laser hybrid welding of steels with a high yield point [52–56]; investigations on the technology of rotational friction welding of butt and tee joints of plate metal from steels with a high yield point in the shop conditions of mounting tower sections (instead of bolted joints) [57–63]; investigations of technology of MAG welding with self-shielded flux-cored wire (SSA method) of butt and tee joints of thick-walled high-quality castings of rotor bushings and nacelle load-carrying structure from steel castings and cast iron; investigations of technological conditions of laser and hydroabrasive cutting of plate metal from steels with a high yield point.

1. (2010) Global gaps in clean energy R&D: Update and recommendations for international collaboration. In: *IEA Report for the Clean Energy Ministerial*.
2. Fichaux, N. Delivering today the energy of tomorrow. *http*://www.windplatform.eu/fi-leadmin/ewetp_docs/Events/Europ ean_Wind_Initiati-ve_JP.pdf
3. (2010) Energy. In: *Ann. report 2010 on public grants from energy research programmes ForskEL, EDDP/ERP, ELforsk, DSCR energy and environment and energy projects of the Danish National Advanced Technology Foundation*.
4. Beurskens, J. Developing offshore wind energy now and in the future. *http*://www.we-at-sea.org/leden/docs/conference2010/l.pdf
5. (2009) TPWind: The way forward. In: *6th Frame Work Programme*, March.
6. Profile of the Danish wind industry. *http*://www.e-pages.dk/windpower/21/
7. RenewableUK (BWEA). *http*://www.bwea.com/pdf/publicat ions/CapReport.pdf
8. Doing business with wind turbine manufacturers. *http*://www.bvgassociates.co.uk/LinkClick.aspx?fileticket=YceP A-zeHDQc%3D&tabi- d=101
9. American wind power surmounted challenges in 2010. *http*://www.awea.org/rn_release_0 1-06-l l.cfm
10. AWEA 3rd Quarter 2010 Market Report. *http*://www.awea.org/documents/r eports/2010_third_quar-ter_report.pdf
11. Winds of change. A manufacturing blueprint for the wind industry. *http*://www.awea.org/ la_pubs_reports.cfm
12. (2010) *WindVision 2025. A strategy for Quebec*. Canadian Wind Energy Ass.
13. VESTAS V 112 3.0 MW offshore. *pdf.www*.vestas.com
14. ENERCON wind energy converters. Products overview. *pdf. www*.enercon.de
15. GAMESA G128-4,5 MW. *pdf.www*.gamesacorp.com
16. SIEMENS wind turbine. New dimensions. *pdf.www*.siemenswindpower.com
17. Repower system. The 5 MW megawatt power plant with 126 meter rotor diameter: Technical data. *pdf. www*.repower.com
18. GE power & water. *pdf. www*.gewindenergy.com
19. Ruukki wind towers. *Reaching the heights with Ruukki. Ruukki- Engineering-Wind-tower-reaching-the-heights.pdf*
20. Acona, D., Weigh, J. (2011) Wind turbine materials and manufacturing fact sheet. *US Dep. of Energy*, 1–8.
21. Aldeman, M. Building the wind turbine supply chain: The next steps workshop. *http*://renewableenergy.illinois-state.edu/wind/conferences/
22. Gudmestad, O.T., Sarkar, A. (2010) Offshore deployment and marine operation for offshore wind turbines. In: *NORCOWE WP3 Meeting Proc*. (7 June 2010).
23. Fischer, T., Kuhn, M. (2010) Importance and mitigation of loading on offshore wind turbines on monopole support structures in cases of non-availability. In: *Proc. of 20th Int. Offshore and Polar Energy Conf*. (Beijing, 20–25 June 2010), 644.
24. Chou, J.-S., Tu, W.-T. (2011) Failure analysis and risk management of a collapsed large wind turbine tower. *Eng. Failure Analysis*, **18**, 295–313.
25. Innovative composite hub for wind turbines. *http*://cordis.europa.eu/data/PROJ _FP5/ACTIONeq DndSESSIONeqll2362005919nd DOCeql021ndTBLeq EN_PROJ.htm
26. (2010) RAPORT. In: *Energetyka wiatrowa w Polsce*, Nov.
27. 166 Sprawozdafi projektow wykonanych w ramach funduszy badawczych Unii Europejskiej — programu WIND ENERGY. *http*://cordis.europa.eu/
28. (2010) *RFSR-CT-2006-00031: High-strength steel tower for wind turbine*: Final report.
29. Paschold, R., Dirksen, D. (2005) Submerged arc welding of steels for offshore wind towers. *Svetsaren*, 60(**1**), 13–17.
30. Torstensson, B., Ivarson, P. (2005) ESAB welding solutions for windmill tower production. Processes and equipment for increased productivity. *Ibid*., 60(**2**), 14–19.
31. Efficient welding in the wind tower manufacturing industry. In: *ESAB Brochure XA00126920*.

32. Man, E., Lafleur, W. (2008) SIF Group at the foundation of Dutch wind energy. *Svetsaren*, 63(**1**), 18–22.
33. Sharpe, M. (2009) Robotic fabrication of wind turbine power generators. *Welding J.*, 88(**8**), 40–44.
34. (2009) Wind turbine welding system uses linear motion modules. *Ibid.*, 88(**8**), 50–51.
35. Wind energy. An Oerlikon market solution. In: *Brochure Air. Liquid. Welding.*
36. (2009) *RFSR-CT-2005-00042. Fatigue behavior of high strength steels welded joints in offshore and marine systems*: Final report.
37. (2009) *RFSR-CT-2006-00029. Improvement in steel utilization and manufacturing by recent break-through in high-power fibre laser welding*: Final report.
38. Thorny, C., Sepold, G., Seefeld, T. et al. (2002) Industrial implementation of laser/GMA welding and mechanical properties of the welds. In: *Proc. of Supermartensitic Stainless Steels Conf.* Brussels: KCI, 147–155.
39. Sepold, G., Thorny, C., Seefeld, T. et al. (2003) CO_2-laser GMA hybrid welding — Aspects of research and industrial application. In: *Proc. of Lasers in Manufacturing Conf.* Stuttgart: AT-Fachverlag, 149–156.
40. Staufer, H. (2004) Laser hybrid welding of ships. *Welding J.*, 83(**3**), 39–43.
41. Thorny, C., Seefeld, T., Vollertsen, F. (2005) Application of high-power fibre lasers in laser and laser-MIG welding of steel and aluminium. In: *Proc. of IIW Ann. Assembly Conf.* (Prague, 10–16 July 2005), 88–98.
42. Staufer, H., Graf, T. (2003) Laser hybrid welding drives VW improvements. *Welding J.*, 82(**1**), 42–48.
43. Reutzel, E.W. et al. (2006) Joining pipe with hybrid laser-GMAW process: Weld test results and cost analysis. *Ibid.*, 85(**6**), 66–71.
44. Staufer, H. (2006) Laser hybrid welding and laser brazing at Audi and VW. *Welding in the World*, 50(**7/8**).
45. Ozden, H. (2007) Investigating fiber lasers for shipbuilding and marine construction. *Welding J.*, 86(**5**), 26–29.
46. Staufer, H. (2007) Laser hybrid welding in the automotive industry. *Ibid.*, 86(**10**), 36–40.
47. Defalco, J. (2007) Practical applications for hybrid laser welding. *Ibid.*, 86(**10**), 47–51.
48. Stridh, L.-E. (2007) Welding of 13 % Cr-steels using the laser-hybrid process. *Svetsaren*, 62(**1**), 34–36.
49. Ohlsen, F. (2009) *Hybrid laser arc welding*. Cambridge: Woodhead.
50. Li, C., Muneharua, K., Takao, S. et al. (2009) Fiber laser-GMA hybrid welding of commercially pure titanium. *Materials and Design*, **30**, 109–114.
51. Kelly, S.M. et al. (2009) Using hybrid laser arc welding to reduce distortion in ship panels. *Welding J.*, 88(**3**), 32–36.
52. Wind tower consumable selection guide. *www*.lincolnelectric.com
53. *http*://content.lincolnelectric.com/pdfs/products/literature/mc05114.pdf
54. *http*://www.bernardwelds.com/articles/article4.htm http
55. *http*://weldingdesign.com/process es/news/wdf_11004/
56. *http*://www.hobartbrothers.com/aboutus/fillermetals_high-strength_pipe/
57. Linert, T.J. et al. (2003) Friction stir welding studies on mild steel. *Welding J.*, 82(**1**), 1–9.
58. Ozekcin, A. et al. (2004) A microstructural study of friction stir welded joints of carbon steels. *Int. J. Offshore and Polar Eng.*, 14(**4**), 284–288.
59. Norris, I.M., Thomas, W.M., Martin, J. et al. (2007) Friction stir welding — Process variants and recent industrial developments. In: *Proc. of 10th Int. Aachen Welding Conf. on Welding and Joining, Key Technologies for the Future* (Aachen, 24–25 Oct. 2007).
60. Defalco, J., Steel, R. (2009) Friction stir process now welds steel pipe. *Welding J.*, 88(**5**), 44–48.
61. Santos, T.F. (2009) A friction stir welding of UNS S32205 duplex stainless steel. In: *LNLS Activity Report*.
62. Saeidet, T. et al. (2010) EBSD investigation of friction stir welded duplex stainless steel. *World Academy of Sci., Eng. and Techn.*, **61**, 376–379.
63. Feng, Z. et al. (2005) Friction stir spot welding of advanced high-strength steels — A feasibility study. In: *SAE Int. Report 01-1248*.

INCREASE OF STRENGTH CHARACTERISTICS OF SPIRALLY-WELDED PIPES OF STRUCTURAL DESIGNATION

A.S. PISMENNY, A.S. PROKOFIEV, R.S. GUBATYUK, A.A. PISMENNY, V.V. POLUKHIN, R.V. YUKHIMENKO and **A.R. GAVRIK**

E.O. Paton Electric Welding Institute, NASU, Kiev, Ukraine

Influence of high-temperature thermomechanical treatment (HTTMT) on strength properties of welds on spirally-welded pipes made from 08kp (rimmed) steel of 1 mm thickness was studied. It is shown that HTTMT of welds in low-carbon steel joints allows producing sound welded joints of pipes with high service properties.

Keywords: *high-frequency welding, spirally-welded pipes, weld, weld strength, blank of structural designation, calculation technique, tread rings, samples*

High requirements made to manufacture and operation of hulls from seamless pipes operating under pressure is a well-known fact [1]. A prime cost of manufacture of the seamless pipes, however, is higher than that of the welded ones, therefore, it is reasonable to evaluate the perspectives of application of spirally-welded pipes (SWP) for manufacture of pressure vessel hulls. High-frequency welding (HFW) as a high efficient and low waste process of joining is applied for manufacture of SWP of various diameters [2].

Usage of HFW in SWP manufacture allows:

- produce various diameter pipes from a strip of equal width due to change of angle of weld inclination in a welded joint;
- produce large diameter pipes and tubular welded structures using relatively simple technological process in comparison with manufacture of longitudinally-welded pipes;
- produce thin-wall pipes of large diameter with high accuracy;
- provide low investments.

A tendency of increase of the requirements to quality of welded pipes, in particular, on index of strength

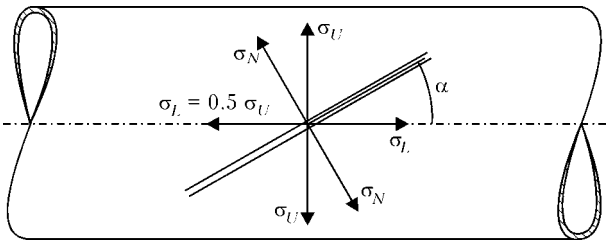

Figure 1. Scheme of stresses affecting spiral weld: σ_N — normal; σ_L — longitudinal; σ_U — circumferential stress

of welded joints [3] is observed at present time. In this connection improvement of HFW by means of automation, respectively, of the welding process as well as the operations for manufacture control [4] and its combination with thermomechanical treatment should be considered for the evaluation of perspective of SWP application as an alternative of the welded pipes.

Optimum relationships of pressure of medium being transported and specific quantity of metal of the high-pressure vessels are to be followed for obtaining of acceptable economic indices in operation of high-pressure tanks. This is directly related to the strength indices of applied grades of steels and strength of pipe welds [5].

High speed of welding in comparison with arc processes and capability of manufacture of thin-wall and specifically thin-wall pipes, having ratio of diameter to wall thickness 50 and more, should be referred to significant advantages of SWP manufacture as a result of development and improvement of HFW method.

Formation of a weld in the process of HFW takes place in an electric welding pipe mill, where rate of deformation in obtaining of welded joint can be realized in a range from 15 to 65 % and more depending on blank material and necessary level of contact pressure for removing of a low-melt phase [6–8].

The weld is formed under pressure in a solid phase at submelting of the welded edges that increases area of the weld and promotes minimization of its thickness

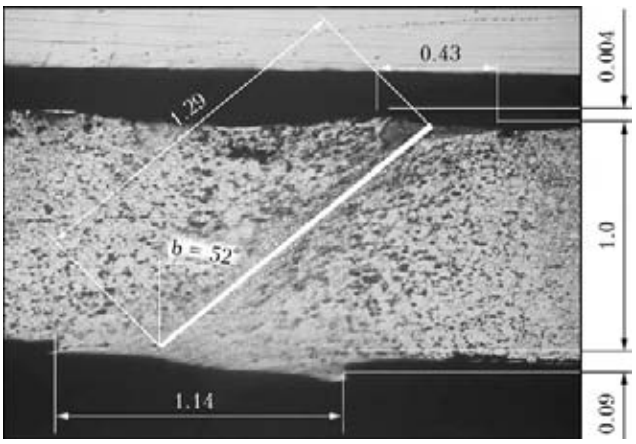

Figure 3. Transverse macrosection (×30) of SWP joint (face of SWP — below)

directly in a process of upsetting, i.e. oncoming mutual deformation of heated edges of the items, in compressed space, and further rolling of edges. At the same time the process of weld formation takes place under conditions of guided flow and deformation of the metal of edges at their mutual sliding over various mating surfaces under complex spatial conditions in the electric welding pipe mill.

Weld zone is the most important element in SWP. Longitudinal welds are exposed to higher loads than transverse ones as a result of internal pressure in operation. In this case the spiral weld takes to some extent intermediate position. Its under load stress value depends on angel of the weld to axle of the pipe (Figure 1). At that the loads affecting it make 60–70 % of the loads affecting longitudinal weld [9].

The spiral weld in a process of formation is exposed to complex influence of a series of factors [10, 11], i.e. bending of initial metal of the strip along a radius of produced pipe; strip stretching at an angle of inclination of spiral weld to generant of produced pipe; rolling of obtained weld; differentiated heating of base metal as well as welded edges in welding; forced cooling of obtained weld; heating for removing of residual stresses and normalizing of weld metal structure.

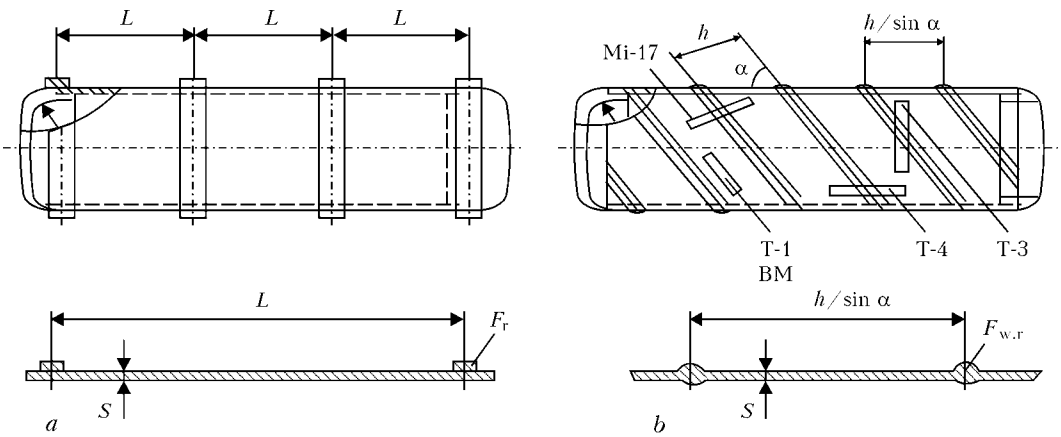

Figure 2. Scheme of cutting out of samples: *a* — hull from thin-wall pipe and with thread rings; *b* — same, but from SWP; T-1 — samples from base metal; Mi-17 — samples of welded joint with classical positioning of weld; T-4 — samples Mi-18 with oblique-like welded joint cut out along generant of SWP; T-3 — samples Mi-18 (special) with oblique-like welded joint cut out along radial surface of SWP; F_r, $F_{w.r}$ — area of thread ring and weld reinforcement, respectively

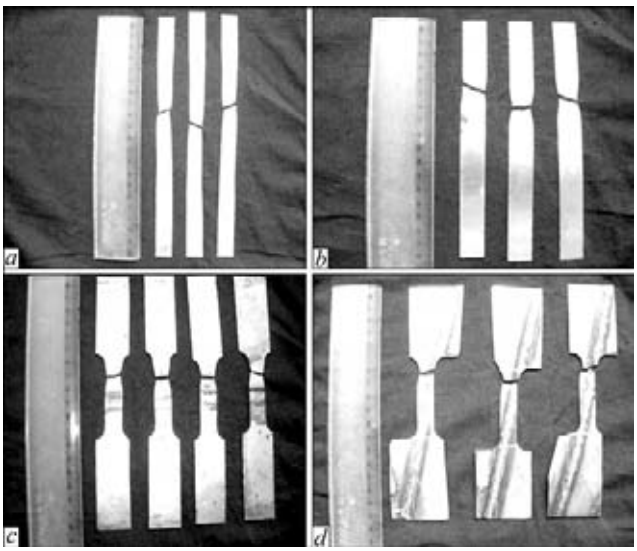

Figure 4. Appearance of the samples T-1 (*a*), Mi-17 (*b*), T-4 (*c*) and T-3 (*d*)

It should be taken into account that edges of the strip are cold-hardened as a result of cutting of roll of sheet for strip, thus, their welding is performed in hardened state, and weld temperature reaches 1200 °C in the process of HFW, i.e. metal of SWP is exposed to HTTMT during welds' performance.

The aim of the present work lies in evaluation of influence of HTTMT on strength properties of SWP. For this SWP with the welds exposed to HTTMT were manufactured on laboratory unit at the E.O. Paton Electric Welding Institute.

The areas with various positioning of the spiral weld (Figure 2) were chosen over a body of SWP. The samples cut out from the body of SWP were used for investigations, determination of strength properties and performance of metallographic investigations.

Diameter of SWP made from 08kp steel was 108.3 mm; thickness of used strip S = 1 mm; width of used strip h = 101 mm; inclination angle of spiral weld to generant of the produced pipe $\alpha = 25°$.

Figure 3 shows a macrosection of a joint. Welded edges of the strip with a lap heated with high frequency currents were delivered into the welding rolls, where upsetting with removing of submelted metal took place, and then the weld formed was exposed to rolling at high temperatures. The weld in cross-section

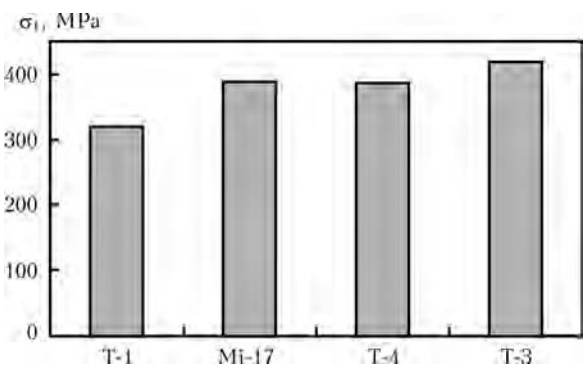

Figure 5. Tensile strength of the samples tested in accordance to cutting scheme (see Figure 2)

deviated from a vertical line per angle β, approximating to 52° as a result of complex plastic strain. At that its length made 1.29 mm at base metal thickness 1 mm that significantly improves the conditions of failure resistance of the welded joint [12].

External weld reinforcement made 0.9 mm, width was 1.14 mm, and internal one equaled 0.04 mm at width 0.43 mm. At that upset force made 1600 H and area of contact spot was 1 mm^2.

The following samples in accordance with DSTU 3245–95 [13] (see Figure 2) [14] were chosen from the produced pipe: T-1 — 3 pcs, Mi-17 — 3 pcs, T-4 — 4 pcs, T-3 (Mi-18) special — 3 pcs, and were exposed to tensile tests.

Tensile strength of T-1 sample made 320 MPa; Mi-17 — 404.4, 380.7, 383.2; T-4 — 384.2, 389.5, 390.5, 394.4; T-3 — 445.4, 407.3 and 408.4 MPa.

Failure of all samples took place along the base metal (Figure 4). Formation of Chernov lines (Luders' lines) (Figure 4, *b*) indicate the presence of displacements of surface layers of metal under effect of circumferential stresses σ_U (see Figure 1) [15]. It can be seen from Figure 5 that normal and longitudinal stresses (σ_N and σ_L) of the weld samples (see Figure 1) exceeded standard failure stress of the base metal samples by 22 % and circumferential stresses σ_U by 30 %, that is, obviously, caused by HTTMT.

Four samples were cut out from SWP for performance of metallographic investigations of the hardened weld. They included sections of spiral weld and were taken uniformly along the length of welded structure.

Macrostructure of a weld zone shows no lacks of fusion, discontinuities, pores and other defects at large magnification.

It is determined that structure of the base metal near the HAZ is polygonal ferrite with carbon precipitates along the grain boundaries in a form of tertiary cementite [16] as well as separate round carbide inclusions.

Change of the structure from pure ferrite to ferrite-pearlite is observed further at transfer from the base metal to weld direction. At that, the round inclusions of cementite gradually dissolve and pearlite revealing in a form of spots with higher etching than ferrite (see Figures 3 and 6, *a*) is formed at their place.

The closer to the weld, the higher is the process of pearlite formation at former places of carbide accumulation (Figure 6, *b*). Change of HAZ metal structure from ferrite to ferrite-pearlite is an evidence of heating of metal in this zone up to temperature of dissolution of iron carbide (over A_{c_1} point) with subsequent cooling [16].

Hardness of this ferrite-pearlite structure somewhat higher than that of ferrite in the base metal structure and makes, approximately, *HV* 180–200, i.e. exceeds hardness of the base metal by 12–25 %. Hardness of the base metal is on the level of *HV* 160, and size of grains larger than in the weld metal (see Figure 6).

Metal in the weld region (Figure 6, *b*) has ferrite structure with uniformly distributed carbides, size of the grains is smaller than in the base metal and HAZ, that is an evidence of heating up to temperature field of homogeneous austenite, i.e. exceeding A_{c_3} point [16]. Hardness of this area is higher than base metal hardness and makes around *HV* 180–190.

It is determined that hardness of weld and HAZ metal exceeds that of the base metal by 12–25 % (Figure 7).

HTTMT affect causes metal hardening in the weld and near-weld zone. Application of HTTMT promotes hardening of the weld metal in SWP, that in turn increases strength indices of pipe itself as a blank of structural designation.

Method for calculation of indices of strength of SWP with weld exposed to HTTMT was approved at the E.O. Paton Electric Welding Institute for evaluation of influence of treatment on strength indices of SWP itself as a blank of structural designation. Existing and approved techniques [1, 12, 15, 17] were used for calculation. At that the strength indices of SWP were compared with those of seamless pipe of similar geometry.

The following allowances were accepted:

• pipe blanks have similar geometry, diameter and wall thickness *S*;

• both pipe blanks withstand similar internal pressure *P*;

• hardning was observed in weld zone as a result of HTTMT of SWP, i.e. strength indices in the weld are higher than in the base metal;

• the calculation were performed taking into account sequential installation of external thread rings

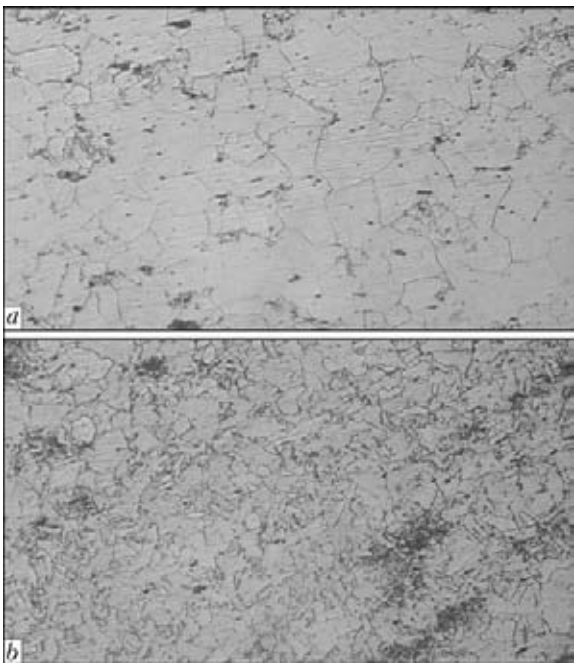

Figure 6. Microstructure (×400) of the base (*a*) and weld metal (*b*)

(effect of thread rings equal to effect of hardened weld in SWP) over the pipe blank, manufactured from seamless pipe, for compensation of effect of hardened weld in the blank from SWP.

The calculations performed showed that:

• the external thread rings are to be installed in series over the pipe blank with calculated distance *L* for preventing the loss of shape of pipe blank manufactured from seamless pipe under effect of limiting external pressure *P*;

• distance *L* between the external thread rings over the pipe blank, manufactured from seamless pipe,

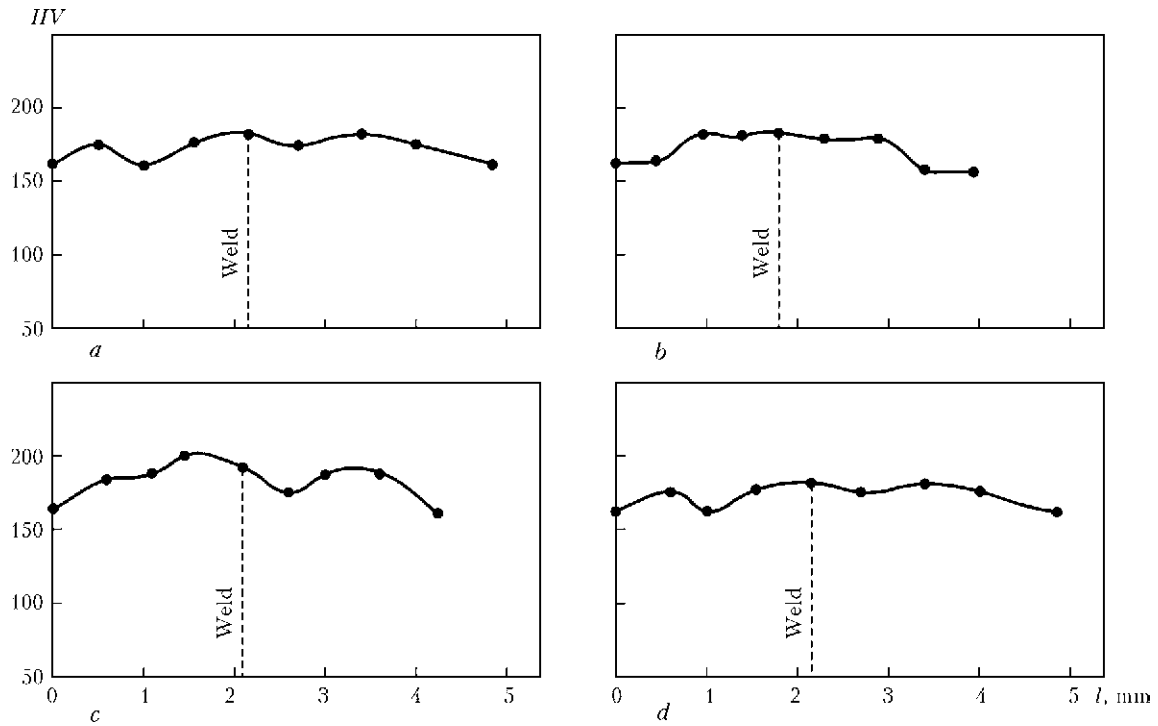

Figure 7. Hardness distribution across the welded joint: *a* — sample T-1; *b* — Mi-17; *c* — T-4; *d* — T-3

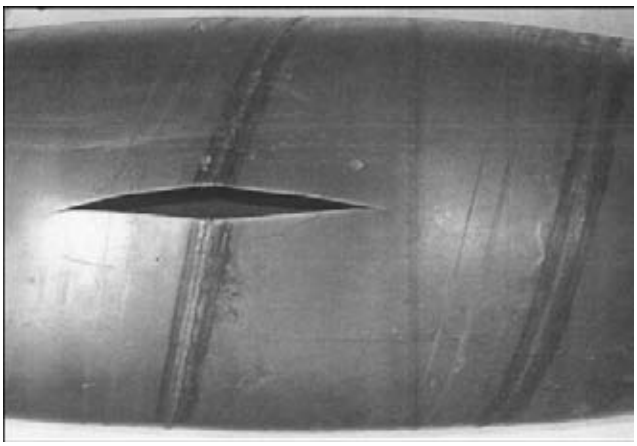

Figure 8. Failure of cylindrical surface of hull

should exceed 2 or more times (depending on steel grade) distance between the winds of the hardened weld $h/\sin\alpha$, i.e. $L > h/\sin\alpha$; density of strip winding increases at $h/\sin\alpha \to 1 << L$ and strength of welded SWP rises, correspondingly;

• sum effect of the hardened weld exceeds strengthening effect of the thread rings per unit of length of SWP.

Results of calculations were experimentally verified using a real sample of SWP. Fragment of SWP with welded-in blind plugs was used as a model of pressure vessel which was pressurized using internal pressure and brought to failure [1]. Hydrostatic failure pressure exceeded calculated one by 18 % in failure of the model of vessel hull. The vessel hull acquired barrel-like form that is an evidence of shape loss. The failure itself took place along the generant of cylindrical surface of the hull, i.e. along the base metal (Figure 8).

CONCLUSIONS

1. Weld, exposed to HTTMT, acquires a gain factor equal 1.22–1.31 relative to the base metal, and hardness exceeds that of the base metal by 12–15 %.

2. Failure stress of the samples with weld exceeds standard stress of failure of the base metal samples by 22–30 %.

3. HTTMT of the welds in SWP from structural low-carbon steels, in particular 08kp, allows obtaining quality joints with high service indices that increases structural strength of SWP by 18 %.

4. Designing and manufacture of welded structures using SWP as a blank of structural destination acquire further investigation as for higher strength steels.

1. (1976) *Safe operation of vapor boilers, vessels and pipelines*. Ed. by V.I. Chernega. Kiev: Tekhnika.
2. Gulyaev, G.I., Semenov, O.A., Shvedchenko, A.A. et al. (1989) *Creators of steel arteries*. Dnepropetrovsk: Promin.
3. Kiuchi, M. (2011) Novel tendencies in production of arc welded pipes. *Novosti Chyorn. Metallurgii za Rubezhom*, **1**, 55–58.
4. Wiebe, J., Scheller, W. (2010) Blick ueber den Tellerrand. *Praktiker*, **6**, 248–251.
5. (2009) At OJSC Uraltrubprom was set in operation the arc welding pipe mill 630 for production of arc welded pipes. *Svarshchik*, **4**, 5.
6. Tabelev, V.D., Kareta, N.L., Panasenko, A.I. et al. (1985) Structure and phase composition of welds made by capillary soldering under pressure. *Avtomatich. Svarka*, **11**, 26–29.
7. Lebedev, V.K., Tabelev, V.D., Pismenny, A.S. (1993) Impact toughness of butt joints soldered with plastic deformation of base metal. *Ibid*., **8**, 29–31.
8. Tabelev, V.D. (1991) On formation of joints in soldering with plastic deformation of base metal. In: *Consumables and technology of soldering*. Kiev: PWI.
9. Annenkov, N.I., Kolyupanov, O.V. (1996) State-of-the-art of production and applications of spirally-welded pipes. *Stroitelstvo Truboprovodov*, **4/5**, 12–18.
10. Efimov, O.Yu., Yuriev, A.B., Ivanov, Yu.F. et al. (2008) Thermomechanical strengthening of large diameter fittings. *Izvestiya Vuzov, Chyorn. Metallurgiya*, **12**, 49–53.
11. Kolbasnikov, N.G., Zotov, O.G., Duranichev, V.V. et al. (2009) Effect of high deformations in hot state on structure and properties of low-carbon steel. *Metalloobrabotka*, **4**, 25–31.
12. Majzel, V.S., Navrotsky, D.I. (1973) *Welded structures*. Leningrad: Mashinostroenie.
13. (2003) *DSTU 3245–95*: Welded steel cylinders for liquefied carburated hydrogen gases at pressure up to 1.6 MPa. General technical requirements. Kyiv: Derzhspozhyvstandart.
14. (1983) *Catalogue of specimens for testing of metals*. Ed. by V.K. Lebedev. Kiev: PWI.
15. Pisarenko, G.S., Agarev, V.A., Kvitka, A.L. et al. (1973) *Resistance of materials*. Kyiv: Vyshcha Shkola.
16. Goudremont, E. (1959) *Special steels*. Ed. by A.S. Zajmovsky, M.L. Bernshtejn. Vol. 1. Moscow: Metallurgiya.
17. *GOST 8696–74*: Spirally-welded pipes with spiral weld of general purpose.

COLD RESISTANCE AND LAMELLAR FRACTURE RESISTANCE OF WELDED JOINTS ON STEEL 06GB-390

V.D. POZNYAKOV, A.Yu. BARVINKO, Yu.P. BARVINKO, A.G. SINEOK and **A.N. YASHNIK**
E.O. Paton Electric Welding Institute, NASU, Kiev, Ukraine

The paper presents results of investigation of resistance of steel 06GB-390 to lamellar-tough and lamellar-brittle fractures, as well as of evaluation of impact toughness (KCV_{-40}) of the weld and HAZ metals of butt joints on this steel (as-welded and after heat treatment). The joints were welded in free and rigidly restrained states. It is shown that steel 06GB-390 is not susceptible to lamellar-tough and lamellar-brittle fractures, while impact toughness of the weld and HAZ metals of the butt joints hardly changes in any of the cases.

Keywords: *arc welding, low-alloy steels, oil storage tanks, HAZ metal, impact toughness, heat treatment of welded joint, welding in rigid contour, welding strains, lamellar fracture*

Because of fluctuations of oil prices in the world markets, the CIS and European countries are active in intensive construction of tanks with a capacity of 50,000–75,000 m^3. In the majority of cases such tanks have the basic and protective walls, this excluding the need for making fire dikes around each tank. As a rule, the 24–30 mm thick rolled plates of steels with $\sigma_y \geq 345$–440 MPa are used to manufacture the lower ring of the tank wall. The regulatory documents [1, 2] recommend steels 09G2S, 15G2ANNb, 10G2FB, 18G2AV etc. with a carbon content of 0.1–0.2 % and sulphur content of up to 0.035–0.040 % to be used to manufacture the lower rings of walls of high-capacity tanks. The long-term experience in construction and operation of different-capacity tanks made by using the above steels shows that reliability and performance of metal structures is at a high level, provided that requirements of these regulatory documents are kept to.

At the same time, new high-strength low-alloy steels of the 06GB (strength class 390) and 06G2B (strength class 440) grades have been intensively applied in the last years in Ukraine for fabrication of welded metal building structures. A distinctive feature of these steels is their low (almost 2 and 7 times lower than indicated in specifications [1, 2]) concentration of carbon and sulphur (Table 1), which should ensure their low sensitivity to cold cracking and, at the same time, high impact toughness at negative temperatures. This is confirmed by the data of study [3], which are indicative of the fact that steels 06GB and 06G2B in the quenched + tempered state at thickness of the rolled plates equal to 8–50 mm have a uniform structure across the plate section (Figure 1), high mechanical properties and high cold resistance (Table 2), and are characterised by good weldability [4]. Also, according to all indicators these steels are promising for fabrication of high-capacity tanks.

However, in selection of steels for fabrication of tanks it is necessary to take into account peculiarities of operation of individual structural wall and bottom elements. It is a known fact that, unlike the vertical and horizontal welds of the walls, the circumferential one-sided welds connecting branch pipes to the wall are made under the rigid contour conditions as well (Figure 2, section *1–1*). At wall thicknesses $t \geq 25$ mm, the volume of the deposited metal is sufficiently big, this causing substantial transverse shrinkage and for-

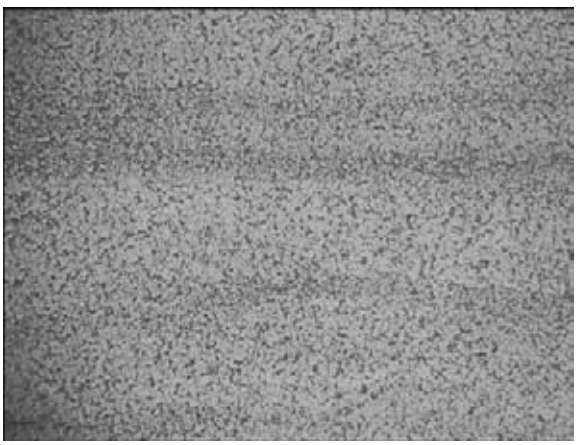

Figure 1. Microstructure (×100) of 26 mm thick rolled metal of steel 06GB

Table 1. Chemical composition of steels 06GB and 06G2B, wt.%

Steel grade	*t*, mm	C	Mn	Si	V	Nb	S	P	C_{eq}
06GB	26	0.06	1.27	0.20	0.037	0.014	0.004	0.007	0.29
06GB	30	0.07	1.27	0.27	0.036	0.013	0.005	0.006	0.31
06G2B	30	0.07	1.42	0.20	0.057	0.038	0.007	0.008	0.34

Table 2. Mechanical properties of steels 06GB (class 390) and 06G2B (class 440)

Steel grade	t, mm	σ_y, MPa	σ_t, MPa	δ_5, %	ψ. %	KCV_{-40}. J/cm^2	σ_y/σ_t
06GB	26	393	498	32.0	80.6	265	0.79
06GB	30	391	477	34.4	79.7	364	0.82
06G2B	30	467	554	33.5	80.4	303	0.84

mation of high residual stresses. Apparently, this may lead to formation of cold cracks in the weld metal. In addition, as the circumferential welds are inspected by the visual-optical method or by the dye penetrant method, this does not exclude the presence of sharp stress raisers in the welded joints, which may lead to decrease in their resistance to brittle and tough fractures. The probability of brittle fracture in the presence of high residual stresses and at low temperatures is evidenced by the data of study [5]. Study [6] also shows that increase in the level of residual stresses and formation of heterogeneous structure in the welded joint lead to a 20–25 % decrease in impact toughness. Moreover, as follows from studies [7, 8], plastic deformation plays a decisive role in probable initiation of not only the brittle fracture but also the tough one.

The stressed state of the welded joints between the strengthening cover plate and wall (Figure 2, section *2–2*) and in the assembly of welding of the thickened bottom edge of bottom box to the wall (Figure 3) is a bit different. Welding strains here act in a direction of the wall thickness and bottom, this initiating their lamellar cracking.

Formation of lamination is characteristic of the rolled plates at $t \geq 20$ mm. The key factor affecting formation of lamellar fractures is the presence of sulphide or oxide inclusions. They are extended in the process of rolling of the plates to form a stringer or laminated structure [9, 10]. Study [10] shows that the quality of steel in Z direction is well described by standard characteristics of ductility ψ_Z and impact toughness KCV. To eliminate lamination in welded structures the authors of study [11] recommend decreasing the sulphur content of steel to S ≤ 0.01 %, and in study [9] it is suggested that steels with S ≤ ≤ 0.007 % and $\psi_Z \geq 25$ % should be classed with those having high resistance, and steels with S > 0.020 % and $\psi_Z \leq 8$ % — with those having low resistance to lamellar cracking.

In this connection, it is necessary to evaluate resistance of rolled plates of steels of the 06GB and 06G2B types to formation of lamellar cracks, and resistance of welded joints to lamellar-brittle fracture, as well as check whether their cold resistance will change in welding in a rigid contour. So, investigations in this area became the purpose of this study.

Steel 06GB 20, 26 and 30 mm thick, and butt joints on this steel 26 mm thick were chosen as investigation objects.

Resistance of the steels to lamellar fracture was evaluated according to GOST 28870–90 by the results of tests of three specimens cut out from the welded joints made by manual arc welding using electrodes

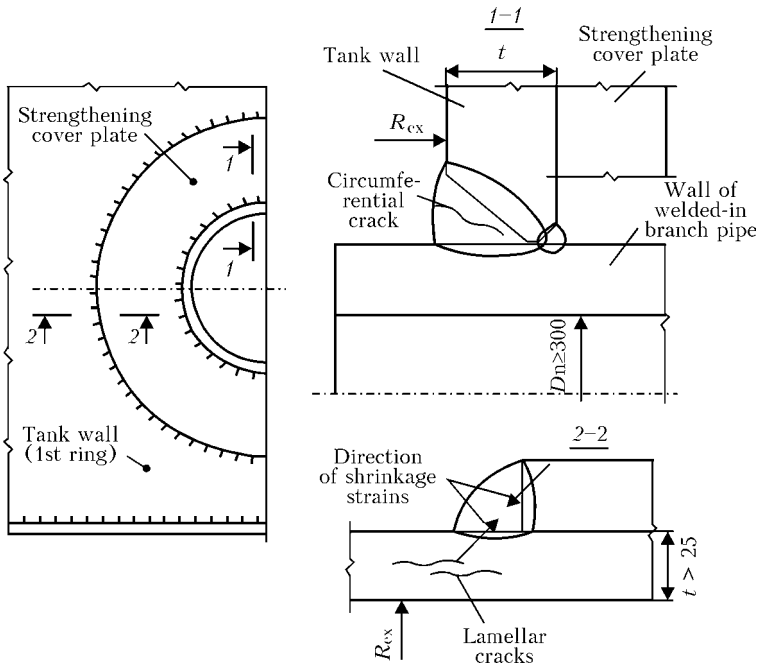

Figure 2. Schematic of the assembly of welding of branch pipe into the lower wall ring by indicating location of probable formation of lamellar cracks

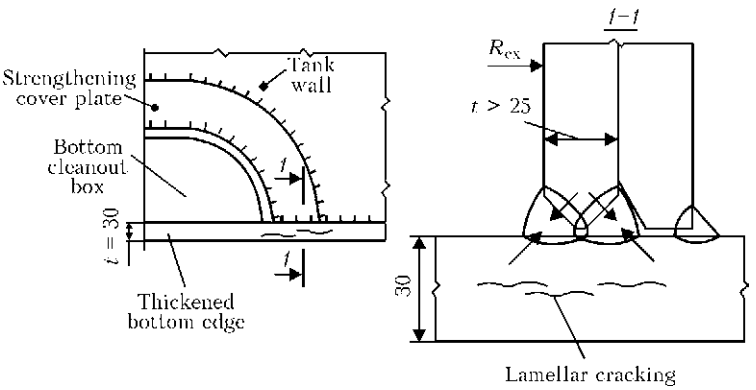

Figure 3. Schematic of formation of lamellar cracks in locations of joints between the wall and thickened edge of bottom cleanout box

Table 3. Results of tensile tests of 06GB steel specimen in *Z* direction

t, mm	σ_y, MPa	σ_t, MPa	δ_5, %	ψ, %
20	428; 437; 444 436	510; 513; 510 511	45.1; 45.9; 44.4 45.0	81.1; 78.8; 81.2 79.6
26	388; 388; 385 387,2	506; 506; 500 504	46.6; 48.1; 48.9 47.9	81.2; 81.1; 81.2 81.1
30	380; 358; 373 370	489; 482; 484 485	35.3; 36.8; 37.6 36.6	71.6; 69.7; 67.9 69.7

OK 53.70. Structural elements of the billets welded and shape of cross sections of the welded joints and welds met requirements imposed on the joints of the T8 type according to GOST 5264–80. Initial and end regions of the welded joints not less than 30 mm long were removed. Specimens for tests according to GOST 1497–84 were made from the remaining part of the welded joints. The scheme of cutting out of specimens is shown in Figure 4. The specimens were tested at +20 °C. The values of σ_y, σ_t, δ_5 and ψ_Z were determined during the tests. The test results are shown in Table 3.

Comparative evaluation of mechanical properties of steel 06GB, 26 and 30 mm thick, along (see Table 2) and across the rolled plate shows that this steel has no anisotropy of properties. By the value of reduction in area ψ_Z this steel can be classed with the top group of resistance to lamellar fractures, i.e. Z 35.

Resistance of welded joints on steel 06GB, 26 and 30 mm thick, to lamellar-brittle cracks was evaluated from the results of impact bend tests of the specimens (type IX according to GOST 9454–78) made from the cruciform welded joints, similar to those used for evaluation of resistance of the steel to lamellar fracture. The specimens from the 30 mm thick welded joints were made only in the as-welded state, while those from the 26 mm thick joints — also after their heat treatment (tempering at 620 °C for 2 h). The scheme of cutting out of specimens is shown in Figure 5. Notches on the specimens were made along the fusion line (FL), in the HAZ metal at a distance of 2 mm from FL, and in the base metal at a distance of 8 mm from FL. The specimens were tested at –40 °C.

Results of the impact bend tests of the specimens (Table 4) are indicative of the fact that tempering has no significant effect on impact toughness of both base metal and FL and HAZ regions of the welded joints. Cold resistance of HAZ metal of the welded joints on steel 06GB is at a level of the base metal ($KCV_{-40} \geq$ $\geq$ 220 J/cm^2), and is much in excess of the requirements given in specifications for the steel ($KV_{-40} \geq$ $\geq$ 98 J, which corresponds to $KCV_{-40} \geq$ 123 J/cm^2) [12]. Decrease in impact toughness, compared to the base metal, in FL of the welded joints was observed in all the cases. KCV_{-40} of the 26 mm thick joints on this steel in the as-welded state ranged from 42 to 305 J/cm^2 (the average value being 130.8 J/cm^2 by the results of testing seven specimens), while after high-temperature tempering it varied from 87 to

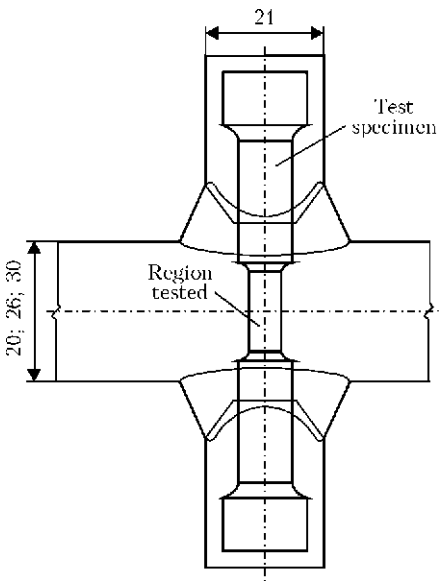

Figure 4. Scheme of cutting out of specimens from the welded joints made in accordance with GOST 28870–90

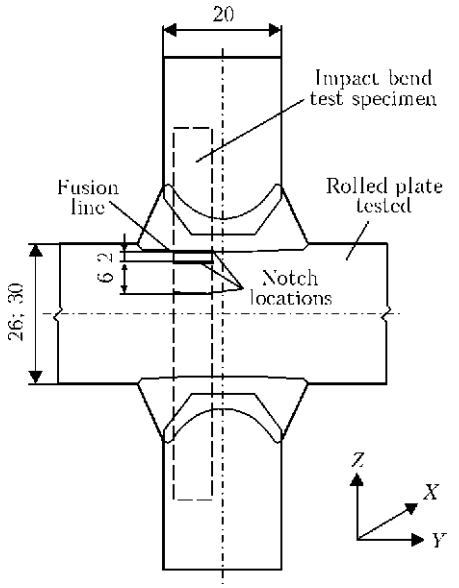

Figure 5. Scheme of cutting out of specimens from cruciform welded joints with indication of locations of notches

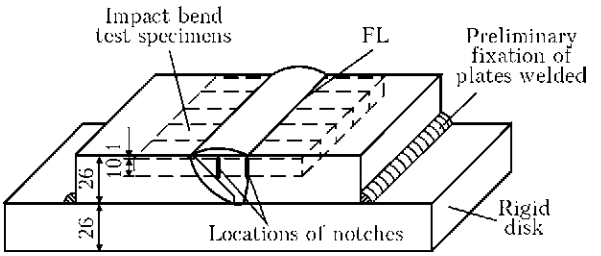

Figure 6. Scheme of cutting out of specimens from butt joints made in rigid contour with indication of locations of notches

197 J/cm^2 (the average value being 128 J/cm^2 by the results of testing three specimens). The almost 35 % lower values of impact toughness, compared to the base metal, were obtained in testing of the specimens with a notch made along FL, which were cut out from the 30 mm thick welded joints. This decrease can be explained by violation of homogeneity of chemical composition and structure of metal in the given region of a welded joint. At the same time, it should be noted that even in the as-welded state the values of impact toughness of the butt joints on steel 06GB were much higher than the level of the requirements imposed on the rolled plates recommended for fabrication of high-capacity tanks [2].

Special investigations were carried out to experimentally check the effect on cold crack resistance and impact toughness of the weld and HAZ metals of the welded joints by the rigidity of their restraining. Four butt joints (S8 according to GOST 5264–80) were made from the 26 mm thick plates by the developed welding technology using 4 mm diameter electrodes OK 53.70 and preheating to a temperature of 70 °C. Two of them were welded in the unrestrained state (joints 1 and 2), and another two (joints 3 and 4) — in the rigidly restrained state (Figure 6). As evidenced by the data of study [13], the value of residual stresses in the HAZ metal of such joints varies from 0.5 to 1.0 of yield stress of the base metal.

Table 4. Results of impact bend tests of specimens made from welded joints on steel 06GB in *Z* direction

t, mm	Notch location	KCV_{-40}, J/cm^2	
		As-welded	After heat treatment
26	FL	163; 253; 305; 98; 77; 42	87; 197; 101
	In HAZ metal (FL + 2 mm)	332; 294; 325; 345; 346; 347	348; 348; 347
	In base metal (FL + 8 mm)	321; 333; 328	347; 345; 345
30	FL	181; 281; 240; 85	–
	In HAZ metal (FL + 2 mm)	334; 335; 326; 223	–

Table 5. Results of impact bend tests of specimens made from 26 mm thick butt joints on steel 06GB

Welding condition	Heat treatment	KCV_{-40}, J/cm^2	
		FL	Weld metal axis
In unrestrained state	No	342; 371; 338 / 350	282; 246; 209 / 246
	Tempering	339; 340; 341 / 340	290; 240; 220 / 250
In rigidly restrained state	No	339; 342; 340 / 340	244; 251; 200 / 232
	Tempering	248; 341; 343 / 311	246; 246; 172 / 221

After welding, joints 2 and 4 were subjected to high-temperature tempering at 620 °C for 2 h. Then macrosections were made from all the welded joints to check the presence/absence of cold cracks in the welded joints, and specimens (type IX according to GOST 9454–78) were prepared for impact bend tests. Some specimens had notches in FL, and some — in the weld metal. Results of the impact bend tests of the specimens carried out at –40 °C are given in Table 5.

As indicated by analysis of the macrosections, all the welded joints were free from cracks, this evidencing high resistance of the welded joints on steel 06GB made by the above technology to cold cracking. Independently of the rigidity of restraining, impact toughness of the weld metal and overheated region of the HAZ metal of the said welded joints was several times higher than the requirements imposed on the rolled plates used to fabricate tanks for oil and oil products both in the as-welded state and after high-temperature tempering [14]. High-temperature tempering has no substantial effect on cold resistance of the welded joints on steel 06GB.

CONCLUSIONS

1. 20, 26 and 30 mm thick rolled metal of steel 06GB has high resistance to lamellar fracture. In reduction

in area, it can be classed with the top group of quality, i.e. Z 35.

2. Values of KCV_{-40} of the base and HAZ metals obtained from the results of standard tests of the specimens cut out from the welded joints on steel 06GB across the weld axis and in Z direction are almost identical, this evidencing their high resistance to lamellar-brittle fracture.

3. Welded joints on steel 06GB made by manual arc welding using electrodes OK 53.70 and preheating to 70 °C are characterised by high resistance to cold cracking.

4. Rigidity of restraining and high-temperature tempering have no substantial effect on cold resistance of the weld metal and overheated region of the HAZ metal of the welded joints on steel 06GB made by using electrodes OK 53.70. At a test temperature of –40 °C their impact toughness is several times higher than the requirements imposed on the rolled metal of welded tanks intended for storage of oil and oil products. The test results obtained allow a conclusion that the requirement to perform heat treatment of individual welded joints can be revised as the sufficient experience is accumulated in operation of the tanks using the said steels.

1. (1998) *API Standard 650*: Welded steel tanks for oil storage. 9th ed. Nov.
2. (2003) *PB 03-605–03*: Rules for designing of vertical cylindrical steel tanks for oil and oil products. Moscow.
3. Kovtunenko, V.A., Gerasimenko, A.M., Gotsulyak, A.A. (2006) Selection of steel for critical building welded structures. *The Paton Welding J.*, **11**, 27–31.
4. Mikhoduj, L.I., Kirian, V.I., Poznyakov, V.D. et al. (2003) Sparsely-alloyed high-strength steels for welded structures. *Ibid.*, **5**, 34–37.
5. Kennedy, H.E. (1945) Some causes of brittle failure in welded mild steel structures. *Welding J.*, **11**, 588.
6. Maccocaire, C. (1991) Repair welding: how to set up a shop. *Ibid.*, **8**, 54–56.
7. Stepanov, A.V. (1974) *Principles of practical strength of crystals*. Moscow: Nauka.
8. Bernshtejn, M.L., Zajmovsky, V.A. (1970) *Structure and mechanical properties of metals*. Moscow: Metallurgiya.
9. Hrivnak, I. (1982) Weldability of steels — state-of-the-art and technological projection. In: *Proc. of 11th Meeting of Coordination Center of CMEA countries-members* (Bratislava, May 1982).
10. Girenko, V.S., Bernatsky, A.V. (1985) Anisotropy of properties of rolled metal and serviceability of welded structures. *Avtomatich. Svarka*, **12**, 13–18.
11. Newly published specifications for lamellar tearing in Japan *Doc. IIW IX-1255–82*.
12. *TU U 27.1-05416923-085:2006*: Rolled plates welded from quality steel of 355–590 strength classes for machine-building. Introd. 04.02.2007.
13. Makhnenko, V.I., Poznyakov, V.D., Velikoivanenko, E.A. et al. (2009) Risk of cold cracking in welding of structural high-strength steels. *The Paton Welding J.*, **12**, 2–6.
14. *GOST 31385–2008*: Vertical cylindrical steel tanks for oil and oil products. General specifications. Introd. 2009.

IMPROVEMENT OF THE TECHNOLOGY FOR SUBMERGED-ARC WELDING OF COPPER TO STEEL

V.N. KOLEDA

E.O. Paton Electric Welding Institute, NASU, Kiev, Ukraine

The paper gives results of investigations of the effect of some techniques on iron content of the weld metal in copper to steel joints made by submerged-arc welding. A new method was developed for welding of copper to steel by using a split electrode consisting of different-diameter wires. The method allows controlling heat input into the copper and steel edges, simplifies the process of tracking the weld line by electrode, and provides the required quality of the welds.

Keywords: *submerged-arc welding, split electrode, two wires, dissimilar joints copper + steel, edge preparation, welding parameters, electrode displacement, mechanical properties of joints*

Wide application of copper as structural material at enterprises of metallurgical and electrotechnical industries involves a difficulty in providing high performance of the welded joints on copper parts operating under conditions of high temperatures, pressures, aggressive environments, etc. In particular, this concerns the welded joints between copper and steel, as these metals are characterised by different values of thermal conductivity, melting temperature and linear and volumetric expansion factors [1]. In this connection, it is a topical task to improve the technological processes used to join these metals.

As shown by analysis of literature data, submerged-arc welding is most promising for making of copper to steel joints 5–40 mm thick. This method is characterised by high productivity and high efficiency of the arc, and often allows welding of metals of medium and large thicknesses in one pass without preheating [2, 3]. Moreover, this process provides a high level of quality and consistency of properties of the welded joints, and features improved sanitary-hygienic working conditions. At the same time, one of the drawbacks of submerged-arc welding is that it is impossible to visually observe the weld metal solidification process.

When making the copper to steel joints under conditions of arc welding the steel edge is subjected to a direct effect by the arc. Penetration of the steel edge should be minimal to limit the iron content of the weld metal, provide the required ductility of the joints

and minimise the sensitivity of the weld metal to solidification cracking [4, 5].

Investigations of physical-mechanical properties of the copper to low-carbon steel welded joints operating at high values of variable temperatures [6, 7] showed that at an iron content of up to 2 wt.% the weld metal has strength equal to that of the base metal (copper) over the entire temperature range. The iron content of more than 7 wt.% in copper causes a dramatic decrease in ductile properties of the joints, which may lead to hot cracking. Comprehensive evaluation of mechanical properties, long-time strength, thermal-fatigue life, amount of accumulation of alternating plastic strains to fracture and character of fractures showed that in operation of the copper to low-carbon steel welded joints under conditions of elevated and variable temperatures the optimal iron content of the weld metal is 3–6 wt.%.

The purpose of this study was to improve the technology for submerged-arc welding of copper to steel to produce the weld metal of the welded joints free from defects in the form of pores, lacks of penetration, cracks, slag inclusions, lacks of fusion with the base metal and undercuts, provide the optimal iron content of the weld metal (from 3 to 6 %), and simplify the process of tracking the weld line by electrode.

Series of experiments were carried out to optimise the technology for welding of copper to steel with different thicknesses of the weld edges. In these experiments the angle between the steel and copper edges was varied from 0 to 45°, the welding wire diameters were varied from 2 to 4 mm, and length of displacement of the electrode towards copper was varied by 0.2 to 1.2 of thickness of the base metal. In welding of the copper to steel specimens (5+5), (10+10) and (20+20) mm thick the welding parameters were varied depending on the thickness within the following ranges: welding current — 300–450, 500–700 and 1000–1300 A, arc voltage — 32–38, 34–40 and 40–46 V, and welding speed — 18–20, 16–18 and 8–10 m/h.

Welding was performed by using wire of the MNZhKT5-1-0.2-0.2 grade and flux of the AN-60 grade by the submerged-arc method. Prior to welding the wire was subjected to mechanical cleaning, and the flux was baked at a temperature of 400–450 °C for 2 h. Surfaces of the specimens of copper M1 (0.01 % O) and steel St3 were cleaned by cleaning wheels to prevent ingress of dirt or oxides to the welding zone. The method of additional gas shielding under a flux layer was used to increase resistance of the welded joint to porosity [8].

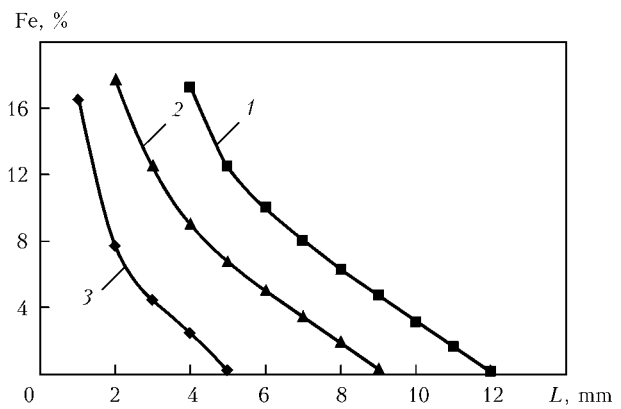

Figure 1. Iron content of weld metal versus length L of electrode displacement towards copper in one-electrode welding of copper to steel at different thicknesses of weld edges: *1* — (5+5); *2* — (10+10); *3* — (20+20) mm

The ABS welding head located over a movable table and VSZh-1600 power supply were employed for welding. The process was carried out at a current of reverse polarity and constant characteristic of the power supply.

Stability of the process was fixed during welding, and detachability of the slag crust and formation of the welds — after welding. Lacks of penetration, lacks of fusion, slag inclusions, cracks, pores and other defects were detected by visual examination of the welds. Then chips were taken from the upper part of the welds to determine the content of iron in the weld metal by the «wet» chemistry method. The investigations showed that the welding process was stable in all the cases, and detachability of the slag crust and formation of the welds were good. No pores or other defects were detected in the weld metal.

Optimal welding parameters and diameters of the wires providing complete penetration of the weld edges, good weld formation and detachability of the slag crust were selected depending on the thicknesses welded.

It was established that for all thicknesses the optimal preparation of the steel edge is at an angle of 30°. The copper edge can be remained non-grooved. In welding of the 20 mm thick joints the angle of the copper edge equal to 30° permits improvement of formation of the welds, although this leads to some increase in their iron content. Preparation of the steel edge at an angle of 45° leads to formation of the lacks of fusion on the side of steel, especially on the 5 and 10 mm thicknesses welded. In welding of the 20 mm thick specimens this edge preparation can be used when the copper edge remains non-grooved. However, this may cause decrease in the iron content of the weld metal to less than 3 %.

In further experiments the steel edge was prepared at an angle of 30°, and no groove was made on the copper edge for all the thicknesses welded.

The investigations showed (Figure 1) that the iron content of the weld metal within the recommended 3–6 % ranges for thicknesses of 5 mm was provided at displacement of the electrode from the weld line to 2–3 mm towards copper, for thicknesses of 10 mm — to 5–7 mm, and for thicknesses of 20 mm — to 8–10 mm.

Displacement of the electrode towards copper to a length less than the above ones leads to a dramatic increase in the iron content of the weld metal and

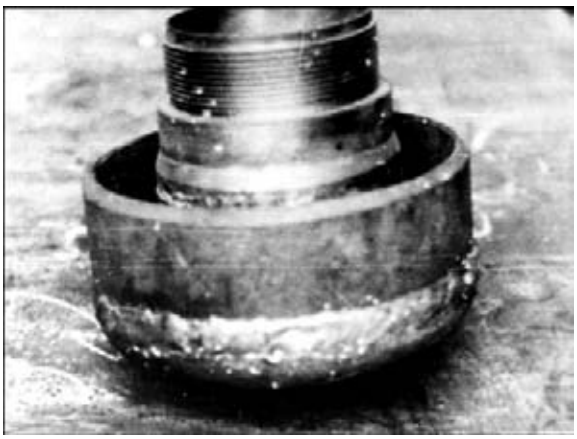

Figure 2. Appearance of a lance after welding of copper snout to steel ring

probable lacks of fusion with the copper edge, which may be related to transfer of the arc to the steel edge.

When the electrode is displaced towards copper to a length above the said ranges, incipient melting of the steel edge takes place only due to the heat of the molten metal pool, while this causes decrease in the iron content of the weld metal and formation of joints of the type of the brazed ones at the weld-steel fusion line. Also, it may cause lacks of fusion on the side of steel.

It was noted that defects in the form of lacks of fusion on the side of the steel edge or incomplete penetration of the copper edge may form at the beginning of welding of copper to steel with the 20 mm thick edges. At the end of welding the weld may displace towards steel, this causing a dramatic growth of its iron content and formation of transverse cracks. At the initial moment of welding the temperature of the copper plate has low values, which leads both to decrease in the depth of penetration of the copper edge and decrease in mobility of the arc, thus causing narrowing of the welds. Therefore, lacks of penetration or lacks of fusion on the side of the steel edge may form before achievement of equilibrium between heat input and heat removal to the copper plate.

At the end of welding the edge effect causes increase in temperature of the weld edges as the weld

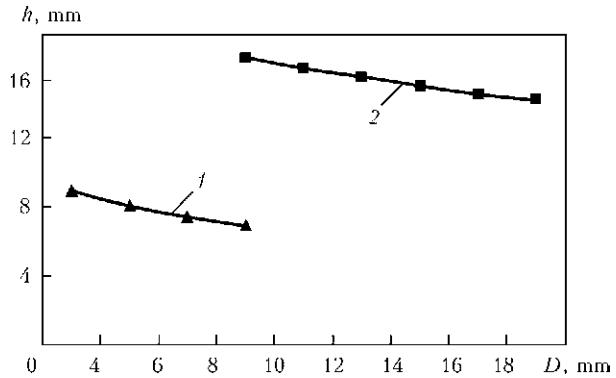

Figure 3. Effect of distance D between wires on edge penetration depth h in split-electrode welding of copper to steel with different thicknesses of weld edges. Here and in Figures 4–6: *1* — (10+10); *2* — (20+20) mm

pool approaches the end of the plates, which promotes increase in mobility of the arc and widening of the molten metal pool. As a result, more intensive melting of the steel edge leads to increase in the iron content of the weld metal. Particularly dangerous are the cases when the arc transfers to the steel edge. In such cases the weld displaces towards steel, and dramatic growth of its iron content may lead to formation of transverse cracks.

No such defects are usually detected in welding of specimens with the 5 and 10 mm thick edges. For welded joints with the 20 mm thick edges the dangerous zone at the beginning and end of welding may amount to several centimetres.

Also, such defects may form in the welded joints in transfer of the arc to the steel edge because of accidental deviations of the welding wire from its feed axis, or in beating of the welding head during movement. This is dangerous because the arc, once caught on the steel edge, continues burning with inclination to steel even after restoration of all welding parameters. Often this happens in welding of copper to steel with the 20 mm thick edges, which makes it impossible to produce sound joints when the process is performed using one electrode.

The selected conditions for welding of copper to steel with the 5 and 10 mm thick edges, edge preparation and other process parameters were recommended for welding of lances at the Frunze Metallurgical Works in Konstantinovsk. Industrial testing of this technology showed good results.

Application of the submerged-arc welding method for welding of a steel ring manufactured by refining of molten metal during melting [9] to a cast copper snout of a lance (Figure 2) allowed replacement of manual TIG welding in argon atmosphere, avoidance of the necessity to use preheating of a workpiece, simplification of the welding process and improvement of quality of the joints.

As in welding of copper to steel using one electrode even insignificant deviations of the latter from the weld axis may lead to deterioration of quality of the welded joints, while under industrial conditions it is very difficult to maintain the minimal deviation within the specified limits, it was of interest to develop such techniques that would assure the sound welded joints over wider ranges of probable deviations of the electrode from the weld axis. Also, these techniques should allow elimination of rejects at the beginning and end of welding. One of such techniques can be welding using a split electrode that sets the required width of the welds and decreases the current at the arc burning on the side of the steel edge, which, in our opinion, should have a positive effect on the quality of the welded joints. Fused-agglomerated flux was used to prevent porosity in split-electrode welding of copper to steel [10].

Series of experiments were carried out to study the possibility of using the split electrode for welding of

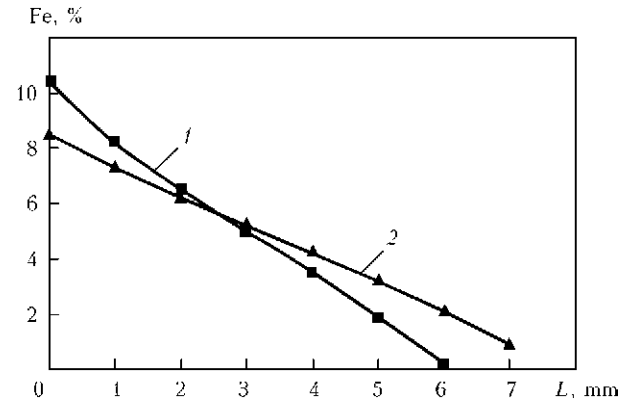

Figure 4. Iron content of weld metal versus length L of electrode displacement towards copper in split-electrode welding of copper to steel at different thicknesses of weld edges

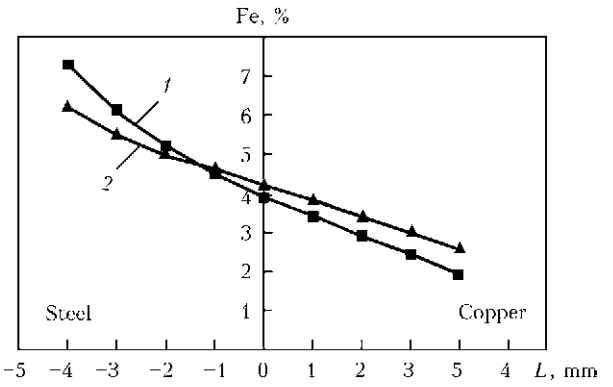

Figure 6. Iron content of weld metal in copper to steel joints versus length L of electrode displacement towards copper in welding of copper to steel by using split electrode consisting of different-diameter wires

copper to steel with the 10 and 20 mm thick edges. The effect of distance between the electrodes, welding parameters, edge preparation and displacement of the electrodes from the weld line on the quality of the welded joints was investigated during the experiments.

As proved by the investigation results on the effect of distance between the wires in the split electrode on the depth of penetration of the copper edge (Figure 3), the use of the split electrode and increase in distance between the wires in it lead to decrease in the depth of penetration of the weld edges. It was noted that two separate pools are formed in the welded joints with the 20 mm thick edges at a distance between the wires in the split electrode equal to 18 mm or more. So, the optimal distances between the wires in the split electrode were selected to be equal to 0.5–0.7 of thickness of the weld edges.

As the depth of penetration of the weld edges at the said distance between the wires was approximately 20 % less than in welding with one electrode under the same process conditions, it was necessary to accordingly increase the welding current at the split electrode.

As follows from Figures 1 and 4, the split-electrode welding technology widens the ranges of probable deviations from the weld axis, compared to one-electrode welding. However, the necessity to increase the current by 20 % or more, to set the electrode displacement to a specified distance from the weld line and keep strictly to this distance during welding does not allow recommending this method for further laboratory and industrial tests.

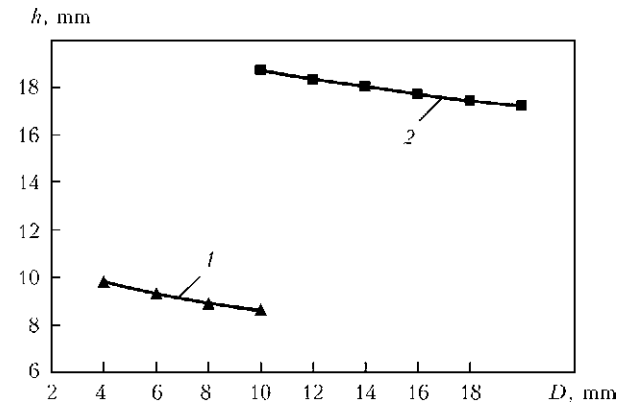

Figure 5. Effect of distance D between wires on edge penetration depth h in welding of copper to steel with different thicknesses of weld edges by using split electrode consisting of different-diameter wires

Based on the results obtained with welding using the split electrode consisting of wires of the same diameters, it was suggested using the split electrode consisting of the different-diameter wires for welding of copper to steel, owing to which it is possible to control heat input into the copper and steel edges.

As seen from Figures 3 and 5, the use of welding with the split electrode consisting of the different-diameter wires (wire diameter on the side of steel is 30–40 % of wire diameter on the side of copper) made it possible to increase the depth of penetration of the weld edges, compared to welding with the split electrode consisting of wires of the same diameters. Welding parameters in both cases were identical.

The trend to formation of two separate molten metal pools was noted in welding with the split electrode consisting of the different-diameter wires at a distance between them equal to more than 18 mm. The optimal distances between the wires in the split electrode are 0.5–0.8 of thickness of the weld edges. In this case it is indicated to increase the welding current by about 10 % compared to welding with one electrode.

Series of experiments on welding of copper to steel with the 10 and 20 mm thick edges were carried out to study the effect of electrode displacement from the weld line on the iron content of the weld metal. Dis-

Figure 7. Appearance of copper to steel welded specimens after bend tests

placement of the split electrode consisting of the different-diameter wires was varied from 0 to 4 mm from the weld line towards copper and towards steel. The steel edge was grooved at an angle of 30°, and the copper edge remained intact.

As follows from Figure 6, the use of the split electrode consisting of the different-diameter wires made it possible to substantially increase the ranges of probable deviations of electrodes from the weld line and, at the same time, assure the high quality of the welded joints.

Based on the results obtained, it was established that a smaller-diameter wire should be set along the weld line and the specified splitting would automatically define the length of displacement of a bigger-diameter wire towards copper. This will substantially simplify the operation of preparation prior to welding and eliminate any possible mistake of an operator. Moreover, an accidental deviation of the electrode from the weld line will have no considerable effect on the quality of the welds.

Keeping to these recommendations will make it possible to produce sound welds with an iron content of 3 to 6 %, thus providing a high level of their mechanical properties at room and elevated temperatures, and allowing avoidance of defects at the beginning and end of welding. Specimens of such joints in tensile tests fracture in the base metal (copper) at σ_t = 200–210 MPa and withstand the bend angle of 180° (Figure 7). The improved technology for welding with the split electrode consisting of the different-diameter wires was tested for welding of copper to steel with the 20 mm thick edges to make solid plates of continuous casting moulds, and can be recommended for wide commercial application.

CONCLUSIONS

1. The optimal edge preparations, welding parameters and length of displacement of electrode from the weld line towards copper were selected, providing sound welds in one-electrode welding of copper to steel with thickness of the weld edges ranging from 5 to 10 mm.

2. It was established that defects may form at the beginning or end of the welds in one-electrode welding of copper to steel with the 20 mm thick edges, which does not guarantee production of sound welded joints.

3. Testing of welding with the split electrode consisting of two wires of the same diameters showed that in welding of copper to steel to provide the sound welds it is necessary to increase the welding current by 20 % or more, compared to one-electrode welding.

4. The suggested method for welding of copper to steel using the split electrode consisting of two wires of different diameters allows controlling heat input into the copper and steel edges and simplifies tracking the weld line by the electrode. This improved technology can be recommended for welding of copper to steel with the 10 to 20 mm thick weld edges.

1. Gurevich, S.M. (1990) *Reference book on welding of nonferrous metals*. Kiev: Naukova Dumka.
2. Shekhter, S.Ya., Reznitsky, A.M., Pyankov, V.V. (1973) Welding of copper to steel in production of blast furnace lances. *Avtomatich. Svarka*, **11**, 55–57.
3. Ilyushenko, V.M., Bosak, L.K., Grishin, L.I. (1966) Automatic submerged-arc welding of copper to large thickness steel. *Ibid.*, **6**, 73.
4. Ivashchenko, G.M., Dzhevaga, I.M., Lebedev, O.M. (1971) Mechanical properties of joints in surfacing of aluminium bronze on carbon steels. *Ibid.*, **8**, 52–55.
5. Shutov, A.S. (1970) On optimal composition of weld metal in fusion welding of copper to low-carbon steel. *Ibid.*, **11**, 17–19.
6. Rotach, A.P. (1985) *Increase in serviceability and life of copper to low-carbon steel welded joints operating at high and variable temperatures*: Syn. of Thesis for Cand. of Techn. Sci. Degree. Leningrad.
7. Pavlyuk, S.K., Rotach, A.P., Vecher, A.V. (1986) Properties of weld metal in copper to low-carbon steel joints at elevated temperatures and their resistance to thermal fatigue. *Problemy Prochnosti*, **3**, 15–19.
8. Koleda, V.N., Ilyushenko, V.M. (2010) Optimisation of parameters of additional gas shielding in submerged arc welding and surfacing of copper and its alloys. *The Paton Welding J.*, **11**, 38–41.
9. Koleda, V.N., Ilyushenko, V.M., Biktagirov, F.K. et al. (2011) Refining of metal in melting of copper and its alloys from waste. *Sovremen. Elektrometallurgiya*, **1**, 33–37.
10. Koleda, V.N., Ilyushenko, V.M. (2010) Fused-agglomerated flux for welding and surfacing of copper and its alloys. In: *Proc. of 5th Int. Conf. on Welding Consumables. Technologies. Production. Quality. Competitiveness* (Kiev, May 2010), 117–123.

Remarkable dates

DEVELOPMENT OF TECHNOLOGY OF AUTOMATIC SUBMERGED ARC WELDING OF ARMOR STEELS

The technology of automatic submerged arc welding of armored steels was developed 70 years ago for the first time in the world by staff-scientists of the Electric Welding Institute under leadership of Evgeny O. Paton. Based on self-regulation of arc processes the new generation of welding machines was designed, installations for welding of tanks, self-propelled artillery guns, air-bombs were projected. As a result the USSR refused from lend-lease supply of American and English tanks, and Soviet Army was completely provided with the best tanks of the Second World War.

Perfidious attack of Germany against USSR broke the planes of Evgeny O. Paton to construct an all-welded bridge across the Dnieper. The Electric Welding Institute on the request of its director was evacuated to the Urals (Nizhny Tagil) and arranged at the territory of the F.E. Dzerzhinsky Uralvagonzavod. All 37 staff-scientists of the Institute were involved into activity of the plant, maximally expanding the implementation of high-speed welding into production of cargo cars and air-bombs, simultaneously creating their own experimental and industrial facility.

At the beginning of October 1941, three thousand scientists of the Komintern Kharkov Plant arrived at Nizhny Tagil, where at the design bureau under leadership of M.I. Koshkin the best medium tank T-34 was built. The plants were joined into one enterprise — the Komintern Ural Tank Plant No. 183. At the latter and also at the plants of Chelyabinsk, Stalingrad, Gorky, Orenburg and other cities the production of tanks was organized. The manufacturers were forced to overcome significant organizational and technological difficulties. A weak point in armor body shops were areas of welding of armor plates of thickness of tens of millimeters. The hundreds of skilled welders were involved into this operation performing manual multilayer arc welding using consumable electrodes.

In November 7,1941, the USSR was imposed the USA law on lend-lease, i.e. sale, rent or exchange for raw materials of armament and provisions. In February 11, 1942, the USA President F. Rusvelt sent a message to I.V. Stalin about shipping of 449 light and 408 medium tanks. In July 18, the Leader of the USSR replied that American tanks easily broke out from German shells and according to tactical and technical characteristics were considerably inferior both to Soviet and also to German ones. The rejection of proposed aid was an evidence of not only high quality of Soviet machinery but also confidence in accelerating of tanks production by domestic industry.

E.O. Paton directed efforts of scientists on the solution of problems of submerged arc welding of armored steels and designing machines for manufacture of complex three-dimensional structures with rela-

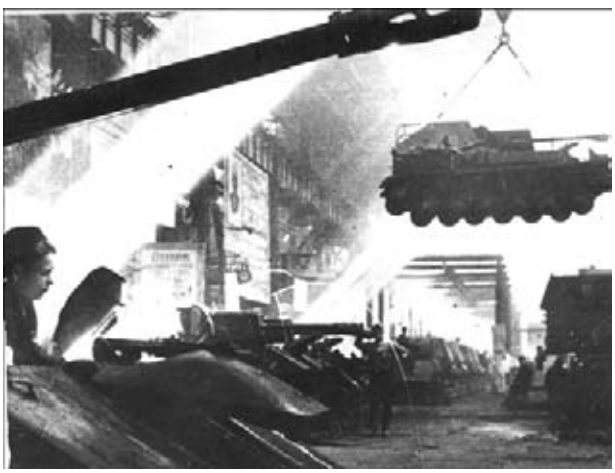

Production of tanks and self-propelled machines at one of the shops of Ural Tank Plant

Generals express gratitude to Evgeny O. Paton (movie shot)

They welded tanks during 1941–1944: *from left to right sitting* G.Z. Voloshkevich, P.I. Sevbo, B.E. Paton, M.N. Sidorenko, A.E. Asnis, M.N. Tishchenko, M.M. Grokhotov; *standing* M.F. Aleksandrov, D.M. Rabkin, K.K. Fride, S.A. Ostrovskaya, V.E. Paton, L.M. Gutman, T.M. Slutskaya

tively short welds. The first of these problems became cracks initiating during automatic welding of alloyed hardened steels. Nobody in the world could solve this task. The proposal of EWI scientist V.I. Dyatlov and B.A. Ivanov, engineer of the Komintern Kharkov Plant, appeared to be unexpected and rather simple, namely to place a low-carbon filler wire into the groove. It resulted in decrease of carburization of weld metal, «brittle» cracks disappeared, process efficiency increased.

In January 1942, the first body of tank T-34 was welded, the firing of which showed its higher robustness as compared to that produced in manual welding. The same year V.I. Dyatlov disclosed the phenomenon of self-control of arc processes with consumable electrode. The studies of this phenomena, carried out by B.E. Paton together with A.M. Makara, P.I. Sevbo and M.N. Sidorenko, were used to create simple and reliable welding machine. The simplified automatic welding heads with constant speed of electrode feeding, in spite of fluctuations of power in electric circuits, started their stable operation and high quality of weld metal was guaranteed. The design group prepared projects of 20 specialized machines for automatic submerged arc welding of different assemblies of tank and 8 for welding of air-bombs and ammunition. At the body workshop on production line 16 machines were assembled for automatic submerged arc welding of base assemblies of tank, which were implemented also at other plants. To provide wide application of new machinery A.A. Morozov, N.A. Kucherenko (T-34) and Zh.Ya. Kotin (IS and KV), the designers of tanks, corrected the projects to meet the requirements of automatic welding. By the end of 1943, the Electric Welding Institute installed more than 50 machines at the plants of People's Commissariat of Tank Industry. Its colleagues trained welders, worked at the plants as instructors, setters-up, inspectors. Putting into operation of one machine released seven welding transformers. The efficient output of production from a unit of industrial area was several times increased. Plants saved up to 42 % of power. The efficiency of automatic welding far surpassed the efficiency of previous technology. One machine replaced 10–14 people.

And again the problem. The successful application of automatic welding could be interrupted as far as reserves of flux AN-1, melted before the war in Donbass, were coming to the end. E.O. Paton proposed to apply instead of a flux the slag of Ashin blast furnace (disclosed by A.I. Korennoj). There were no sulphur in the slag and metallurgists added manganese ore, so the country produced a new welding material: flux ASh. In March 2, 1943 E.O. Paton, the first one of the Ukrainian academicians, was awarded the title of Hero of Socialistic Labor. During years of war he was decorated with three orders, and group of the Institute with orders and medals.

During years of war the colleagues of the Institute published more than dozen of printed works among which are the third edition of monograph of E.O. Paton «Automatic high-speed submerged arc welding», «Manual on welding of armor structures», monograph of B.E. Paton and A.M. Makara «Experimental investigation of automatic submerged arc welding process».

At the beginning of 1945, the submerged arc welding was used at 52 plants. During years of war 4 mln m of welds were welded using automatic machines, 5 mln kW·h of power was saved, the labour consumption in manufacture of tank body was 5 times decreased. In total during the years of war 102,857 tanks and self-propelled artillery guns were produced in the Soviet Union. The Electric Welding Institute won the competition by correspondence with Krupp concern (Germany), where all armor machinery was welded using manual electrodes and the quality of joints was not high. In the USA only in 1944 the technology of automatic welding of armor steels was developed. The USA lend-lease supplies to Soviet Union amounted about 4 % of their production in USSR. Instead of this 300,000 t of chromium and 32,000 t of manganese ore were obtained by the USA for that time.

It should be noted that «Uralvagonzavod» obtained additional «qualification», it became a large tank building enterprise. However, the E.O. Paton Electric Welding Institute implemented there new technologies for a long time. In 1982 the Ural citizens invited delegation of PWI to the ceremonies devoted to the 40-anniversary of automatic welding of tanks.

Prof. A.N. Kornienko, PWI

NEWS

PLASMA-ARC WELDING OF LARGE-SIZED PRODUCTS FROM CARBON MATERIALS TO METALS

Welding equipment and technology were developed by PWI Zaporozhie Center of Plasma Technologies with the purpose of replacement of pressure multiampere contacts by welded contacts in such electric metallurgy installations as electrolyzers for aluminium and magnesium production, furnaces for graphitization, silicon carbide synthesis, etc. The cause for replacement of pressure contacts is the transient electric resistance on metal–carbon material interface, increasing tens and hundreds of times during operation, whereas welded contacts change their transient resistance by one to two orders of magnitude less.

ECP macrosection

Such a replacement ensures a considerable saving of power (up to 18 %), and also allows developing new rational designs of energy- and resource-saving electrolyzers and Acheson furnaces based on welded electric contact assemblies.

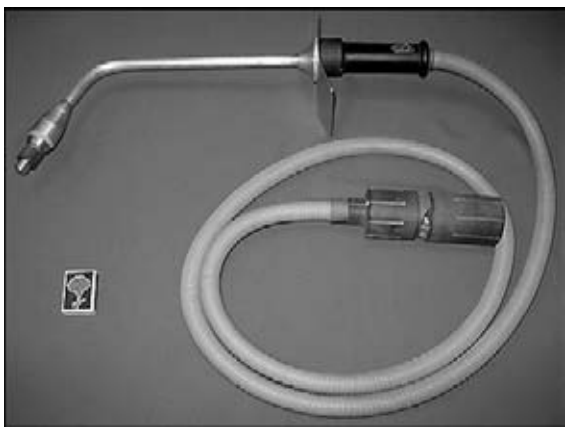

Acrotron

Welded joints of the type of metal + carbon material are made by a nozzle-free plasma generator — arcotron, operating with a new type oxide cathode, so that the process is performed in open air without application of shielding gases or fluxes. Power to arcotron is supplied from DC welding sources with a steeply falling external volt-ampere characteristic.

The main design element of any welded electric contact assembly is electric contact plug (ECP), each of which is capable of carrying the current load from 300 up to 600 A. Individual ECP are used to create contact assemblies for 10–225 kA. Contacts between ECP, current-carrying parts and buses are provided using various types of welded-in and welded-on jacks (metal conductors), thus ensuring failure-safe operation of welded joints at higher temperatures and alternating loads of installation thermal cycles.

TECHNOLOGY AND EQUIPMENT FOR MICROPLASMA SPRAYING OF BIOCERMET COATING ON ENDOPROTHESES

PWI developed technology and equipment for microplasma spraying of a bilayer biocermet (titanium–hydrooxyapathite (HA)) coating for endoprostheses. Here a possibility was achieved of deposition by microplasma spraying of a titanium coating with controllable porosity (pore size of 50–150 μm) by application of wire microplasma spraying.

Spraying of bilayer biocermet coating is performed in microplasma spraying unit MPN-004 with consumed power of up to 2.5 kW, including a power source with water cooling module, gas block, plasmatron, as well as irreplaceable wire feed mechanism and powder feeder MPD-004.

Microplasma spraying differs from the current plasma methods by application of a low power plasma jet (1–2 kW), allowing reduction of spraying spot diameter to 3–8 mm in deposition of hydrooxyapathite that ensures an essential (by 2–3 times) lowering of powder consumption in spraying on small-sized implants compared to regular plasma spraying. In addi-

tion, microplasma spraying technology allows forming a HA layer with a high degree of crystallinity (88–98 %), which can be controlled by variation of the spraying mode. Spraying of Ti-layer with a controllable porosity is performed by microplasma spraying of Ti-wire.

A combination of porous Ti-coating with an outer HA layer ensures the strength of its adhesion to endoprostheses surface of 24–25 MPa and subsequent active growing of bone tissue into the coating.

Developed bioceramic coating (Ti–HA) and technology of its microplasma spraying are recommended for deposition on hip joint endoprostheses, as well as on other kinds of endoprostheses, including dental, inerspinous cages, etc.

Microplasma spraying technology can be also used for deposition of coatings from metals, oxides, carbides on small-sized products, for forming local coatings in the form of spots and strips with transverse dimensions of 3–8 mm, as well as local repair of damaged surface areas.

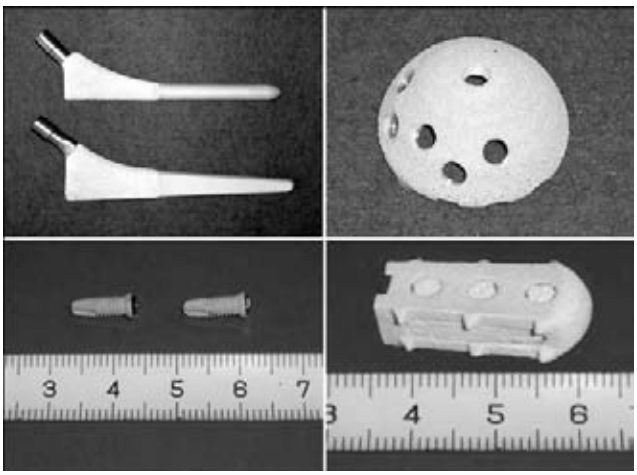

HAND LIQUID-FUEL CUTTER

Autogenous Equipment Factory «Donmet» (Kramatorsk, Ukraine) offers new Bobukh RK200 hand liquid fuel cutter (gasoline blow torch) «Vognyk 182». The novelty is intended for severing of low-carbon steel from 3 to 200 mm thick.

- gasoline of A-76, A-80, AI-91, A-92, A-95 and other grades designed for engines (GOST 2084–77), and gasoline of «Regulator-91» and «Normal-80» (GOST 51105–97) grades can be used as fuel;
- operation even at a frost of –25 °C is possible;

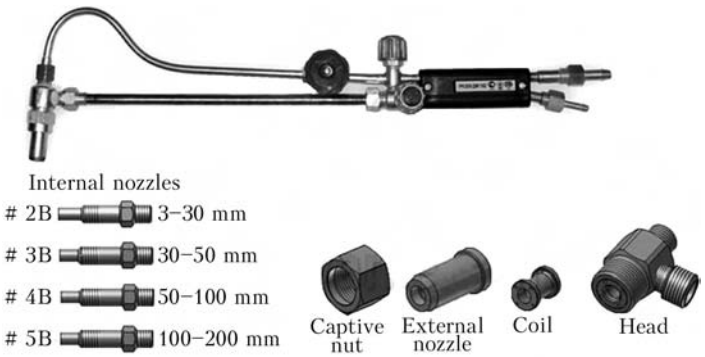

Characteristic features of RK200 cutter «Vognyk 182»:

- absence of asbestos cord and of separate heating flame for evaporation of liquid fuel (gasoline);
- complete combustion of fuel;
- 100 % resistance to back kick;
- reaching the working parameters during 15–30 s;
- length — not more than 555 mm;
- weight — not more than 840 g.

SUBSCRIPTION
FOR «THE PATON WELDING JOURNAL»

If You are interested in making subscription directly via Editorial Board, fill, please, the coupon and send application by fax or e-mail.

The cost of annual subscription via Editorial Board is $324.

Telephones and faxes of Editorial Board of «The Paton Welding Journal»:

Tel.: (38044) 200 82 77, 200 81 45

Fax: (38044) 200 82 77, 200 81 45.

«The Paton Welding Journal» can be also subscribed worldwide from catalogues of subscription agency EBSO.

SUBSCRIPTION COUPON

Address for journal delivery _____

Term of subscription since _____ **20** **till** **20**

Name, initials _____

Affiliation _____

Position _____

Tel., Fax, E-mail

Subscription to the electronic version of «The Paton Welding Journal» can be done at site: *www: rucont.ru*

РУКОНТ
НАЦИОНАЛЬНЫЙ ЦИФРОВОЙ РЕСУРС

We offer for the subscription all issues of the Journal in pdf format, starting from 2009. You can subscribe to individual issues or to the entire archive including all issues over a period of 2009–2011. The subscription is available for natural persons and legal entities.

ADVERTISEMENT
IN «THE PATON WELDING JOURNAL»

External cover, fully-colored:
First page of cover (190×190 mm) – $700
Second page of cover (200×290 mm) – $550
Third page of cover (200×290 mm) – $500
Fourth page of cover (200×290 mm) – $600

Internal cover, fully-colored:
First page of cover (200×290 mm) – $350
Second page of cover (200×290 mm) – $350
Third page of cover (200×290 mm) – $350
Fourth page of cover (200×290 mm) – $350

Internal insert:
Fully-colored (200×290 mm) – $300
Fully-colored (double page A3) (400×290 mm) – $500
Fully-colored (200×145 mm) – $150
Black-and-white (170×250 mm) – $80
Black-and-white (170×125 mm) – $50
Black-and-white (80×80 mm) – $15

- Article in the form of advertising is 50 % of the cost of advertising area
- When the sum of advertising contracts exceeds $1000, a flexible system of discounts is envisaged

Technical requirement for the advertising materials:
- Size of journal after cutting is 200×290 mm
- In advertising layouts, the texts, logotypes and other elements should be located 5 mm from the module edge to prevent the loss of a part of information

All files in format IBM PC:
- Corell Draw, version up to 10.0
- Adobe Photoshop, version up to 7.0
- Quark, version up to 5.0
- Representations in format TIFF, color model CMYK, resolution 300 dpi
- Files should be added with a printed copy (makeups in WORD for are not accepted)